ULTRAFAST OPTICAL NONLINEARITIES IN INGAASP WAVEGUIDE DEVICES.

Peter D. Roberts

A Thesis Submitted for the Degree of PhD
at the
University of St Andrews

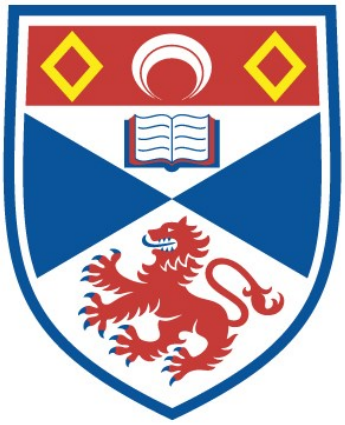

1996

Ultrafast Optical Nonlinearities in InGaAsP Waveguide Devices

Thesis submitted for the degree of Doctor of Philosophy
to the University of St. Andrews
by
Peter D. Roberts, B.Sc.

J. F. Allen Physics Research Laboratories
Department of Physics and Astronomy
University of St. Andrews
North Haugh
St. Andrews
Scotland KY16 9SS

May 1996

ProQuest LLC.
789 East Eisenhower Parkway
P.O. Box 1346
Ann Arbor, MI 48106 – 1346

Th C2B

Declaration

I Peter David Roberts hereby certify that this thesis has been composed by myself, that it is a record of my own work, and that it has not been accepted in partial or complete fulfilment of any other degree or professional qualification.

I was admitted to the Faculty of Science at the University of St. Andrews under Ordinance General No 12 on 1st October 1992.

Signed Date 16 March 1996

I hereby certify that the candidate has fulfilled the conditions of the Resolution and Regulations appropriate to the Degree of Ph.D.

Signature of Supervisor Date

16/03/96.

Copyright

In submitting this thesis to the University of St. Andrews I understand that I am giving permission for it to be made available for use in accordance with the regulations of the University Library for the time being in force, subject to any copyright vested in the work not being affected thereby. I also understand that the title and abstract will be published, and that a copy of the work may be made and supplied to any bona fide library or research worker.

Abstract

This thesis presents an investigation of the enhanced intensity-dependent refractive nonlinearity in optical amplifiers biased to transparency. Nonlinearities in an optical amplifier with a bulk active region and in optical amplifiers containing four, eight and sixteen quantum wells were compared using picosecond and femtosecond duration pulses generated using colour-centre lasers.

Measurements of nonlinear absorptive and refractive dynamics in the amplifiers were performed using pump-probe and time-division interferometry techniques. A curve fitting function was used to distinguish nonlinearities from the measured dynamics. Carrier-heating, caused predominantly by free-carrier absorption, and virtual effects were found to be the most important nonlinearities in optical amplifiers biased to transparency. A strong correlation of the magnitude of the carrier-heating effect with the thickness of the amplifier active regions was observed.

A novel measurement of the intensity dependence of the current required to bias optical amplifiers to transparency was performed using a technique which monitored the opto-electronic voltage across the amplifiers. The measurement showed that the transparency current increased linearly with intensity in the 4 QW and 8 QW amplifiers as a result of carrier-heating. Measurements performed on the 16 QW and bulk amplifiers showed a nonlinear variation of transparency current with intensity. These measurements were supplemented with a pump-probe investigation which revealed a negative trend in the transmission with a time constant in excess of 200 ps. It was suggested that a saturation effect related to the amount of heat added to the carrier distribution through free-carrier absorption was responsible for both of these effects.

All-optical switching of picosecond pulses via the investigated enhanced nonlinearity was demonstrated in a polarisation switch, constructed using the bulk amplifier, and a nonlinear directional coupler. The optical powers required to perform optical switching were 1.6 W and 5.8 W respectively.

Contents

Chapter 1

Introduction

1.1 Semiconductor lasers

The first operating laser was demonstrated in 1960[1] and operational semiconductor lasers were reported two years later[2,3]. The optical gain in early semiconductor lasers was provided by electron-hole recombination in the depletion region of a *p-n* junction, and feedback was provided by polished facets perpendicular to the junction plane. Early semiconductor lasers had very high threshold current densities, and were unable to operate at room temperature. Improvements in their performance were achieved by sandwiching a layer of semiconductor material between two cladding layers of a different semiconductor with a wider bandgap. In 1969, a 'heterostructure' laser constructed using a combination of GaAs and AlGaAs was operated in pulsed mode at room temperature[4-6], and a laser operating in continuous wave (CW) mode at room temperature was reported in the following year[7,8]. By the early 1970's, AlGaAs/GaAs lasers had become useful and practical laboratory tools.

Lateral confinement of the carriers in semiconductor lasers was proposed in 1967[9] to limit the spread of carriers in the active layer, and thereby reduce the threshold current. Early carrier confinement was achieved by injecting current to lasers via a stripe contact which ran along a central region of the laser[10]. Optical gain in these 'gain guiding' lasers was confined to the vicinity of the stripe, and the mode was similarly confined. A further improvement to the performance of semiconductor lasers was made through lateral confinement of the field perpendicular to the junction plane by adding a higher bandgap material on either side of the active region of the laser[11]. The higher bandgap material acted as a barrier to the diffusion of electrons and holes,

and in addition guided the optical mode when material with an appropriate refractive index was chosen.

1.1.2 Quantum Wells

With the development of heterostructure lasers and the advent of molecular beam epitaxy (MBE) machines capable of forming very thin (<20 nm) layers of semiconductor, came the idea of producing an active region composed of a number of thin layers separated by layers of a material with a greater bandgap. It was predicted by Henry[12] that this structure would produce discrete steps in the optical absorption of a semiconductor. Quantisation of the optical absorption edge as a consequence of this discrete structure (quantum wells) was observed for the first time in GaAs/AlGaAs by Dingle *et al*[13] in 1974. A laser containing quantum wells was first demonstrated by Van der Ziel *et al*[14] in the following year.

In a bulk semiconductor, the density of states increases as the square root of energy, while in quantum wells, the increase is step-like (a comparison of the bulk and quantum density of states is shown in figure 1). To provide a high gain from a semiconductor laser requires population inversion of levels with a high density of states, and in a bulk semiconductor laser, this can only be achieved by first filling the lower energy levels. Quantum well lasers are advantageous because their peak gain is associated with levels at the bottom of the band, and the current required to reach an equivalent gain is significantly reduced. A second advantage of quantum well structures is that the bandgap is dependent on the thickness of the quantum wells, and the operating wavelength of a laser may therefore be tuned by changing the thickness of the wells.

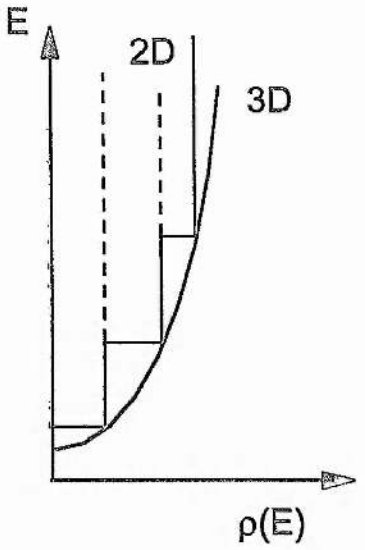

Figure 1. The density of states in a quantum well (2D) and bulk (3D) structure.

The predicted advantages of quantum-well semiconductor lasers over their bulk counterparts were realised through work of Tsang who optimised the growth of quantum wells by the molecular beam epitaxy technique[15]. Subsequently, Tsang investigated the effects of varying the number and thickness of wells and optimised the height and thickness of the barriers between the wells. By increasing the proportion of Al in the outer layers of the lasers to confine the optical mode, he produced lasers containing four quantum wells with thresholds of 250 A/cm^2.[16] In addition to this, Tsang also developed a design of graded index waveguide for separate optical confinement, which further improved the performance of the quantum well lasers[17]. The structure of quantum well lasers developed by Tsang is commonly used today, and the optical amplifiers used in this thesis are of the separate confinement heterostructure design.

In the 1980's it was realised that it was possible to suppress the growth of line defects in the structure of quantum well lasers by incorporating strain between adjacent layers of semiconductor. The increased reliability provided by these strained layers has allowed the development of quantum well lasers which produce output powers of the order of Watts.

1.1.3 Long-Wavelength Semiconductor lasers

Early development of semiconductor lasers was concerned with AlGaAs/GaAs structures which provided light in the 0.8 to 0.9 μm wavelength range. However, considerable interest was also placed in the development of longer wavelength semiconductor lasers capable of operating in the 1.1 to 1.6 μm range. Lasers operating in this wavelength range are of distinct relevance to the telecommunications industry through their utility in optical fibre communications networks. Initially, interest was concentrated on lasers operating at 1.3 μm, as this corresponded to the wavelength of dispersion-free optical fibres, and was important for the establishment of long distance fibre-optic cables. As the field of fibre optics was developed, it became possible to engineer fibres in such a way that the zero of dispersion could be shifted to longer wavelengths. This allowed the construction of fibres which had near-zero first-order dispersion at 1.55 μm, the wavelength of minimum loss (~0.2 dB/km) in silica. Interest in, and the subsequent commercial application of, semiconductor lasers was transferred to this longer wavelength.

The material system used to make semiconductor lasers operating at ~1.55 μm is InGaAsP/InP. The active region of the lasers is made from $In_{1-x}Ga_xAs_yP_{1-y}$ quaternary alloy, the relative proportions of In and Ga (x), and As and P (y) being varied to control the wavelength produced, and the cladding is formed from InP. The combination of InGaAsP and InP is used because of the good match between the lattice constants of the two materials (the variation of lattice constant with alloy composition is shown in figure 2). CW operation at room temperature of an InGaAsP laser at 1.1 μm was first demonstrated in 1976[18], with operation of a laser at 1.55 μm reported in 1979[19-21]. InGaAsP lasers have been developed to the point where they are commercially exploited as sources in long distance fibre-optic communications links at both 1.3 and 1.5 μm.

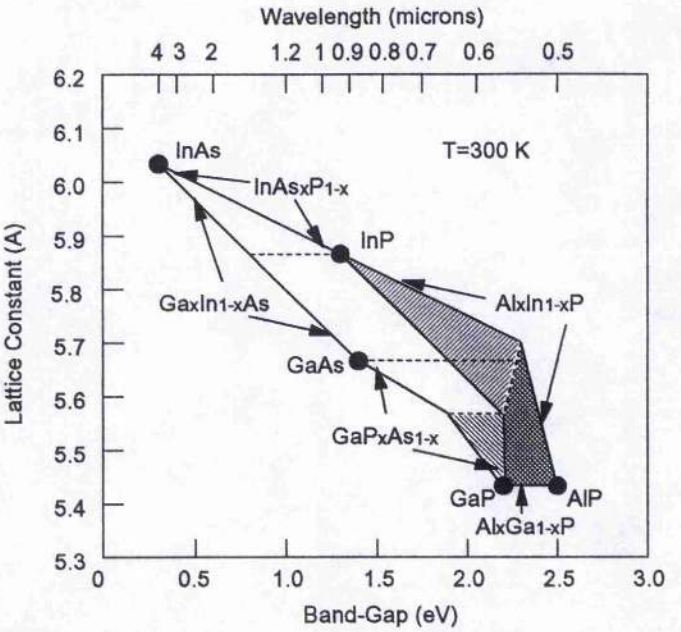

Figure 2. Band gap and lattice constant for $In_{1-x}Ga_xAs_{1-y}P_y$ (clear region) and $(Al_xGa_{1-x})_yIn_{1-y}P$ (shaded regions) obtained by varying compositions x and y. Dashed lines separate indirect-bandgap regions (shown downward sloping hatch). Dotted lines show the wavelength range for a semiconductor laser whose quaternary active layer is lattice-matched to the binary compound[22].

In parallel with the development of the role of long-wavelength semiconductor lasers as sources in communications networks, there has been growing interest in the potential application of semiconductor structures to provide all-optical switching, and in particular all-optical multiplexing and demultiplexing of signals from communications links.

1.2 Optical Switching

1.2.1 Introduction

In recent years, switching of optical signals has become a primary goal for researchers in the field of optoelectronics. In the 1980's, the term 'optical computing' was fashionable, and it was widely believed that electronic computers would eventually be superseded by optical equivalents with operational speeds orders of magnitude greater than that available through electronics. More recently, the thinking has been that optical means may be useful for providing parallel processing of images (for

example performing Fourier transforms), and a considerable amount of attention has been paid to potential application of all-optical switches as multiplexers and demultiplexers of optical signals from communication fibres.

Currently, multiplexed optical signals arriving at a termination of a fibre-optic cable are detected and converted into electrical signals, the signal is processed and then emitted by a semiconductor laser. The speed of this detection and re-emission process is limited firstly by the speed of the electronic processing of the signal and secondly by the response of the laser emitter. As demand increases for access to the internet and for other digital communications, the bandwidth necessary to provide communications networks capable of providing these needs will increase correspondingly. For a number of years therefore, researchers have been investigating ways of performing all-optical switching of optical communications signals which will operate at speeds adequate to conform to these requirements. Practically speaking, there is a requirement for optical switches operating at a rate of ~100 Gbit/s[23] (a switching speed of ~ 10 ps)

Current research into all-optical switching in semiconductors can be broadly divided into two categories, switches which operate via inter-band effects, and those which are based upon virtual nonlinearities (*i.e.* transitions to states which only exist for a period which is determined by the energy of the states via the Heisenberg uncertainty principle) .

1.2.2 Instantaneous Nonlinearities

In conventional linear optics, the induced polarisation in a material depends linearly upon the strength of the optical field in the material in a manner that can be described by the relationship

$$P(t) = \chi^{(1)} \cdot E(t) \qquad (1)$$

where P(t) is the polarisation, E(t) is the field and $\chi^{(1)}$ is the linear susceptibility of the material. In nonlinear optics, the optical response of a material can be described by generalising equation (1) and expressing the polarisation as a power series

$$P(t) = \chi^{(1)} \cdot E(t) + \chi^{(2)} \cdot E(t)^2 + \chi^{(3)} \cdot E(t)^3 \qquad (2)$$

where $\chi^{(2)}$ and $\chi^{(3)}$ are the second-order and third-order nonlinear optical susceptibilities. Second-order nonlinear optical interactions can only occur in crystals which do not have an inversion symmetry (noncentrosymmetric crystals), whereas third-order nonlinear optical interactions can occur in both centrosymmetric and noncentrosymmetric materials.

A monochromatic field applied to a media can be expressed as

$$E(t) := \varepsilon \cdot \cos(\omega t) \tag{3}$$

where ω is the frequency of the field and ε is the amplitude. The third-order nonlinear polarisation induced by the field will be

$$P(t)^{(3)} := \left(\frac{1}{4}\right) \cdot \chi^{(3)} \cdot \varepsilon^3 \cdot \cos(3\omega t) + \left(\frac{3}{4}\right) \cdot \chi^{(3)} \cdot \varepsilon^3 \cdot \cos(\omega t) \tag{4}$$

where the first term of the polarisation expression describes the response at frequency 3ω that is caused by an applied field at frequency ω. This is the process of third-harmonic generation where three photons of frequency ω are destroyed and a single photon of frequency 3ω is created. The second term of equation (4) represents a nonlinear contribution to the polarisation at the frequency of the applied field. This term leads to a modification of the refractive index experienced by the propagating wave of frequency ω. The refractive index in the presence of this type of nonlinearity can be represented as

$$n := n_0 + n_2 \cdot I \tag{5}$$

where n_0 is the linear refractive index (refractive index at low intensities), and n_2 is the intensity-dependent component of the refractive index:

$$n_2 := \frac{12 \cdot \pi^2}{(n_0)^2 \cdot c} \cdot \chi^{(3)} \tag{6}$$

where $\chi^{(3)}$ is in S.I. units. The term n_2 is also referred to as the nonlinear index coefficient and is measured in units of cm^2/W.

In general, all-optical switching is achieved by arranging a waveguide structure such that intense light travelling through the waveguide will experience a nonlinear change of phase as a result of the intensity dependent component of the refractive index. The waveguide is constructed so that the induced phase change leads to a modification of its transmission. This may be achieved by interferometrically adding two fields in the waveguide (Mach-Zehnder interferometer[24]), modifying a phase-matching criteria (nonlinear directional coupler[25]) or adding orthogonally-polarised fields (polarisation gate[26]).

1.2.3 Switching via Instantaneous Nonlinearities

Research into switching of intense optical pulses at 1.55 μm has concentrated on using the nonresonant third-order nonlinearity in AlGaAs structures. Waveguides constructed from AlGaAs/GaAs are used because the proportion of Al and Ga can be chosen such that the bandgap of the waveguide is just over twice the energy of a photon at a wavelength of 1.55 μm. This provides considerable reduction of two-photon absorption of the light, which arises at high intensities, whilst allowing for exploitation of the resonant enhancement of third-order nonlinearities which occur at energies close to twice the bandgap.

The method of engineering waveguides with bandgaps just below the two-photon absorption edge (and in some cases the three-photon absorption edge) has been pursued by Stegeman and co-workers at CREOL, Florida, in collaboration with Aitchison and co-workers at the University of Glasgow. The nonlinear coefficient, n_2, in AlGaAs/GaAs waveguides operating in this regime has been measured to be of the order of ~ 10^{-13} cm^2/W [27], and peak powers of the order of 100 W are typically required to achieve nonlinear phase shifts capable of achieving optical switching. The waveguides from which the switches are constructed are typically 2 cm long. These are used in preference to shorter guides because their length allows optical pulses to accumulate greater nonlinear phase shifts on propagation through the waveguides, and

enables switching to be performed at correspondingly lower powers. This reduction in intensity is important to further minimise two-photon and three-photon absorption which have respectively quadratic and cubic dependences on intensity. Nonlinear all-optical switches constructed from AlGaAs waveguides have been demonstrated using directional couplers[25], asymmetric Mach-Zehnder interferometers[24] and polarisation-rotation gates[26].

Recently, multiplexing[28] and demultiplexing[29] of fs signals using AlGaAs nonlinear directional couplers have been demonstrated. Although these results demonstrate that all-optical processing of ultrafast optical signals using instantaneous nonlinearities is possible, in practice the limited size of the nonlinearity is such that the optical powers required are prohibitive (300 W). This implies that practical application of this nonlinearity in the telecommunications industry may be unlikely.

1.2.4 Switching via Carrier-Dynamic-Related Nonlinearities

Optical nonlinearities arising from inter-band transitions of carriers are much larger than those seen for instantaneous nonlinear effects that occur via virtual transitions. The largest contribution to changes of the refractive index is from band-filling, in which initially vacant conduction (or valence) band states become occupied by optically excited electrons (or holes), reducing the size of the absorption coefficient, and thereby changing the refractive index. Early optical switches[30] were based upon this mechanism which offers a large nonlinear effect. More recently, switching has been demonstrated in a nonlinear etalon device in which the refractive index experienced by a TM polarised probe is modified by saturation of the absorption of a TE polarised pump (a quantum well device being chosen with a bandgap such that the TM probe is not absorbed)[31].

The slow recovery time (~1 ns) associated with absorption/loss saturation effects is a severe disadvantage and reverse biasing is often used to sweep carriers out of switches operating via this nonlinearity to enhance the speed of their recovery.

1.2.4 Ultrafast Nonlinearities in Amplifiers Biased to Transparency

In 1991, Grant and Sibbett[32] observed an intensity-dependent refractive index of $-2\times10^{-11}cm^2/W$ in a forward-biased bulk InGaAsP optical amplifier. The amplifier was biased such that optical pulses propagating through it would cause an equal number of stimulated absorptions and stimulated emissions, and the net number of band-to-band transitions induced by the pulses was zero. Because the densities of carriers in the bands of the amplifier were not modified by the pulses, the slow recovery time associated with carrier density reconfiguration was thereby avoided. The nonlinearity was measured by monitoring the spectra of 27 ps duration pulses transmitted by the amplifier using a scanning Fabry-Perot interferometer. The symmetry of spectra transmitted by the amplifier suggested that the recovery time of the nonlinear effect which was modifying the refractive index was considerably less than the pulse duration. Further experimentation using 1 ps duration pulses demonstrated that the recovery time of the effect was of the order of 1 ps. This effect displayed the desired combination of a ps regime recovery time with a refractive index nonlinearity which was more than an order of magnitude greater than that observed for instantaneous nonlinearities in AlGaAs waveguides.

Subsequent to Grant's experimental work, a similar investigation was performed on a multiple quantum well amplifier[33]. The magnitude of the ultrafast nonlinearity observed in the amplifier was similar to that seen in the bulk amplifier used by Grant and Sibbett. In further experimentation, the effect of varying of the number of quantum wells in amplifiers on the size of the nonlinearity was investigated[34]. These studies again involved the technique of monitoring spectra transmitted by the amplifiers to observe refractive nonlinearity. It was demonstrated that the size of the nonlinearity increased progressively with the number of quantum wells in the amplifier.

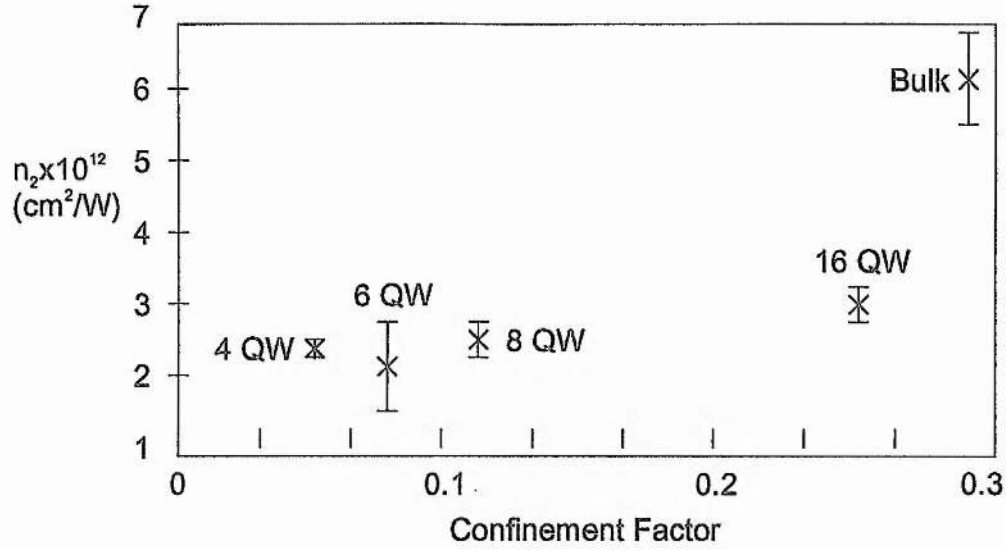

Figure 3. Variation of nonlinear index with active region modal confinement[33].

An amplifier containing a bulk active region displayed the largest refractive index nonlinearity, but it was noted that internal loss in bulk amplifiers is greater than that in quantum well amplifiers and this to some extent offsets the advantage acquired from the size of the nonlinearity. This investigation was concerned only with the size of the nonlinearity in amplifiers biased to transparency and did not provide any information as to the origin of the effect responsible for the intensity-dependent refractive index nonlinearity, other than that it was observed to have a recovery time of approximately 1 ps.

In parallel with the spectral investigations of the nonlinearities in forward-biased InGaAsP amplifiers, work carried out at MIT[35,36] used pump-probe and interferometer measurements to measure variations in the transmission and refractive index of AlGaAs amplifiers and separate the nonlinear effects via their time constants. Two-photon absorption, carrier-heating caused by free-carrier absorption, the optical Stark effect and spectral hole-burning were observed. These effects and their influence on the transmission and refractive index of optical amplifiers are discussed in full in Chapter 2.

It was against this background of considerable interest in the magnitude and origin of the ultrafast optical nonlinearity seen in optical amplifiers biased to transparency that the work described in this thesis was undertaken.

1.3 Experimental Equipment/Techniques

1.3.1 KCl:Tl^0(1) and NaCl:OH^- Lasers

The experiments described in this thesis were performed using KCl:Tl^0(1) and NaCl:OH^- colour-centre lasers. Colour-centres in KCl:Tl^0(1) crystals are associated with neutral thallium atom perturbed by adjacent anion vacancies, whilst those in NaCl:OH^- crystals are formed by two adjacent anion (Cl^-) vacancies in the <110> crystal direction with a neighbouring O^{2-} ion in a halide ion site. Colour-centre gain media are homogeneously broadened, are useful as high-power single-mode lasers[37] and, through their large gain bandwidth, can be mode-locked to produce pulses with sub-picosecond durations[38].

The potential of a colour-centre in a host crystal is influenced by the lattice surrounding it, and its energy levels are strongly broadened by lattice vibrations or phonons. The vibronic broadening of energy levels of a colour-centre is represented in figure 4.

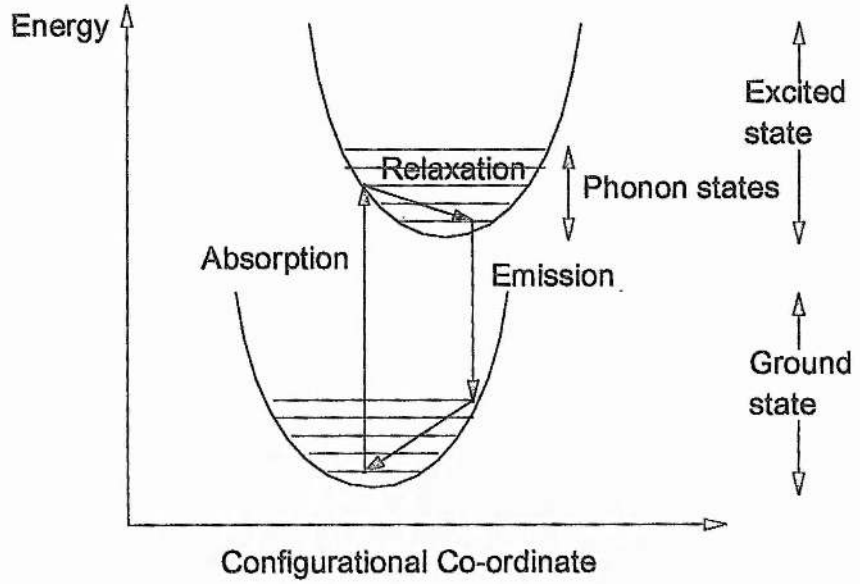

Figure 4. The electronic and phonon states of a colour-centre shown as a function of the configurational co-ordinate (distance from a vacancy to its neighbouring ions).

The configurational co-ordinate in Figure 4 refers to the distance from a lattice vacancy to its nearest neighbouring ions. The ground and excited electronic states of the colour centre are represented by two parabolas, with phonon states within each

electronic state being represented by horizontal lines. Excitation from the ground state to an excited electronic state is rapidly followed by the emission of phonons to the lowest phonon state of the excited state, referred to as the Relaxed Excited State. The electron spontaneously decays from the Relaxed Excited State to the ground electronic state, where further emission of phonons allows it to reach its lowest energy state. The cross-section for emission of phonons is much greater than the cross-section for the spontaneous decay of an electron from the Relaxed Excited State, and the centre is an effective four-level system. Vibrational broadening of the electronic states leads to the very large gain bandwidths of colour-centre lasers, and allows them to be modelocked to produce ultrashort pulses.

A KCl:$Tl^0(1)$ laser was used to generate pulses of 100 fs duration which were used in the experiments described in Chapters 2 and 3 of this thesis. The absorption band of the colour-centre in KCl:$Tl^0(1)$ is centred at 1.06 μm, and the laser is tunable from 1.4 - 1.63 μm[39], although the limited bandwidth of the mirrors used in the laser cavity meant that it was only capable of operating between 1.48 and 1.6 μm. The laser was pumped optically using 2 W of 1.06 μm light from a Nd:YAG laser, and typically yielded a typical output power of 200 mW.

Experiments described in Chapters 4 and 5 of this thesis were performed using a NaCl:OH^- colour-centre laser. The output from NaCl:OH^- lasers is tunable from 1.37 - 1.85 μm, and they have been demonstrated to produce 3 W of output power when pumped with a 10 W Nd:YAG laser[36]. The laser used here was tuneable between 1.47 and 1.58 μm. Colour-centres in NaCl:OH^- lasers are trapped by O^{2-} ions and unlike colour-centres in KCl:$Tl^0(1)$ lasers, do not migrate through the crystal. The output from NaCl:OH^- lasers is thus not subject to fading over a period of use of a few months which is observed in KCl:$Tl^0(1)$ lasers.

In order to obtain laser action from either of the KCl:$Tl^0(1)$ and NaCl:OH^- crystals, it is necessary to maintain them at cryogenic temperatures. The laser cryostat used to keep the crystals at low temperatures were developed at St. Andrews University.

The configuration of the resonator cavity used for the colour-centre lasers was based on one originally used for dye lasers.

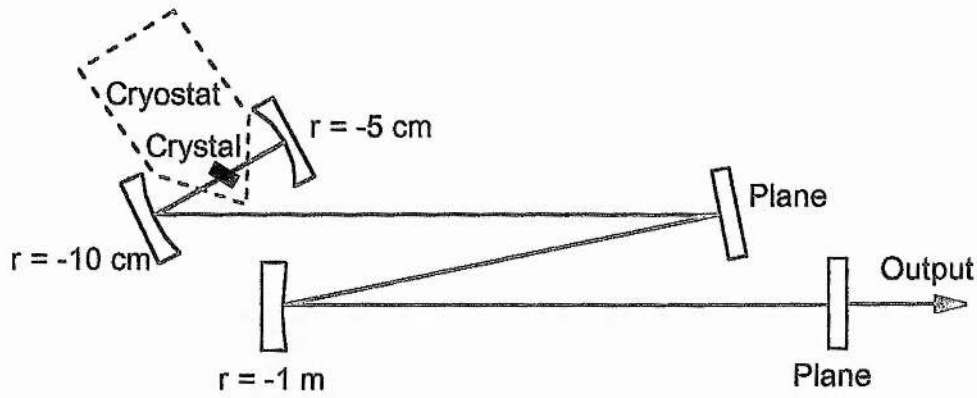

Figure 5. Schematic of the resonator configuration used for the KCl:Tl^0(1) and NaCl:OH^- colour-centre lasers.

The -10 cm and -5 cm radius of curvature mirrors were chosen to provide a spot size in the crystal of the order of 10 - 20 μm, whilst being relatively insensitive to misalignment of the mirrors. The -1m radius of curvature mirror increased the size of the spot in the colour-centre crystal to ~30 μm, providing better stability and matching the modes of the pump and the laser beams. The length of the cavity was matched to the length of the cavity of the Nd:YAG pump laser (183 cm).

1.3.2 Mode-locking

The colour-centre lasers used in the experiments described in this thesis were operated in three different regimes. The first of these, continuous wave (CW) operation was used when low intensity light was required to measure the linear properties of optical amplifiers. To produce CW light from the laser, its cavity was shortened by ~ 1 cm so that pulses from the acousto-optically mode-locked Nd:YAG laser were not synchronous with light propagating in the laser cavity.

The second regime of operation whereby pulses of 10 - 30 ps duration were produced involved synchronous pumping. The length of the laser cavity was carefully adjusted to match that of the acousto-optically mode-locked Nd:YAG pump laser. Synchronous pumping refers to a situation where pump pulses are synchronised with pulses in a laser cavity, providing a peak of gain to the laser pulse to the detriment of photons which are temporally displaced from the pulse. This mode-locking technique is useful for colour-centre lasers because they have relatively short upper-state lifetimes

and large gain cross-sections, which allow the pump pulse to saturate the gain, bringing it below threshold and shortening the trailing edge of the laser pulse.

The third regime of operation of the colour-centre lasers was coupled-cavity mode-locking. To produce coupled-cavity mode-locking, a laser cavity is constructed as an interferometer, and a nonlinear element is introduced into one of the arms of the interferometer[37,40,41]. Both Fabry-Perot[39] and Michelson[42,43] interferometer type cavities have been used to produce mode-locking of colour-centre lasers. In experiments described in this thesis, the Fabry-Perot (shown in Figure 6) and Michelson arrangements were used variously to overcome limitations of the intensity of light coupled into the nonlinear cavities arising from the limited range of mirror reflectivities available.

An intense pulse propagating through the nonlinear element included in the nonlinear arm of the interferometer experiences a phase shift proportional to the intensity across its profile. By arranging a suitable phase difference between the arms of the interferometer, it is possible to add pulses in the main cavity to pulses returning from the nonlinear arm such that there is constructive interference at the centre of the pulses and destructive interference at the wings of the pulses. In this way, the duration of the pulse in the main cavity of the laser is reduced. The element in the nonlinear arm of the interferometer setup used for experiments in this thesis was an erbium-doped optical fibre, with a fibre nonlinearity of approximately 2 $W^{-1}km^{-1}$. The length of the fibre was short (20 cm) to facilitate generation of pulses with sub-100 fs durations.

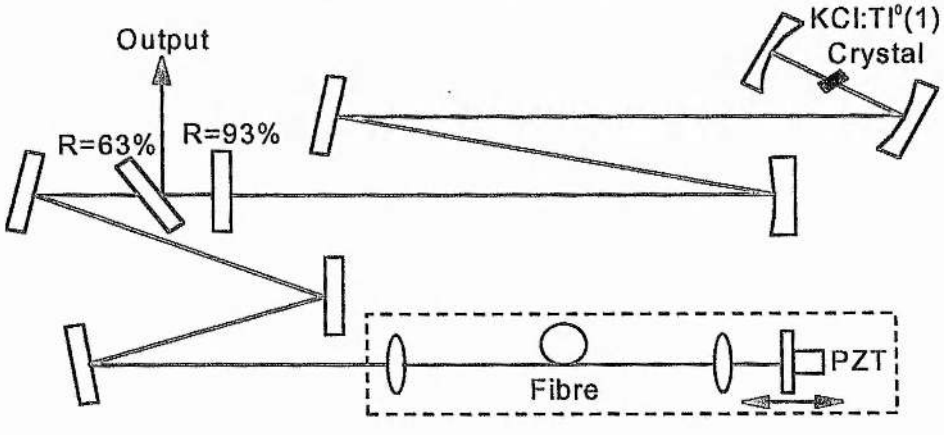

Figure 6. Schematic of the KCl:Tl^0(1) colour-centre laser in a nonlinear Fabry-Perot configuration.

1.3.3 Diagnostics

Large area germanium photodiodes were used to detect the average intensity of light used in many of the experiments in this thesis. In the experiments described in Chapters 2 and 3, ultrafast nonlinear effects are transformed from measurements in the time domain to spatial measurements. The photodiodes used to measure the transmission of the experiments in these chapters were connected to an amplifier which was designed to make their response linear. The response of the photodiodes was calibrated against a thermal power meter over the tuning range of the lasers.

A scanning-autocorrelator was used to monitor the pulses produced from both the synchronously-pumped and the coupled-cavity mode-locked lasers. The autocorrelator utilised second harmonic generation from type I phase matching of two input beams. The autocorrelator worked by splitting an incident beam into two beams of equal intensity, reflecting one from a static retro-reflector and reflecting the other from a retro-reflector mounted on a loudspeaker before recombining the two beams and passing them through a $LiNbO_3$ crystal. Second harmonic light generated in the $LiNbO_3$ by the incident beams was detected using a photo-multiplier tube. The loudspeaker was modulated by a rounded sawtooth waveform which caused the temporal overlap of two beams of pulses to vary.

The two beams incident on the $LiNbO_3$ crystal were collinear, and when pulses in the beams were not temporally overlapped, the $LiNbO_3$ crystal produced an output at a background level as a result of each beam independently generating second harmonic light. When overlapped pulses were incident on the LiNbO3 crystal the intensity of light produced was four times the background level, resulting in a detected signal with a pulse to background ratio of 3:1

Light produced by the crystal provided real-time information on the duration of pulses in the incident beam. Because what was being measured was pulse autocorrelations, the function produced was symmetric, and information relating to the temporal profile of the pulses was lost. The autocorrelator was calibrated by monitoring its output whilst translating the static retro-reflector through a known distance. To calculate the duration of pulses from their autocorrelation, it was necessary to assume that the pulse was a given shape (Gaussian for actively mode-

locked lasers, and $Sech^2$ for passively mode-locked lasers) and divide the duration of the autocorrelation by a corresponding constant.

For the experiment described in chapter 4 of this thesis, pulses of greater than 30 ps duration were generated using the NaCl:OH⁻ laser. The translation of the loudspeaker was limited to around 5 mm and was not capable of measuring these long pulse durations. A synchroscan streak-camera with a resolution of approximately 6 ps was used instead of the autocorrelator to measure these 'long' pulses. In the streak-camera a beam of light incident on the slit of the streak camera is imaged onto a photocathode (designed to work at 1.5 μm), from which electrons are released as a beam, and then focused using electrostatic lenses onto a phosphor screen at the far end of an imaging tube. The image of the slit is swept across the phosphor screen by applying a voltage ramp to a pair of deflector plates. When an optical pulse is incident on the photocathode, it liberates a packet of electrons which are 'streaked' to form an image on the phosphor screen corresponding to the intensity profile of the pulse.

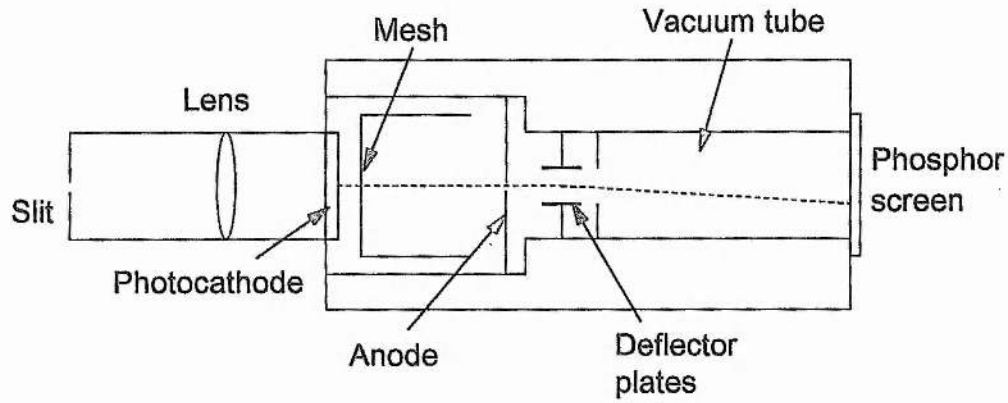

Figure 7. Schematic of the streak camera

The voltage ramp applied to the deflectors was triggered using pulses from the laser (or equivalently from a pump laser). The pulses were detected using a photodiode, the pulse train from which was used to trigger a tunnel diode oscillator oscillator which in turn produced a signal which was doubled and amplified to a power of several watts. Although the sreak camera had a poorer resolution than the autocorrelator, it was advantageous in that its response was linear, and the profile of pulses which it detected could be readily monitored.

Measurements of the spectra of pulses transmitted by optical switches described in Chapter 5 were required to demonstrate that the effect causing the optical switching was faster than the duration of the switched pulses. These spectral measurements were performed using a scanning Fabry-Perot interferometer which was of an in-house design and construction. The interferometer was fabricated from two plane 95% reflecting dielectric mirrors, one mounted on a precision translation stage, and the other on a mirror mount. The spectral width measured by the interferometer was adjustable by varying the separation of the mirrors using the mirror mount. Calibration of the interferometer was performed by moving the mirrors together until they touched and then winding the translation step back by a known distance. A correction factor of 14 μm was added to the mirror separation to take account of the thickness of the mirror coatings.

1.4 Summary

In this chapter, a brief history of the development of semiconductor lasers from simple *p-n* junctions to quantum well separate-buried-heterostructure lasers was presented. The origin of the third-order virtual refractive index nonlinearity was outlined, and the current state of all-optical switching of light at 1.55 μm using virtual nonlinearities was discussed. A brief discussion of all-optical switching via real-carrier transitions was followed by a summary of experimental investigations of the size and nature of the enhanced ultra-fast refractive index nonlinearity seen above the bandgap in optical amplifiers biased to transparency.

The principles of operation of the laser sources used in experiments described in this thesis was explained, and the various modes of operation in which they were used was discussed. The chapter ended with a summary of the main items of diagnostic equipment which were used for experiments described in later chapters.

The main body of this thesis describes an investigation of the above-bandgap ultra-fast nonlinearity in amplifiers biased to transparency. This nonlinearity is attractive because it is of a magnitude which could permit optical-switching of picosecond pulses produced using semiconductor diode lasers, and also offers the possibility of production and switching of optical pulses using monolithic devices.

References

[1] T. H. Maiman, Nature 187, 493 (1960)
(A. L. Schalow and C. H. Townes. Phys. Rev. 12, 1940 (1958))

[2] R. N. Hall, G. E. Fenner, J. D. Kingsley, T. J. Soltys and R. O. Carlson, Phys. Rev. Lett. 9, 366 (1962)

[3] M. I. Nathan, W. P. Dumke, G. Burns, F. H. Dills and G. Lasher, Appl. Phys. Lett. 1, 62 (1962)

[4] H. Kressel and H. Nelson, RCA Rev. 30, 106 (1969)

[5] I. Hayashi, M. B. Panish and P. W. Foy, IEEE J. Quantum Electron. QE-5, 211 (1969)

[6] Zh. I. Alferov, V. M. Andreev, E. L. Portoni and M. K. Trukan, Sov. Phys. Semicond. 3, 1107 (1970)

[7] I. Hayashi, M. B. Panish, P. W. Foy and S. Sumski, Appl. Phys. Lett. 17, 109 (1970)

[8] Zh. I. Alferov, V. M. Andreev, D. Z. Garbuzov, Yu. V. Zhilyaev, E. P. Morozov, E. L. Portnoi and V. G. Trofim, Sov. Phys. Semicond. 4, 1573 (1970)

[9] J. C. Dyment, Appl. Phys. Lett. 10, 84 (1967)

[10] J. E. Ripper, J. C. Dyment, L. A. D'Asaro and T. L. Paoli, Appl. Phys. Lett. 18, 155 (1971)

[11] H. Kressel and J. K. Butler, Semiconductor Lasers and Hterojunction LEDs. New York Academic Press, 1977

[12] P. S. Zory, Quantum Well Lasers, Academic Press Inc., 1993

[13] R. Dingle, W. Weigmann and C. Henry, Phys. Rev. Lett. 33, 827 (1974)

[14] R. C. Miller, R. Dingle, A. C. Gossard, R. A. Logan, W. A. Norland and W. Wiegmann J. Appl. Phys. 47, 4509 (1976)

[15] W. T. Tsang, Appl. Phys. Lett. 34, 473 (1979)

[16] W. T. Tsang, Appl. Phys. Lett. 39, 786 (1981)

[17] W. T. Tsang, Appl. Phys. Lett. 40, 217 (1982)

[18] J. J. Heish, J. A. Rossi and J. P. Donnelly, Appl. Phys. Lett. 28, 709 (1976)

[19] S. Akiba, K. Sakai, Y. Matsushima and T. Yamamato, Electron. Lett. 15, 606 (1979)

[20] G. D. Henshall and P. D. Greene, Electron Lett. 15, 621 (1979)

[21] I. P. Kaminow, R. E. Nahori, M. A. Pollack, L. W. Stulz and J. C. Dewinter, Electron. Lett. 15, 763 (1979)

[22] H. C. Casey Jr. and M. B. Panish, Heterostructure Lasers, Parts A and B. New York Academic Press (1978)

[23] D. A. O. Davies, M. A. Fisher, D. J. Elton, S. D. Perrin, M. J. Adams, G. T. Kennedy, R. S. Grant, P. D. Roberts and W. Sibbett, Electron. Lett. 29, 1710 (1993)

[24] K. Al-Hemyari, A. Villeneuve, J. U. Kang, J. S. Aitchison, C. N. Ironside and G. I. Stegeman, Appl. Phys. Lett. 63, 3562 (1993)

[25] K. Al-Hemyari, J. S. Aitchison, C. N. Ironside, G. T. Kennedy, R. S. Grant and W. Sibbett, Electron. Lett. 28, 1090 (1992)

[26] P. A. Snow, I. E. Day, I. H. White, R. V. Penty, H. K. Tsang, R. S. Grant, Z. Su, W. Sibbett, J. B. D. Soole, H. P. Leblanc, A. S. Gozdz, N. C. Andreadakis and C. Caneau, Electron. Lett. 28, 2346 (1992)

[27] G. I. Stegeman and P. Li Kam Wa, Nonlinear Optical Materials and Devices for Applications in Information Technology, Kluwer Academic Publishers (1995)

[28] J. U. Kang, G. I. Stegeman and J. S. Aitchison, Electron. Lett. 31, 118 (1995)

[29] A. Villeneuve, K. Al-Hemyari, J. U. Kang, C. N. Ironside, J. S. Aitchison and G. I. Stegeman, Electron. Lett. 29, 721 (1993)

[30] P. A. Li Kam Wa, J. E. Stich, N. J. Mason, J. S. Roberts and P. Robson, Electron. Lett. 21, 26 (1985)

[31] I. Gontijo, D. T. Neilson, J. E. Erlich, A. C. Walker, G. T. Kennedy and W. Sibbett, Paper CTuD4, Conference on Lasers and Electro-Optics, Baltimore (1995)

[32] R. S. Grant and W. Sibbett, Appl. Phys. Lett. 58, 1119 (1991)

[33] M. A. Fisher, H. Wickes, G. T. Kennedy, R. S. Grant and W. Sibbett, Electron Lett. 29, 1185 (1993)

[34] D. A. O. Davies, M. A. Fisher, D. J. Elton, C. P. Seltzer, M. J. Adams, G. T. Kennedy, P. D. Roberts, R. S. Grant and W. Sibbett Annual Meeting IEEE Lasers and Electro-Optics Society (LEOS) (1993)

[35] C. T. Hultgren and E. P. Ippen, Appl. Phys. Lett. 59, 635 (1991)

[36] C. T. Hultgren, D. J. Dougherty and E. P. Ippen, Appl. Phys. Lett. 61, 2767 (1992)

[37] R. Beigang, K. Klameth, B. Becker, Z. Yoon and H. Welling, Opt. Commun. 65, 383 (1988)

[38] L. F. Mollenauer and R. H. Stolen, Opt. Lett. 9, 13 (1984)

[39] G. T. Kennedy, Ph.D. Thesis (1993)

[40] P. N. Kean, X. Zhu, D. W. Crust, R. S. Grant, N. Langford and W. Sibbett, Opt. Lett. 14, 39 (1989)

[41] K. J. Blow and B. P. Nelson, Opt. Lett. 13, 1026 (1988)

[42] R. S. Grant and W. Sibbett, Opt. Commun. 86, 177 (1991)

[43] F. Ouellette and M. Piche, Opt. Commun. 60, 99 (1986)

Chapter 2

Measurement of Ultrafast Gain Dynamics

2.1 Introduction

As part of the evaluation of the potential applicability of forward-biased semiconductor optical amplfiers as ultrafast all-optical switches, it is desirable to obtain information on the nature and magnitude of the nonlinear absorption mechanisms which occur in the amplifiers. Pump-probe experiments utilising ultra-short pump and probe pulses allow these nonlinear absorption mechanisms to be isolated and measured in the time domain. In this chapter, results from pump-probe measurements of absorption-related nonlinearities in amplifiers operating at the transparency point are presented and discussed. Four amplifiers were used for these experiments. The structure of the active regions of each of the amplifiers was different in that both bulk and multiple quantum well devices (MQW) were investigated. One amplifier contained a bulk active region, and three others had four quantum wells, eight quantum wells and sixteen quantum wells respectively. The relative magnitudes of the absorptive nonlinear effects in the amplifiers were measured.

The chapter begins with a description of the pump-probe technique. Previous work on the investigation of gain nonlinearities in optical amplifiers using this method is reviewed, and this is followed by a discussion of the type and size of the nonlinearities that have been observed. The results of measurements performed during the course of this project are presented and the relative magnitudes of the nonlinearities which have been resolved are determined by using a suitable fitting algorithm.

2.2 Background

2.2.1 Pump-Probe Measurements

Pump-probe experiments are a practical and accurate means of providing time-domain measurements of ultrafast dynamics in semiconductors. The principle of a pump-probe experiment is to induce nonlinear effects in a medium using a high intensity pump pulse, and then monitor the transmission characteristics of a low intensity probe pulse in the medium. The time delay between the low intensity probe pulse and the high intensity pump pulse is varied in a predetermined manner, and the corresponding changes in the transmission of the probe pulse are recorded.

In general, a beam of optical pulses is split into a high intensity pump beam and a low intensity probe beam. The probe beam travels a longer optical path than the pump beam before both are incident on a sample. Upon propagation through (or reflection from) a semiconductor, the pump pulse alters the gain and refractive index of the semiconductor, and the transmission of the probe pulse is affected accordingly. The probe pulse is separated from the pump pulse using a polarising beam-splitter or some other method of discrimination and its intensity is measured independently of the pump pulse. The transmission of the probe pulse is determined as a function of its delay relative to the pump pulse, thus giving information on both the size and temporal nature of gain nonlinearities in the semiconductor

Measuring the transmission of an amplifier as a function of the delay between pump and probe pulses allows measurements of ultrafast effects to be transformed into measurements of relative displacement. The resolution thus obtained is well in excess of the response time of ultrafast detectors. Typically, the position of the mirror determining the delay between the pump and probe can be determined to the order of one micron. This corresponds to a time resolution of ~3 fs, and the resolution of the pump-probe measurement is therefore limited only by the duration of the detected pump and probe pulses.

Pump-probe investigations of optical amplifiers described in the literature have tended to be influenced directly by the availability of ultrashort pulse sources in particular spectral bands, in parallel with the development of optical amplifiers operating at those wavelengths. Research in the late 1980's involved dye lasers, used

in the near infra-red to investigate gain dynamics in AlGaAs amplifiers biased close to the transparency point[1]. It was observed that the propagation of high intensity pump pulses through the AlGaAs amplifiers heated the distribution of carriers in the amplifiers via the creation of hot carriers, or by the removal of cool carriers through stimulated emission. The heated carrier distribution returned to the temperature of the semiconductor lattice through the emission of optical phonons with a time constant of 0.9 ps.

With the development of techniques to reduce the duration of pulses generated by dye lasers, the increased temporal resolution of gain dynamics in AlGaAs optical amplifiers revealed evidence of a second nonlinearity with a recovery time of between 150 and 300 fs[2,3].

The development of InGaAsP amplifiers with bandgap transitions around 1.5μm, combined with the availability of coupled-cavity mode-locked KCl:Tl^0(1) lasers, opened up the possibility of pump-probe investigations of gain dynamics in a new material[4,5]. Experiments with pump and probe pulses of around 150 fs duration revealed gain dynamics that were more complex than those seen in AlGaAs. Carrier heating was still an important mechanism in amplifiers operating at gain, but amplifiers biased to transparency or loss also exhibited a positive transient with a recovery time of ~ 200 fs. Mark and Mork[6,7], and Hall *et al.*[8] have concluded that this transient is a result of spectral hole burning in combination with a delay in the heating of the carrier distribution.

2.2.2 Four-Wave Mixing Experiments

In parallel with pump-probe investgations of gain dynamics in optical amplifiers, experiments using four-wave mixing have given complementary evidence of the nature and recovery times of nonlinearities present in InGaAsP amplifiers. Four-wave-mixing experiments do not require ultra-short laser pulse sources to resolve ultrafast transients. This is because the measurement of time dynamics is transformed into a measurement of frequency response. A number of groups have investigated nonlinear effects in InGaAsP amplifiers using four-wave-mixing experiments[9-12]. The results of these experiments initially appeared to be contradictory, with different groups finding very different relative magnitudes of carrier heating and spectral hole

burning. This apparent contradiction has subsequently been shown to be a consequence of the level of forward bias current applied to the amplifier[13]. A high bias current (>200mA) will fill the bottom of the conduction band, reducing the effect on the gain of raising the carrier temperature, and allowing spectral hole burning to dominate the response of the amplifier. In contrast, for a bias current of the order of 10 mA, at wavelengths close to the transparency point, heating of the carrier distribution is the primary effect which dominates spectral hole burning. Time constants measured in amplifiers operating in this regime agree well with results acquired through pump-probe experiments.

2.2.3 Gain/Loss Saturation in InGaAsP Amplifiers

The passage of a high intensity pump pulse through an optical amplifier will alter the gain or absorption experienced by a subsequent probe pulse. Even if the intensity of the pump pulse is not great enough to induce any nonlinear mechanisms in the amplifier, the pump pulse will still influence the transmission of the probe by modifying the carrier density distribution in the amplifier. If the amplifier is biased to absorb incident light then the pump pulse will create electron-hole pairs thereby increasing the carrier density and reducing the loss experienced by the probe pulse. If the amplifier is biased to gain then the passage of the pump pulse will reduce the carrier density, and gain experienced by the probe pulse will be reduced. The deviation of the carrier density away from its equilibrium state will recover with a time constant determined by the rate of recombination (for carrier densities above the equilibrium), or by the supply of carriers from the current source (for carrier densities below the equilibrium).

The recovery of the carrier density to its equilibrium level in an InGaAsP optical amplifier is dependent on the doping of the amplifier, but is typically of the order of a few hundreds of ps, for forward bias currents of a few tens of milliamps[14]. The pump-probe experiments described in this chapter were performed with a maximum time delay between the pump and probe pulses of around 7 ps. On this timescale, changes in the carrier density were apparent as steps in the transmission of the probe pulse at zero time (ie. where the pump and probe pulses overlap).

If an optical amplifier is biased such that the number of stimulated emissions and absorptions caused by the propagation of a pump pulse is the same, then there will be no net change in the density of carriers in the amplifier. The amplifier is referred to as being biased to transparency. When this is the case, the transmission of a probe pulse will be not be modified by changes of the carrier density. When performing pump-probe measurements, the absence of a step up (reduced loss) or a step down (reduced gain) in the transmission of a probe pulse indicates that the amplifier is biased to transparency.

2.2.4 Ultrafast Nonlinear Gain in InGaAsP Amplifiers

When the intensity of a pump pulse propagating through an optical amplifier is sufficiently high, the transmission of the corresponding probe pulse will be modified by additional nonlinearities in that amplifier. The strongest nonlinearity in InGaAsP optical amplifiers biased at and around transparency is carrier heating[13], which may be caused by any one of three different mechanisms.

The first mechanism by which the carrier distribution may be heated is free carrier absorption. This is the process by which an electron in the conduction band (or a hole in the valence band) absorbs a photon, and is excited to a state with excess energy. Once excited to this high energy state the carrier thermalises with the carrier distribution via carrier-carrier scattering (with an associated time constant of 100 - 200 fs[8]), raising the temperature of the carrier distribution. In order that the carrier may be excited to the high energy state, a simultaneous interaction with a phonon is necessary. This is to transfer the momentum required as a consequence of the structure of the conduction (or valence) band. It is because of this requirement that a carrier undergoes a simultaneous interaction with photon and a phonon of the correct momentum that free-carrier absorption only becomes an important carrier heating mechanism for high intensitiy incident light. The free-carrier absorption coefficient in a bulk InGaAsP amplifiers has been measured to be approximately 19 cm^{-1}.[6] Although the free-carrier absorption coefficient is dependent on the doping of the active region of the amplifier, it is believed that the amplifier which was used to obtain this

measurement was of the same construction as those which were used for the experiments described in this thesis.

Two-photon absorption is the second mechanism through which a carrier distribution may be heated. Two-photon absorption refers to the mechanism by which two-photons are absorbed simultaneously by a carrier in the valence band, causing an interband transition. If the two-photons are of equal energy (as is the case in the pump-probe experiments described later in this chapter) the final excited state of the carrier is identical to that which would have resulted from the absorption of a single photon of twice the energy. The mechanism by which two-photon absorption occurs may be described in terms of the Heisenberg Uncertainty Principle. A first photon absorbed by a carrier excites that carrier to a state which can be said to exist only for a length of time determined by the Heisenberg uncertainty principle (*i.e.* a virtual state). If a second photon is absorbed by the carrier within that time, the carrier will be excited to a real final state. The transition rate due to two-photon absorption depends quadratically on the intensity of incident light. The effect of two-photon absorption is to excite carriers high up into the conduction and valence bands, thus strongly heating the carrier distribution.

The final mechanism whereby the temperature of a carrier distribution may be increased is through the creation of carriers with energies greater than the average carrier energy via stimulated transitions. Carriers created via stimulated absorption thermalise with the carrier distribution via carrier-carrier scattering, increasing the temperature of the distribution. The effectiveness of this mechanism is determined by the energy of the incident photon relative to the position of the quasi-Fermi-levels in the conduction band. If the energy of a created carrier is close to the quasi-Fermi-energy then it will have a marginal effect on the temperature of the carrier distribution. If however, the created carrier is of considerably greater energy than the quasi-Fermi-level, its effect on the temperature of the carrier distribution will be correspondingly more pronounced. The carrier distribution may also be heated by the stimulated recombination of carriers with energies below the quasi-Fermi-level. Similarly, removing 'hot' carriers or adding 'cool' ones will lower the temperature of the carrier distribution.

Heating electrons in a conduction band broadens the Fermi distribution of the electrons in that band, and reduces the occupancy of states towards the bottom of the band (the regime that is investigated in this chapter using pump-probe measurements). Thus, there are less occupied states available to interact with a probe pulse and its transmission is reduced. Carrier heating will thus lead to a reduction in the transmission of a probe pulse regardless of whether the amplifier is operating at gain or loss. The temperature of the heated carrier distribution returns to the lattice temperature within a time determined by the carrier-phonon scattering time. In InGaAsP the carrier-phonon scattering time is around 160 fs,[15] and the reported recovery time of the carrier temperature in amplifiers biased close to transparency is 0.65 - 1 ps[6,16].

A further nonlinear mechanism present in InGaAsP amplifiers is spectral hole burning. A pump pulse propagating through an amplifier operating in gain will deplete carriers at the wavelength of the pump pulse. A dip is thus created in the gain spectrum, and a probe pulse of the same wavelength will experience a reduced gain. The dip in the carrier distribution will disappear as the carriers thermalise via carrier-carrier scattering within 100 - 200 fs. Spectral hole burning will increase the transmission of a probe pulse propagating through an amplifier which is operating in loss and decrease the transmission of a probe pulse in an amplifier operating in gain. This is distinct from the effect of carrier heating, where the probe transmission is reduced regardless of bias.

2.3 Pump-Probe Experiment

2.3.1 Experimental Configuration

The pump-probe experiment was configured as illustrated in Figure 1.

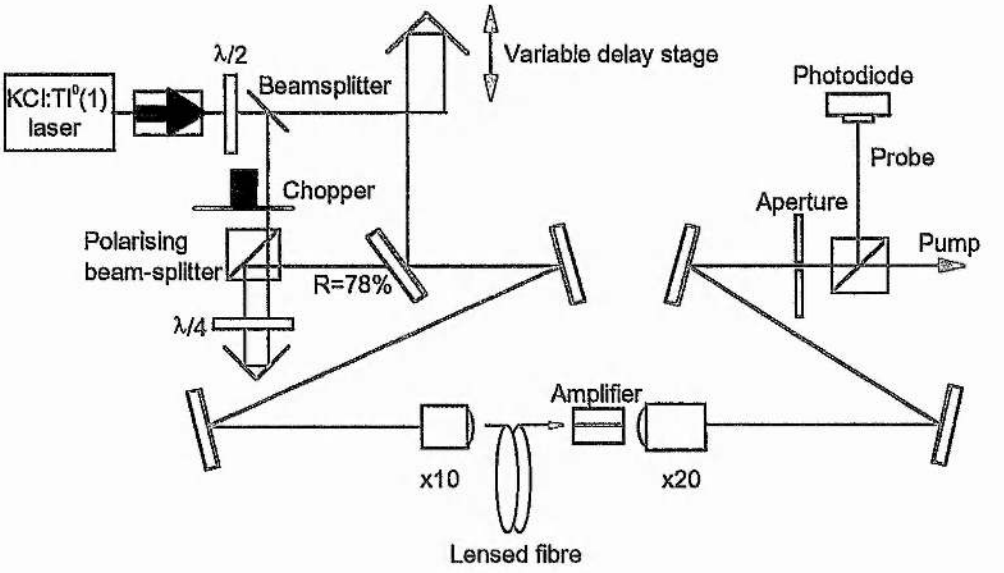

Figure 1. Schematic configuration of pump-probe experiment

A KCl:Tl^0(1) laser was coupled-cavity mode-locked to produce pulses of 100 fs duration at a wavelength of 1525 nm. The beam from the laser was passed through a Faraday isolator to prevent feedback from the experiment interfering with the mode-locking. The polarisation of the beam transmitted by the isolator was rotated to be transverse electric (TE), ie. with the E-field in the plane of the optical bench (and the plane of the amplifier junction), using a half-wave plate before being split into two beams by a 50% beam-splitter.

Light transmitted by the beam-splitter was selected as the pump beam, and was directed onto a retro-reflector mounted on a delay stage. The position of the delay stage was actuated in micron steps by a computer-controlled stepper motor. The pump beam was adjusted until it was incident normally on the retro-reflector. This was to ensure that movement of the retro-reflector by the stepper-motor would not change the alignment of the pump beam, which misalignment would have reduced the

efficiency of the coupling of the pump beam to the lensed fibre, and consequently reduced the intensity of the pump beam coupled to the amplifier.

The portion of the beam reflected by the beam-splitter was used as the probe beam. It was passed through a polarising beam splitter, was rotated to be circularly polarised using a quarter-wave plate, reflected back through the quarter-wave plate (the polarisation of the probe beam was now transverse magnetic (TM), ie. with its electric field perpendicular to the plane of the optical bench) and reflected by the polarising beam splitter. This circuitous method of producing TM polarised light was used because the expermient was a section of the partially constructed Time Division Interferometer which will be described in Chapter 3.

The pump and probe beams were recombined by passing the probe through the back of a 78% reflecting mirror and reflecting the pump from the surface of the mirror. The ratio of the intensities of the recombined pump and probe beams was ~ 20:1. Care was taken to 'walk' the pump and probe beams so that they were as close as possible to being collinear. This was to avoid discrepancies between the coupling efficiency of each of the beams to the lensed fibre. The intensity of the probe pulse was further controlled using a neutral-density attenuator wheel (not shown).

The pump and probe beams were coupled into the amplifier to be investigated using a lensed fibre. The fibre was cleaved to be the shortest length possible (20 cm) in order to avoid any distortion of the pulse through self-phase modulation and group-velocity dispersion. Autocorrelations and spectra of the transmission by the fibre of high intensity pulses were recorded to confirm that no such distortion was present. Light coupled into the amplifier was collected at the output facet using a x20 microscope objective, and focussed through an aperture placed at a distance of 1 m to prevent the detection of unguided light. The probe beam was separated from the pump by employing a polarising beam splitter which reflected the probe and transmitted the pump. The intensity of the transmitted probe beam was measured using a germanium photodiode.

The high intensity of the pump beam relative to the probe beam, and the limited discrimination by the polarising beam-splitter between TE and TM light combined to impose excessive amounts of noise on initial experimental traces obtained from the pump-probe setup. The noise was due to interference between the pump and probe

pulses. This noise was helpful in determining the position of the zero delay between the pump and probe pulse, but obscured the gain dynamics present close to the zero delay point. Discrimination of the probe from the pump was improved by chopping the probe beam and using a lock-in detection system.

A computer program was used to control the position of the delay stage. Each increment of the delay stage was followed by a preset pause (usually 1 second) after which a measurement of the probe intensity was taken from the lock-in detector. Measurements taken in this manner were plotted on the computer's monitor as they were being taken to allow continuous monitoring of the results.

2.3.2Preliminary Results

Pump-probe transmission measurements were performed on an amplifier containing eight InGaAs wells of 8 nm thickness separated by 10nm thick InGaAsP barriers. The average power of the TE polarised pump beam incident on the x10 coupling objective was measured to be 8 mW, corresponding to a coupled peak power of 100 W in the amplifier (the pump pulses were 100 fs duration). The TM polarised probe beam had an average power of 0.3 mW at the x10 objective, corresponding to 3.7 W peak power in the amplifier. The ratio of pump intensity to probe intensity was thus ~ 20:1.

With the power and pulse durations of the pump and probe beams set at the values given above, a number of pump-probe transmission measurements were performed. Each measurement was taken with the forward bias to the amplifier set at a different level. Because the computer screen displayed the results in real-time, it was possible to set the gain (or loss) of the amplifier at a required level, by making adjustments to the bias and monitoring the effect on the transmission of the probe pulses. Figure 2 shows pump-probe transmission plots for the 8 quantum well (QW) amplifier operating at gain, loss and transparency.

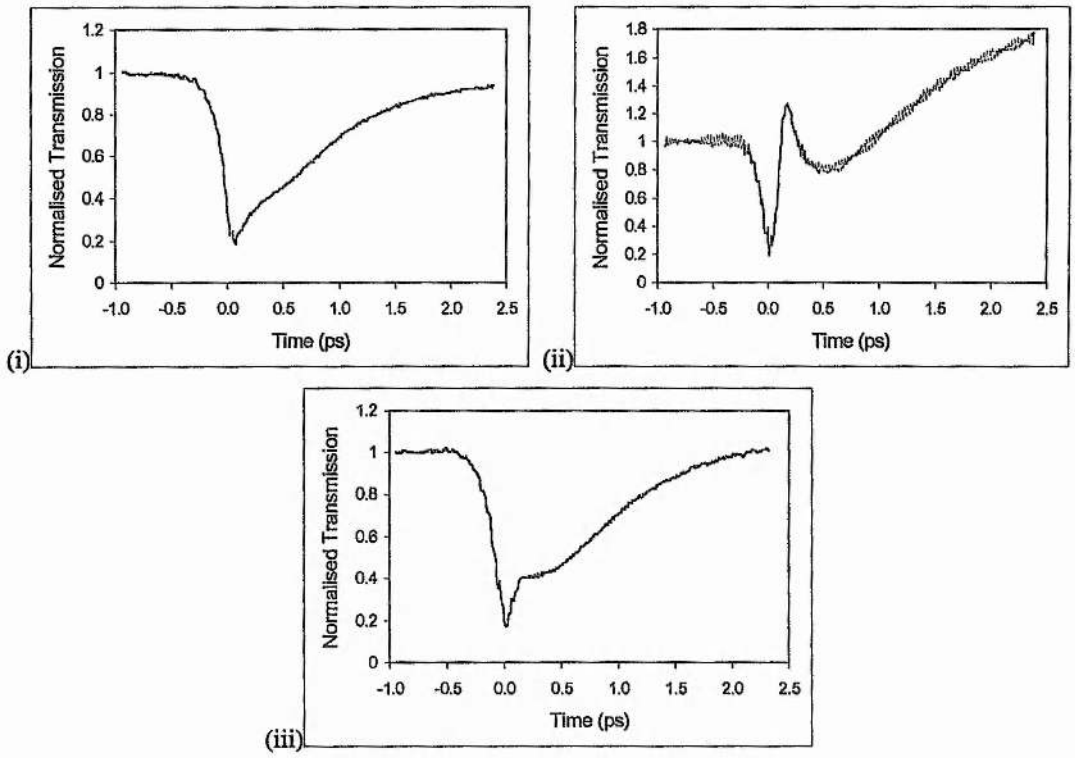

Figure 2. Transmission curves for an 8 QW amplifier operating at gain (i), loss (ii), and transparency (iii).

In all of the plots presented in Figure 2, zero time corresponds to the position of the delay stage where the pump and probe pulses were exactly overlapped. The zero point was determined by observing the autocorrelation of the pump pulse, and adjusting the position of the delay stage until the interference between the pump and probe pulses reached a maximum (a half-wave plate was used to rotate the two beams so that they had TE components of roughly equal magnitude).

The displacement of the delay stage between measurements was set to be 15 fs (5 microns), small enough to record all of the dynamics resolved by the 100 fs pulses.

Each of the plots in Figure 2 has been normalised by dividing the transmission of the probe pulses by the mean of the first twenty data points (ie. points measured when the probe pulse preceeded the pump pulse through the amplifier). The forward bias currents to the amplifier for the results shown were 40 mA, 5 mA and 20 mA for plots (i), (ii) and (iii) respectively.

There are a number of features present in plot (i) which illustrate the effects described in sections 2.2.3 and 2.2.4 of this chapter. The transmission of the probe

pulse can be seen to have recovered to a nearly constant level within 2.5 ps after the arrival of the pump pulse. This recovery is to a level below the initial transmission. This reduction in transmission occured because the pump pulse depleted carriers from the conduction band and reduced the gain experienced by the probe pulse. Full recovery of the gain back to its original value via the injection of new carriers (from the forward bias to the amplifier) occurs within a few hundred picoseconds, too long to be observed by the experiment but short enough to allow complete recovery of the carrier density before the arrival of the next pump pulse.

The carrier distribution was heated by the pump pulse via free carrier absorption (described in section 4.2.4). The probe pulse experienced a reduced gain as a result of the increased carrier temperature. The increasing transmission in plot (i) from a minimum at zero time to the almost constant level seen at 2.5 ps corresponds to cooling of the heated carrier distribution via the emission of longitudinal optical phonons.

Part of the initial downward transient seen in plot (i) is caused by two-photon absorption (describe in section 2.2.4). It has been observed by Mark and Mork[6] that this is a combination of the absorption of one photon from the pump pulse and one from the probe pulse. The two-photon absorption transient thus follows the profile of the pump pulse.

Plot (ii) of Figure 2 shows a result for the 8 QW amplifier operating in the absorption regime. The maximum recorded delay between the pump and probe pulses was not sufficient to show the transmission of the amplifier recovering to a step-like state. However, the transmission can be seen to be increasing above its initial value as a consequence of the pump pulse causing an increase of the carrier density. A positive transient is clearly apparent at ~ 0.2 ps after zero time. Hall *et al*[8] have shown that this dynamic is the result of a combination of spectral hole burning, and a delay in the turn-on of carrier heating caused by the finite thermalisation time (from carrier-carrier scattering) of the distribution. Again, the negative transient associated with two-photon absorption is apparent. The high frequency modulation seen on the trace was due to background noise such as room lighting being detected by the lock-in detector (the intensity of the probe was extremely low, having been attenuated by the amplifier).

Plot (iii) of Figure 2 shows the 8 QW amplifier operating at transparency. No step like change in transmission is seen in this regime, in contrast to the transmission curves recorded in plots (i) and (ii). This is because the pump pulse causes equal numbers of stimulated absorptions and emissions on propagation through the amplifier, and does not alter the carrier density distribution. One method of determining the transparency current in an amplifier (others are described elsewhere in this thesis) is to perform pump-probe measurements of the transmission, altering the bias current for each measurement until the transmission of the probe pulse before and after the pump pulse is the same. The other transients observed in plots (i) and (ii) due to cooling of the heated carrier distribution and two-photon absorption are also seen in plot (iii).

2.4 Investigation of transmission of a range of amplifiers

2.4.1 Preliminary results and qualitative analysis

It was an object of this project to investigate and compare the properties of a bulk InGaAsP amplifier and equivalent InGaAsP amplifiers with different numbers of quantum wells to try to elucidate more information about the complex nonlinear behaviour of froward biased InGaAsP amplifiers. Accordingly, pump-probe experiments were performed on amplifiers whose active regions contained 1, 8, and 16 quantum wells (QW), and on a further amplifier having a bulk active region. The amplifier containing a single quantum well was of similar construction to the 8 QW amplifier described above (with the obvious difference in the number of quantum wells). The bulk amplifier had an active region 200 nm thick. The 16 QW amplifier contained InGaAs wells 6.5 nm thick separated by InGaAsP barriers 8 nm thick. All of the amplifiers were of the buried heterostructure design.

The structure of the 8 QW amplifier is illustrated in Figure 3. Since the InGaAsP layers on either side of the set of quantum wells were only 20 nm thick, a substantial fraction of the mode was not confined to the active region but extended into the doped InP region. The thickness of the InGaAsP layers on either side of the sets of wells in the 1 and 4 QW devices was scaled to maintain a combined undoped layer of constant thickness (~180 nm). The undoped layer in the 16 QW amplifier was

268 nm thick and in the bulk amplifier was 200 nm. The variation of overlap of the mode into the doped regions of the amplifiers will introduce an error into the comparison of the carrier heating terms described later in this chapter.

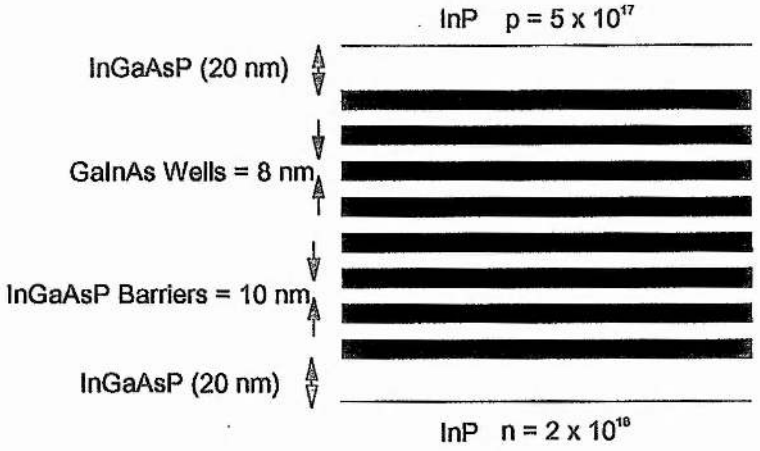

Figure 3. Structure of the 8 QW amplifier

The doping levels shown in Figure 3 are estimations given by BT labs.

Pump-probe transmission results obtained using the bulk amplifier, and the amplifiers containing 1,8 and 16 quantum wells are shown in Figure 3.

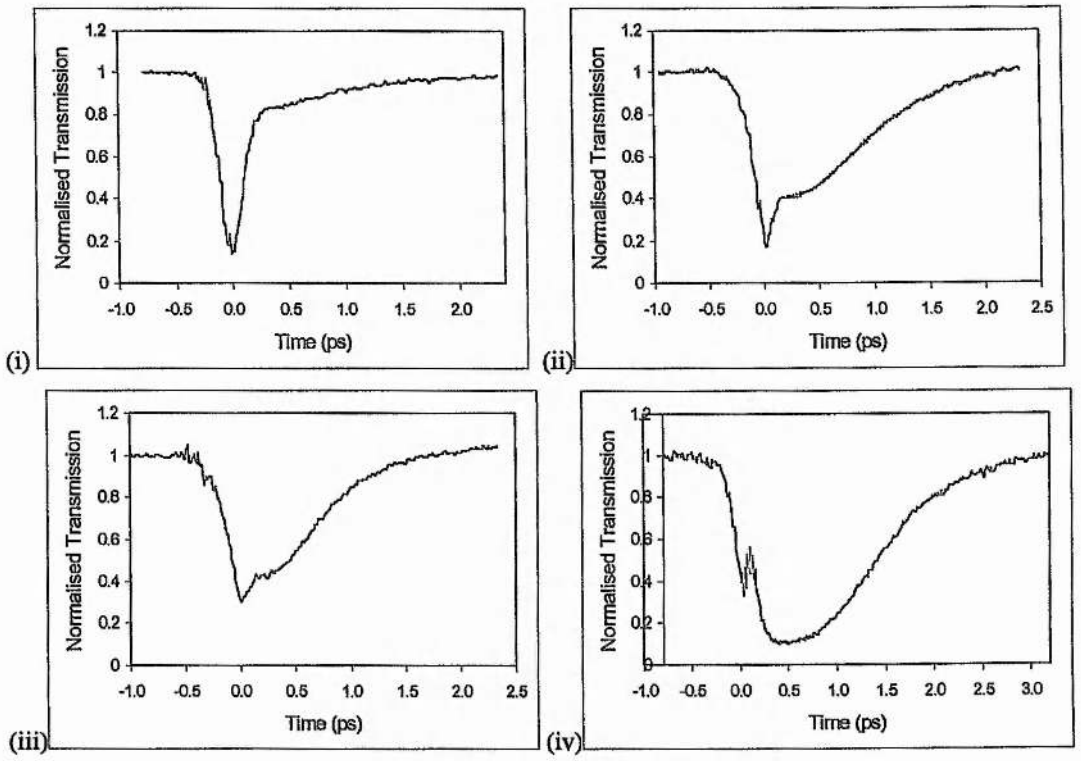

Figure 4. Pump-probe transmission curves for amplifiers with active regions comprising 1quantum well (i), 8 quantum wells (ii), 16 quantum wells (iii) and a bulk region (iv).

Although measurements were performed on each of the amplifiers for a number of different bias currents, the results obtained when the amplifiers were operating at transparency are displayed here only for ease of comparison. All of the results displayed in Figure 4 were obtained with pump and probe pulses of 100 fs duration. The intensity of the pump beam incident at the input facet of the amplifiers was set at 240W peak power (equivalent to 2.1 mW average power, 26 pJ per pulse) for all of the measurements performed.

The curve in plot (i) shows the transmission of an amplifier containing an active region consisting of a single quantum well. The bias current required to reach transparency in the single quantum well amplifier was low (5 mA) because the volume of the active region was small. The confinement factor for the mode in the amplifier was 0.011, the majority of the mode propagating through the cladding layers of the amplifier. The plot is a combination of a dip at zero time and an exponential recovery of transmission. The pronounced dip at zero time was caused by two-photon absorption, the majority of which occured in the cladding layers of the amplifier. The carrier distribution experienced a limited amount of carrier heating, reflecting the very small confinement of the mode in the active layer. This is seen in plot (i) as a shallow recovery of the transmission. The 'heel' at the transition from the two-photon absorption dip to the carrier heating recovery curve corresponds to the delay in carrier heating which is seen as a peak in the other plots of Figure 4.

The transmission curves in plot (ii) and plot (iii) of Figure 4 showing the transmission of the 8 QW and 16 QW amplifiers are very similar. The components seen on these traces are as described for the 8 QW amplifier in relation to Figure 2(iii).

Plot (iv) shows the transmission of the bulk amplifier. There are two main differences between this plot and those obtained from the 8 and 16 QW amplifiers. Firstly, the peak associated with the delayed turn on of the carrier heating is situated on the downward slope of the trace rather than on the upward slope. Secondly, the decrease in transmission of the probe caused by carrier heating is much greater in this plot than in the other plots shown in Figure 4.

These two apparently separate departures from the effects seen in the quantum well amplifiers are both caused by the same effect. The difference in the position of the peak corresponding to the delay of carrier heating is a result of a change in the relative

magnitudes of the effects of carrier heating and two-photon absorption, and not a consequence of differences in the recovery times of the contributing nonlinear effects. In the amplfiers containing active regions containing quantum wells, the confinement of the mode in the active region is relatively low. The effect of two-photon absorption (which occurs in the cladding and the active region) thus dominates over the effect of carrier heating (which occurs primarily in the active region). This means that, following the initial downward transient caused by two-photon absorption, the trend of the transmission curve is upwards. In contrast, the effect of carrier heating in the bulk amplifier is clearly greater than the effect of two-photon absorption, as a consequence of the increased confinement of the mode in the active region. Therefore, the transmission of the bulk amplifier will undergo a further downward trend after the transient due to two-photon absorption has begun to recover.

The effect on the transmission of an amplifier obtained by varying the relative magnitudes of the two-photon absorption and carrier heating contributions is illustrated in Figure 4. The transmission curves shown in Figure 5 were obtained from a model which is fully described in the following section of this chapter.

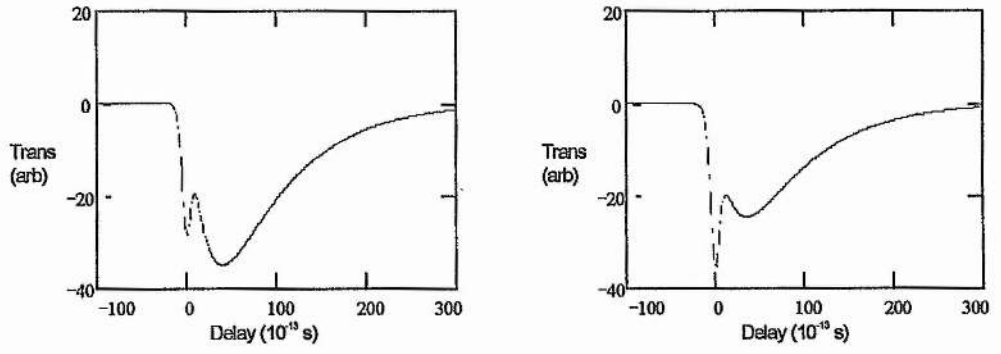

Figure 5. Transmission curves obtained using a response function model. The coefficient representing carrier heating is twice as great in the left hand trace than in the right hand trace.

The two plots shown in Figure 4 were derived with identical time constants and magnitudes for each of the nonlinear effects used in the model, except for the magnitude of the coefficients representing carrier heating. The carrier heating term used for the right hand trace in Figure 4 was twice that used for the left hand trace.

2.4.2 Quantative Analysis of pump-probe transmission results

To make quantitative comparisons of the various absorptive nonlinearities apparent in the transmission characteristics of the four amplifiers, a curve-fitting method that separated transmission changes with different time constants was used. This method was based upon that described by Hall *et al*[16] and Hultgren *et al*[17] of MIT. The method used by these workers involved creating an impulse response function for a semiconductor that contained a term for each of the absorptive effects discussed above. The response function was correlated with a function representing the autocorrelation of a pulse to provide simulations of transmission curves obtained through pump-probe experiments. The time constants for the nonlinear effects were taken from the litereature, and the magnitudes of each of the effects varied until the closest fit to the experimental data was found. The fitting program used for the results in this thesis did not have a facility for correlating functions. Consequently, an alternative function which explicitly included an approximation for the effect of the correlation was formulated as described below. The approximation was based upon the assumption that pulses propagating through the amplifier were $sech^2$ pulses.

The response function used to represent the effect of a high intensity pulse propagating through an optical amplifier is constructed from four separate functions. The first of these is a step function representing the change in transmission caused by a reduction or increase of the carrier density. Although the results shown in Figure 3 were ostensibly obtained with amplifiers that were biased to transparency, in practice it proved difficult to adjust the bias accurately enough to completely eliminate changes in the carrier density distribution. The correlation of a step function and a pulse autocorrelation can be represented by:

$$T(\tau) := \int_{-\infty}^{\infty} a_0 \cdot \Phi(\tau - t) \cdot G(t)^{(2)}\, dt \qquad (1)$$

where Φ is the Heaviside function, $G(t)^{(2)}$ is the autocorrelation of the pulse, and a_0 is the magnitude of the step. This equation is the transmission $T(\tau)$of the probe pulse by the amplifier. The Heaviside function describes the change of transmission of the amplifier which would occur if an impulse of light (*i.e.* a delta function) were to

propagate through it. In other words, the Heaviside function is the 'impulse response' of the amplifier. The effect of a pump pulse propagating through the amplifier is described by the correlation of the pump pulse G(t) with the amplifier's impulse response. To find the effect of this pump-induced change of the transmission of the amplifier on a probe pulse, the expression must be correlated with the shape of the probe pulse. Hence, the transmission of the probe pulse is described by an impulse response correlated with a pump and a probe pulse (represented here as the autocorrelation of the pulse)

In the fitting model used for this thesis, the transmission of the probe pulse from the correlation of the step and pulse autocorrelation are approximated by:

$$R(t) := s\cdot\left[\frac{\sinh\left(\frac{t}{a}\right)}{\cosh\left(\frac{t}{a}\right)\cdot\left(\frac{1}{a}\right)} + a\right] \qquad (2)$$

Where 'a' is the pulse duration measured for a $\text{sech}^2(t/a)$ pulse, and 's' is the amplitude of the step. The first part of the expression in parenthesis is the integral of a $\text{sech}^2(t/a)$ pulse. The duration of the pulse 'a' was divided by a constant to correct for the fact that the expression was the integral of a pulse and not the integral of the autocorrelation of that pulse. The additional 'a' in the parenthisis was inserted to make the function greater than or equal to zero for all values of τ.

Functions derived using equations (1) and (2) are compared in Figure 6

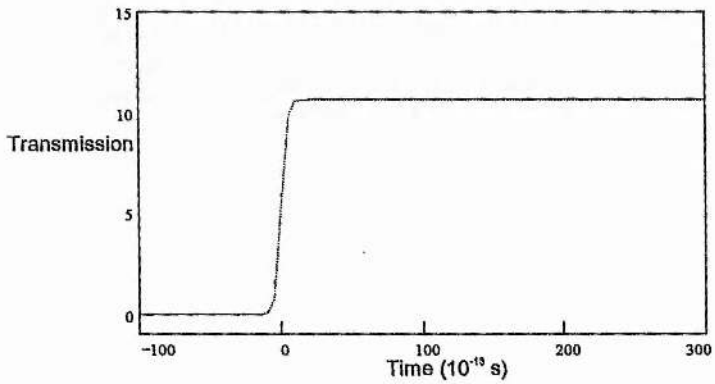

Figure 6. Comparison of a function obtained from the correlation of a pulse autocorrelation with a Heaviside function (solid line), with an approximation function (dashed line)

The program used to generate the curves shown in Figure 5 would not perform correlations with non-integer numbers, or with numbers greater than 1000. Accordingly, the correlation was determined with time calibrated in tens of femtoseconds. The vertical scale of the graph of Figure 5 is marked in arbitary units. As Figure 5 demonstrates, the approximation function closely follows the correlated function.

The second part of the response function represents the decrease in transmission caused by two-photon absorption. Two-photon absorption adiabatically follows the pump pulse profile, and the term required to represent this is simply a correlation of a delta function with the autocorrelation of the pulse profile:

$$T(\tau) := \int_{-\infty}^{\infty} a_3 \cdot \delta(\tau - t) \cdot G(t)^{(2)}\, dt \qquad (3)$$

Where $\delta(\tau - t)$ is the delta function, and a_3 is the amplitude of the function. This is represented in the fitting program used for this thesis by a sech^2 pulse shape

$$R(t) := b \cdot \text{sech}\left(\frac{t}{a}\right)^2 \qquad (4)$$

where b is the intensity of the pulse. Plots derived using equations (3) and (4) are shown in Figure 7.

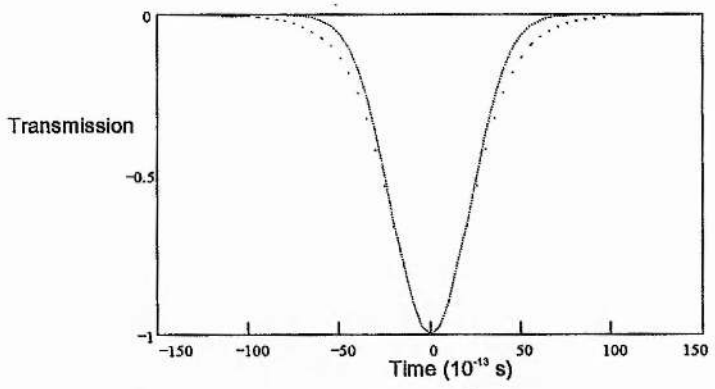

Figure 7. Comparison of a function obtained from the correlation of a pulse autocorrelation with a delta function (solid line), with an approximation function (dotted line)

The correlation function and approximation diverge slightly at their wings, but the effect of this divergence is minimal when the this function is combined with the other functions (see Figure 10 below)

The carrier heating term is an exponential function.

$$T(\tau) := \int_{-\infty}^{\infty} a_2 \cdot \exp\left[-\frac{(\tau - t)}{\tau_2}\right] \cdot G(t)^{(2)}\, dt \qquad (5)$$

where τ_2 is the time constant of the recovery of the heated carriers to the lattice temperature, and a_2 is the amplitude of the term. This expression was approximated in the fitting program used by multiplying the exponential term by the integrated $sech^2$ pulse shape to simulate correlation with the autocorrelation of a $sech^2$ pulse.

$$R(t) := \left[\frac{\sinh\left(\frac{t}{a}\right)}{\cosh\left(\frac{t}{a}\right)\cdot\left(\frac{1}{a}\right)} + a\right]\cdot\left[c\cdot\exp\left[-\left(\frac{t}{ch}\right)\right]\right] \qquad (6)$$

where ch is the time constant equivalent to τ_2 of the exponential and 'c' is the amplitude of the term.

Plots derived using equations (5) and (6), depicted in Figure 7, show that the two functions are in close agreement.

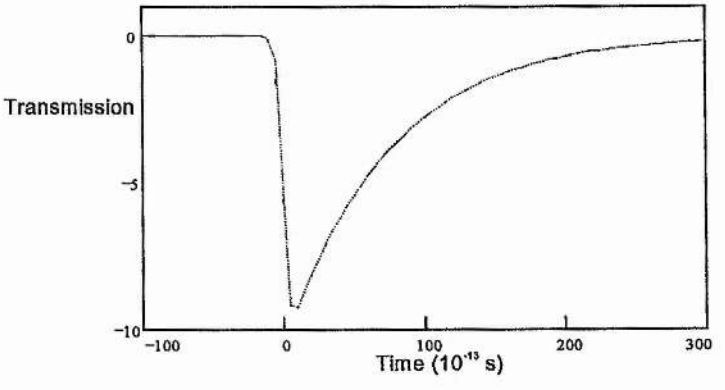

Figure 8. Comparison of a function obtained from the correlation of a pulse autocorrelation with an exponential function (solid line), with an approximation function (dotted line)

The fourth and final term of the response function is a second exponential that represents the delay in the turn on of carrier heating.

$$T(t) := \int_{-\infty}^{\infty} a_1 \cdot \exp\left[-\frac{(\tau - t)}{\tau 1}\right] \cdot G(t)^{(2)}\, dt \qquad (7)$$

This exponential is approximated in the same way as the exponential representing carrier heating.

$$R(t) := \left[\frac{\sinh\left(\frac{t}{a}\right)}{\cosh\left(\frac{t}{a}\right)\cdot\left(\frac{1}{a}\right)} + a \right] \cdot \left[d \cdot \exp\left[-\left(\frac{t}{dy}\right) \right] \right] \tag{8}$$

The function (7) representing the delay in carrier heating, and the approximation function (8) are plotted in Figure 9.

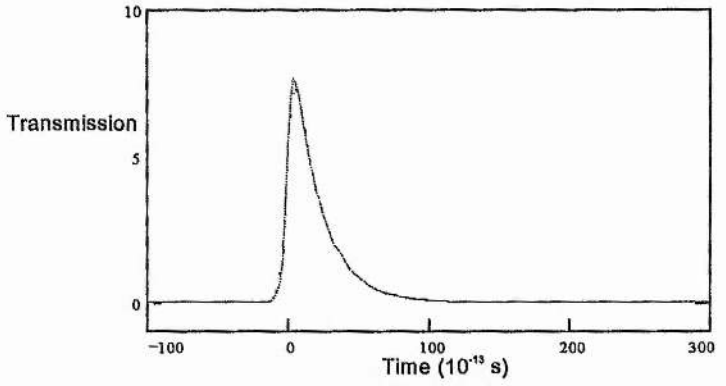

Figure 9. Comparison of a function obtained from the correlation of a pulse autocorrelation with an exponential function (solid line), with an approximation function (dotted line)

The four separate terms of the response function are combined to form an expression representing the experimentally measured change in the probe energy caused by the pump. The combined expression is:

$$T(\tau) := \int_{-\infty}^{\infty} \left[\Phi(\tau - t) \cdot \left[a_0 + a_1 \cdot \exp\left[-\frac{(\tau - t)}{\tau_1} \right] + a2 \cdot \exp\left[-\frac{(\tau - t)}{\tau_2} \right] \right] + a_3 \cdot \delta(\tau - t) \right] \cdot G(t)^{(2)}\, dt$$

In the expression, the exponential functions are multiplied by the Heaviside step function because the system is causal. The form of the combined expression approximating the above is:

$$R(t) := \left[\left[\frac{\sinh\left(\frac{t}{a}\right)}{\cosh\left(\frac{t}{a}\right)\cdot\left(\frac{1}{a}\right)} + a \right] \cdot \left[s + d \cdot \exp\left[-\left(\frac{t}{dy}\right) \right] + c \cdot \exp\left[-\left(\frac{t}{ch}\right) \right] \right] + b \cdot \operatorname{sech}\left(\frac{t}{a}\right)^2 \right]$$

In order to ascertain whether the approximate form of the response function was of adequate accuracy to obtain qualitative measurements, the functions r(t) and

$\Delta W(\tau)$ were plotted, with respective constants set at equivalent values, on a single set of axes.

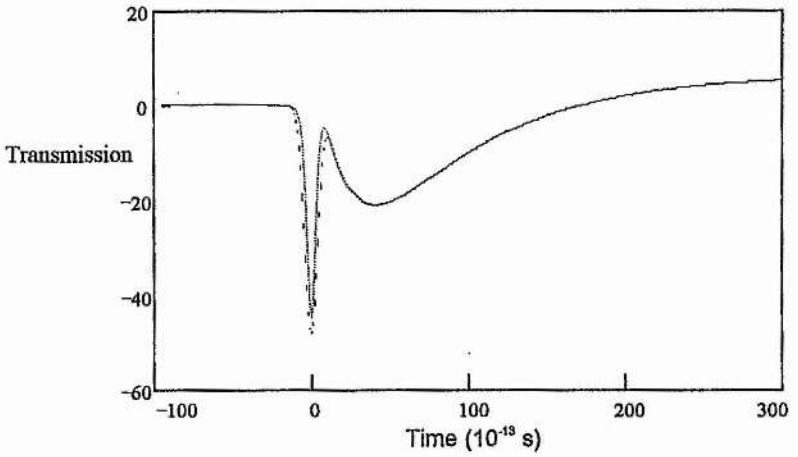

Figure 10. Comparison of a function obtained from the correlation of a pulse autocorrelation with a response function (solid line), with an approximation (dashed line)

It is clear from Figure 9 that the approximate form of the fitting function described above followed closely the form of the fitting function itself. The error incurred by using the approximate function was small in relation to the comparative differences between the transmission curves being compared.

2.4.2 Numerical analysis of pump-probe transmission results

The transmission curves, shown in Figure 4, obtained from the four amplifiers under investigation, were fitted with curves generated using the approximation function described above. The transmission curves are shown below in Figure 7 with the fitted curves plotted on common axes.

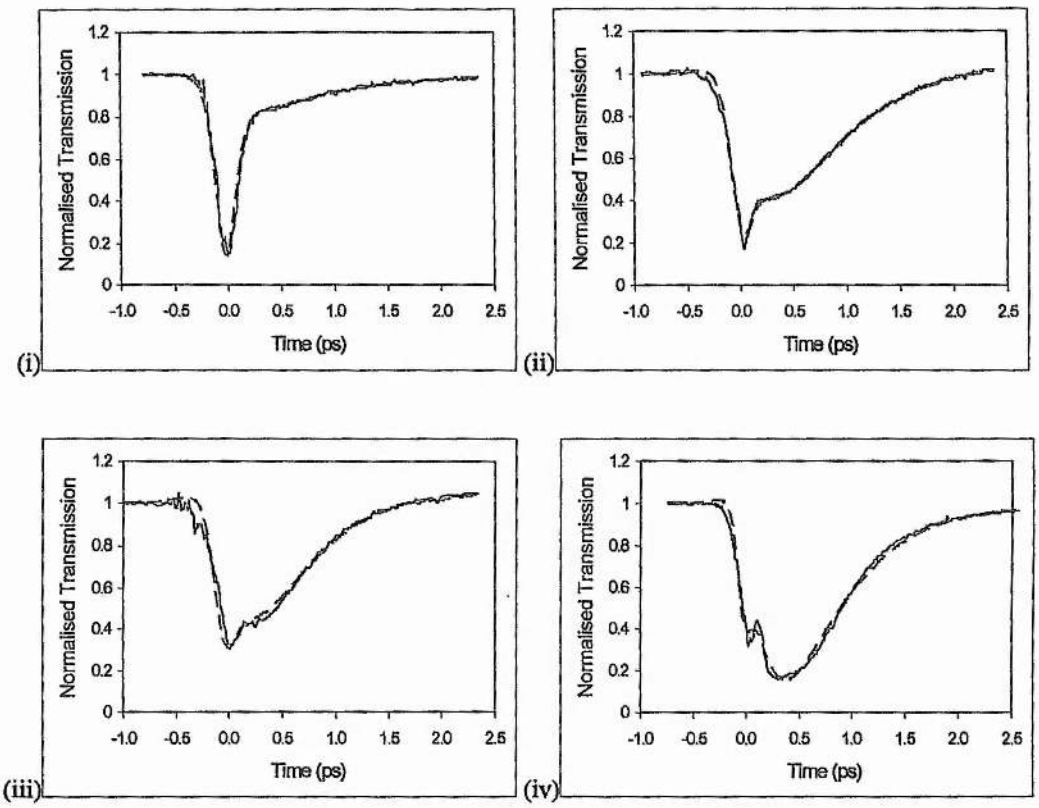

Figure 6. Pump-probe transmission curves for amplifiers with active regions containing 1quantum well (i), 8 quantum wells (ii), 16 quantum wells (iii) and a bulk region (iv). Theoretical curves generated to fit the experimental data are shown as dashed lines.

When fitting these curves, it became apparent that a number of experimental effects had acted in combination with the response function described in section 2.4.2. It was necessary to separate these experimental effects from the results in order to obtain the response functions of the amplifiers.

The resolution of the experimental pump-probe results did not correspond to that which would have been obtained from the correlation of a 100 fs pulse (the duration of the probe and pump pulses) with the response function. Rather, the resolution of the pump-probe traces observed corresponded to a pulse duration of 120 fs in the case of the bulk amplifier, and between 160 and 170 fs in the case of the multiple quantum well amplifiers.

The loss of resolution in the results obtained from the bulk amplifier was due to broadening of the pulses via group velocity dispersion. The effects of group velocity dispersion can be expressed in terms of a critical pulse duration as:

$$T_t := T_i \cdot \left[1 + \left(\frac{T_c}{T_i} \right) \right]^{\frac{1}{2}}$$

where T_i is the duration of the incident pulse, T_t the duration of the transmitted pulse, and T_c the critical pulse duration, ie. the pulse duration for which the output is broadened by a factor of $\sqrt{2}$. The critical pulse duration measured for the bulk amplifier was 72 fs, a value that corresponds with those obtained by previous workers[18,19].

The corresponding critical pulse durations obtained for the multiple quantum well amplifiers were of the order of 120 fs. This value is well in excess of previously observed dispersion in InGaAsP amplifiers refered to in the literature[19]. The additional loss in resolution was therefore postulated as being a result of the pump and probe pulses 'walking off' from each other on propagation through the amplifiers. This was a consequence of the different effective refractive indeces for TE polarised light and TM polarised light in the quantum well amplifiers (the pump was TE polarised, and the probe was TM polarised).

The discrepancy between the resolution of the results obtained from the bulk amplifier and the multiple quantum well amplifiers was normalised by fitting the data with response functions representing different pulse durations.

A second experimental effect introduced an element of uncertainty into the values of the terms obtained from the curve fitting procedure. This was the position of the point of overlap between the pump and probe pulses (zero time on the traces in Figure 6). As previously mentioned, this was determined experimentally by observing the correlation of the pump and probe pulses and estimating the point where the interference between them was at a maximum. However, there was an appreciable degree of uncertainty in this measurement. A variable offset was introduced into the response function so that a 'best fit' with variable offset could be obtained. In all cases, the resulting offset was less than 20 fs, and the corresponding changes to the other fitting terms were less than 10%.

The pump-probe transmission curves being investigated in this section of the chapter were all obtained using amplifiers that were biased to transparency. The transparency current was determined by comparing the intensity of the pulse probe detected before and after the transmission of the pump pulse. However, the resolution

of the screen that was used to monitor the transmission of the probe pulse was such that the accuracy of this determination of the transparency current was limited, and a step component corresponding to a change in the density of carriers in the amplifier is present in each trace. Consequently, the step-like Heaviside function used to fit carrier density changes was not set at zero, but was allowed to vary. By doing this, the step like part of the transmission curves was separated from the rest of the transmission data and did not influence the other fitting parameters.

2.4.3 Fitting Parameters

The parameters obtained for the terms in the approximation function when the function was fitted to the curves as shown in Figure 6 are presented below in Table 1.

	1 QW	8QW	16QW	Bulk
carrier heating term	-1.6	-6.3	-8.6	-17.6
delay/hole burning term	1.5	6.2	8.8	19.4
two-photon absorption term	-0.82	-0.74	-0.70	-0.74
step amplitude	-0.025	0.2	0.20	-0.05

Table 1. Fitting parameters used to fit the approximate response function described in section 2.4.1 to the transmission curves shown in Figure 6 (the throughput was ~50% for all of the amplifiers).

The carrier heating term and the corresponding term representing the delay of carrier heating increase with the size of the active regions in the amplifiers. The two-photon absorption term on the other hand stays approximately the same for all four amplifiers. The behaviour of the fitting parameters in Table 1 can be explained in terms of the confinement factors for the modes in the active region for each of the amplifiers.

Carrier heating in amplifiers operating at or close to the transparency point is predominantly caused by free-carrier absorption as discussed in section 2.2.4. The strength of free-carrier absorption is determined by the free-carrier absorption coefficient, the number of carriers available, and the intensity of the light interacting with them. In the case of the quantum well amplifiers, the amount of free-carrier

absorption observed increases with the number of wells, and therefore with the size of the active region. The corresponding overlap between the pump pulse and the free carriers increases accordingly. Although the confinement factor of the bulk amplifier was only marginally greater than that of the 16 quantum well amplifier, the size of the carrier-heating effect was doubled. This was because the confinement factor calculated was for the entire active region of the amplifiers, including the barriers in the case of the quantum amplifiers. Thus, the overlap between the pump pulse and the free carriers was effectively doubled in the case of the bulk amplifier because there were no barriers in the active region, and this is reflected in the large increase of the carrier heating term as shown in Table 1. The scaling of the carrier-heating term is not strictly linear with the number of quantum wells, and this indicates a limitation of the current theory.

The values of two-photon absorption coefficient given in Table 1 are seen to be essentially independent of the structure of the amplifiers being investigated. This is because two-photon absorption occurs both in the cladding regions and in the active regions of the amplifiers[5], and it is therefore not strongly affected by the confinement of the mode.

The time constants used to fit the approximation function to the data shown in Figure 4 were obtained from the literature. The time constant of the exponential corresponding to the cooling of the carrier temperature from its heated value to the lattice temperature was set at 650 fs for the bulk amplifier and 900 fs for the amplifiers containing quantum wells, values which correspond with those reported by a number of experimenters[5-7,19].

The time constant of the exponential that corresponded to the delay in the 'turn on' of carrier heating was set at 200 fs. This was a consequence of the finite time required for the heat added by free carrier absorption to thermalise from the energetic carriers to the carrier distribution via carrier-carrier scattering. The prior determination of this time constant in the literature is necessarily imprecise because this value is close to the duration of pulses used to investigate InGaAsP. Nevertheless, this seems to be a commonly quoted and accepted value[4,6]. There has been some discussion in the literature as to whether this term is due to spectral hole burning or to the delay in turn-on of carrier heating, the consensus now being that it is a combination of both of these effects. However, in the results under discussion here the amplifiers are biased to

transparency, which is defined as the point where there are no net inter-band transitions, and no spectral hole burning is present. This is confirmed by Table 1, where the magnitude of the delayed carrier heating term is almost equal to the magnitude of the carrier heating term, showing that there is no spectral hole burning occuring in the amplifiers.

It should be noted that the curve-fitting method used in this chapter to compare the magnitudes of the carrier heating and two-photon absorption effects in the four amplifiers cannot give absolute values for the coefficients of these effects. In order to do this a comprehensive model of the type formulated by Mark and Mork[6] would be required. A further limitation of the curve fitting method used in this chapter arises from the interdependence of the fitting terms. Using four varibles in a curve fitting expression necessarily reduced the confidence associated with the values obtained for each term, and an element of good forturne is included in the very clear trends observed in the fitting variables. Despite this, the curve-fitting method used in this chapter was able to provide relative comparisions of the size and the general trends of the effects in the range of amplifiers studied with an accuracy better than +/- 20 % .

2.5 Summary

Pump-probe investigations of the transmission of four amplifiers with different structures were performed using 100 fs pulses. The results obtained when the amplifiers were biased such that they were operating at or close to the transparecny point were compared using a curve-fitting method. With this curve-fitting method it was possible to attribute distinctive separate contributions to the transmission curves resulting from carrier heating, two-photon absorption, linear absorption/stimulated recombination and delayed thermalisation of the carrier distribution. The magnitudes of the effects thus obtained were compared. It was noted that the amount of carrier heating observed, which was almost exclusively caused by free carrier absorption, was closely dependent on the confinement of the mode in the active region of the amplifiers. By contrast, the magnitude of the two-photon absorption term was independent of the amplifier structure. The magnitude of the term seen as a positive peak on the traces obtained at transparency was equal to that of the carrier heating

term, and was thus confirmed to be a result of a delay in the turn-on of carrier heating. No spectral hole burning was observed in the amplifiers when they were biased at the transparency point. An element of experimental good fortune was associated with the very clear trends seen in the nonlinear coefficients derived from the fitting variables. However, the accuracy of the results was estimated to be better than +/- 20% and the general trends observed arose from the physical mechanisms described above.

The results described in this chapter give a clear insight into to the structural dependence of absorptive nonlinearities in InGaAsP optical amplifiers. This, in combination with the following chapter which describes an investigation of the structural dependence of refractive nonlinearities in InGaAsP optical amplifiers, is of considerable value for possible future design of all-optical switching in waveguides biased to transparency.

References

1 M. S. Stix, M. P. Kesler and E. P. Ippen, Appl. Phys. Lett. **48**, 1722 (1986)

2 W. Z. Lin, L. G. Fujimoto, E. P. Ippen and R. A. Logan, Appl. Phys. Lett. **50**, 124 (1986)

3 M. P. Kesler and E. P. Ippen, Appl. Phys. Lett. **51**, 1765 (1987)

4 K. L. Hall, J. Mark, E. P. Ippen and G. Eisenstein, Appl. Phys. Lett. **56**, 1740 (1990)

5 Y. Lai, K. L. Hall, E. P. Ippen and G. Eisenstein, IEEE Photonics Technol. Lett. **2**, 711 (1990)

6 J. Mark and J. Mork, Appl. Phys. Lett. **61**, 2281 (1992)

7 M. Willatzen, J. Mark, J. Mork and C. P. Seltzer, Appl. Phys. Lett. **64**, 143 (1994)

8 K. L. Hall, G. Lenz, E. P. Ippen, U. Koren and G. Raybon, Appl. Phys. Lett. **61**, 2512 (1992)

9 L. F. Tiemeijer, Appl. Phys. Lett. **59**, 499 (1991)

10 K. Kikuchi, M. Kakui, C.E. Zah and T. P. Lee, IEEE J. Quantum Electron. **28**, 151 (1992)

11 J. Zhou, N. Park, J. W. Dawson, K. J. Vahala, M. A. Newkirk and B. I. Miller, Appl. Phys. Lett. **63**, 1179 (1993)

12 K. Kikuchi, M. Amano, C. E. Zah and T. P. Lee, Appl. Phys. Lett. **64**, 548 (1994)

13 A. D'Ottavi, E. Iannone, A. Mecozzi, S. Scotti, P. Spano, J. Landreau, A. Ougazzaden and J. C. Bouley, Appl. Phys. Lett. **64**, 2492 (1994)

14 J. M. Wiesenfield, G. Eisenstein, M. Wegener, D. S. Chemla, G. Raybon and U. Koren, Tech. Digest Ultrafast Phenomena **6**, 296 (1990)

15 H. Lobentanzer, W. Stolz, J. Nsgle and K. Ploog, Phys. Rev. B., **39**, 5234 (1989)

16 K. L. Hall, A. M. Darwish, E. P. Ippen, U. Koren and G. Raybon, Appl. Phys. Lett. **62**, 1320 (1992)

[17] C. T. Hultgren, D. J. Dougherty and E. P. Ippen, Appl. Phys. Lett. **61**, 2767 (1992)

[18] L. Zenento, J. Lightwave Technol. 7, 39 (1989)

[19] K. L. Hall, G. Lenz, A. M. Darwish and E. P. Ippen, Opt. Comm. **111**, 589 (1994)

Chapter 3

Measurement of Ultrafast Refractive Index Dynamics

3.1 Introduction

In order to gain a better insight into the nonlinear mechanisms present in InGaAsP optical amplifiers, it is desirable to perform measurements of refractive index nonlinearities which complement the measurements of absorptive nonlinearities described in Chapter 2. From the perspective of investigating the potential utility of the amplifiers as optical switches, it is preferable to be able to determine what effect the structure of the amplifiers has on the magnitude, speed and sign of the refractive nonlinearities present in the amplifiers. In order to do this, it is first necessary to separate and measure the changes in refractive index caused by each nonlinear effect. This can be done by separating the effects in the time domain, using an interferometric technique based upon the pump-probe technique described in the preceding chapter.

One experimental apparatus by which nonlinear changes of refractive index with different time constants may be separated and measured is the time-division interferometer. In this chapter, the development and implementation of a time-division interferometer (TDI) is described. The TDI was used to measure nonlinear refractive index changes in a range of optical amplifiers. The results of these experiments were compared by using a curve fitting program to separate and quantify the contributions to the nonlinear refractive index changes caused by various nonlinear effects. The results of this comparison are discussed in relation to the results obtained in Chapter 2.

3.2 Background

3.2.1 Relationship between refractive and absorptive nonlinearities

Nonlinear refractive index dynamics are linked to absorptive nonlinear dynamics by the Kramers-Kronig transformation:

$$\Delta n(\omega) = \frac{c}{\pi} \int_0^{\infty} \frac{\Delta g(\Omega)}{(\Omega^2 - \omega^2)} d\Omega \qquad (1)$$

where $\Delta n(\omega)$ is the change in refractive index at a frequency 'ω' associated with a perturbational change $\Delta g(\Omega)$ of gain or absorption. In order to use the Kramers-Kronig transformation it is necessary to be able to integrate the gain as a function of frequency for all frequencies, although in the case of nonlinear changes it is necessary only to integrate over the frequencies at which absorption changes[1].

Useful analyses of the relationship between the nonlinear absorption spectrum and the nonlinear refractive index have been published for virtual nonlinear interactions above the band gap. In particular, Sheik-Bahae *et al* have published [2] an account of the effect of two-photon absorption, electronic Raman and the optical Stark effect on the refractive index of semiconductor optical amplifiers. The investigation concluded that the cumulative effect of these nonlinearities is an instantaneous negative change of refractive index. In particular, photons at energies just above the bandedge, will expereince the negative tail of the refractive nonlinearity arising from two-photon absorption.

The Kramers-Kronig transformation has also been used to determine the effect on the refractive index of a change in carrier density[3-5] and it has been shown that at photon energies just above the bandgap, an increase in the density of carriers in an amplifier will lead to a decrease of the refractive index. From this, it is apparent that linear absorption will reduce the refractive index, whilst carrier-heating, which reduces carrier density at photon energies close to the bandgap will lead to an increase of refractive index.

3.2.2 Previous experiments

Ultrafast optical nonlinearities may be measured in the frequency domain or in the time domain. Four-wave mixing experiments[6,7] performed on optical amplifiers have detected nonlinearities with time constants in agreement with those obtained using pump probe techniques. However, it is not possible to separate the refractive part of a nonlinearity from its absorptive aspect using frequency-domain experiments. Therefore, in order to produce quantitative measurements of separate refractive index nonlinearities it is necessary to use time-domain experiments.

Time-domain investigations of refractive nonlinearities performed in the 1980's were based on Mach-Zhender type interferometer set-ups. An early interferometer experiment passed non-collinear pump and probe beams through a sample such that they intersected inside the sample[8]. The probe beam was thus spatially separated from the pump beam and could be detected without interference from the pump beam. A reference beam was provided which did not pass through the sample, but travelled along a separate path before being recombined with the probe. Phase shifts incurred by the probe beam as a result of refractive index dynamics induced in the sample by the pump beam, were measured via interference between the probe and reference pulses.

More recently, an interferometric measurement of refractive index nonlinearities in doped fibres was performed using a similar Mach-Zhender interferometer technique[9]. The specimen was positioned in one arm of the interferometer, the second arm being a delay for the reference pulse. However, in this experiment the pump and probe beams were of necessity collinear because the specimen was an optical fibre. Thus, rather than spatially separating the probe and the pump beams, they were given orthogonal polarisations. The reference beam did not propagate through the fibre, but travelled along the second arm of the interferometer. The phase shift of the probe was measured by detecting interference patterns formed by the probe and reference beams. A similar technique has been used to measure nonlinear phase shifts in channel waveguides[10].

A limitation to the accuracy of these experiments arose from noise caused by fluctuations in the length of the two arms of the interferometer. Thermal fluctuations in the air through which the probe and reference beams were propagating altered the refractive indices of the arms of the interferometer, varying the relative delay between

the probe and reference pulses. In order to overcome this problem, LaGasse *et al*[11] separated the probe and reference pulses in the time domain rather than separating them spatially. The experimental setup that they described was termed a time-division interferometer (TDI). In the TDI, the reference pulse preceded the pump and probe pulses though the sample by a few hundred picoseconds. The temporal displacement of the reference pulse in relation to the probe and pump pulses was insignificant in comparison to slow thermal fluctuations, and the reference pulse thus experienced the same fluctuations of the refractive index of the air as the probe and pump pulses. After transmission by the sample under investigation, the reference pulse was delayed so that it was temporally overlapped with the probe pulse. Interference between the probe and reference pulses was detected, allowing measurement of nonlinear changes of the refractive index induced by the pump. The pump was eliminated from the detected signal using a chopper referenced to a lock-in detection.

With the growing interest in optical amplifiers, Hultgren and Ippen applied the TDI technique developed by their co-workers at MIT to investigate AlGaAs amplifiers[12]. The TDI setup used for their investigation is shown in Figure 1.

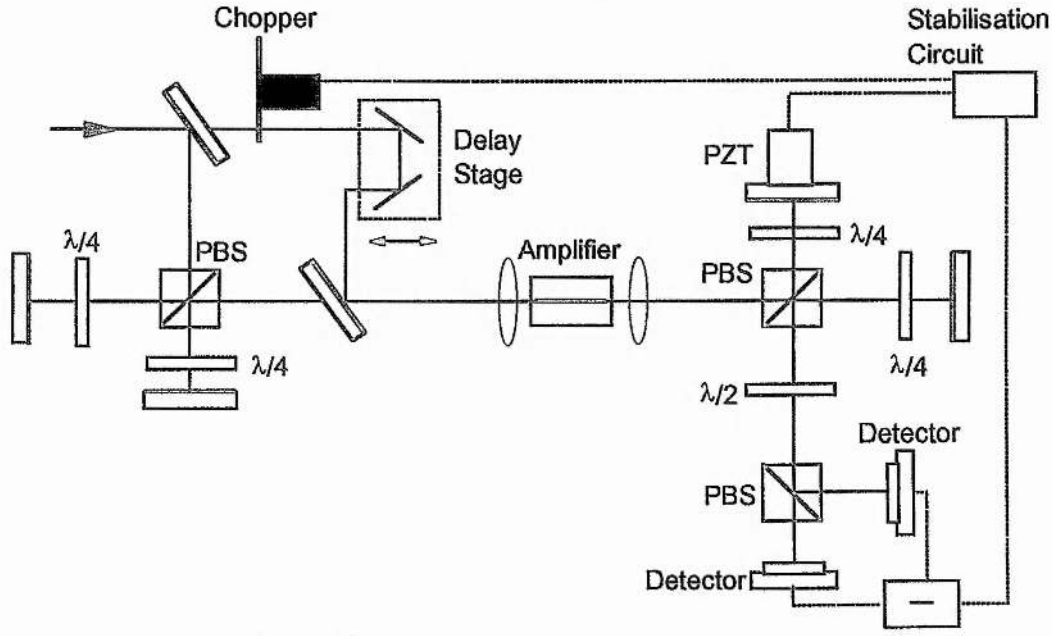

Figure 1. The time-division interferometer

In the experimental setup shown in Figure 1. The interferometer by which phase changes are measured is formed by the four delay arms containing quarter-wave plates. The interferometer is actively stabilised using a piezo-electric transducer which

is referenced to interference produced by the probe and reference beams. The results described in this chapter were obtained using an experimental setup based on that depicted in Figure 1, and a detailed description of the operation of such a time-division interferometer will therefore be deferred until later in this chapter.

At the time of the inception of this project no time-domain measurements of nonlinear refractive index changes in InGaAsP optical amplifiers had been performed. However, since this project was undertaken Hall *et al* published an investigation of femtosecond index nonlinearities in InGaAsP amplifiers[13]. They used a novel interferometer setup which utilised heterodyne detection to measure changes in the refractive index of amplifiers for both co-polarised and cross-polarised pump and probe pulses. The pump, probe and reference pulses were distinguished from each other by using acousto-optic modulators to apply a modulation to each of the pump, probe and reference beams and then detecting the modulation of the beams using an AM/FM radio receiver. The pump beam was chopped, and the modulation of the pump was transferred to the probe through nonlinear interactions in the amplifier under investigation. Modulation of the probe was detected and integrated to yield information on the transmission and phase of the probe. The results of this experiment will be discussed in relation to the results described later in this chapter.

3.2.3 Principles of Operation of the Time-division interferometer

The TDI experiment is analogous to a pump-probe experiment in that the effect of a pump pulse on a probe pulse is measured as a function of the delay between pump and probe pulses. In a pump-probe experiment, changes in the transmission of an amplifier are determined by measuring the intensity of transmitted probe pulses. In the TDI experiment, changes of the refractive index of an amplifier are determined by measuring the variation of the length of optical path travelled by a probe pulse as a function of its delay relative to a pump pulse.

Variation of the path length travelled by the probe pulse is measured by comparing the path travelled by the probe with that travelled by a reference pulse. This is done using an interferometer, which consists of two delay arms on the input side of the amplifier under investigation, and two delay arms on the output side of the

amplifier (as illustrated in Figure 1). On the input side, the length of the delay arm travelled by the reference pulse is less than that travelled by the probe pulse. The reference pulse thus precedes the probe through the amplifier under investigation. The pump pulse is approximately synchronised with the probe pulse and does not interact with the reference pulse.

On the output side of the amplifier, the lengths of the delay arms travelled by the probe and reference pulses are opposite such that the probe and reference become temporally overlapped. The polarisations of the probe and reference pulses are rotated such that they interfere with each other, and the resulting interference patterns are detected using a balanced detector system.

One arm of the interferometer is electronically stabilised using a transducer which is referenced to the interference between the probe and reference pulses. When the pump is absent from the experiment, (*i.e.* when it is blocked by a chopper wheel) the transducer maintains a fixed phase difference between the probe and reference pulses. The length of the stabilised delay arm is held fixed in its stabilised position as the chopper wheel rotates to allow transmission of the pump beam. The pump induces a nonlinear change of the refractive index of the amplifier, altering the path length travelled by the probe pulse, and changing the phase between the probe and reference pulses. The resulting modification of the interference pattern is measured by a balanced detector system and compared with previously obtained values to provide a calibrated value of phase shift induced by the pump pulse.

The length of path travelled by the pump pulse can be modified to resolve refractive index changes in the time domain in a manner analogous to that used in pump-probe experiments.

3.3 Experiment

3.3.1 Experimental setup

The experimental setup by which the principles described in the previous section were realised is illustrated in Figure 2.

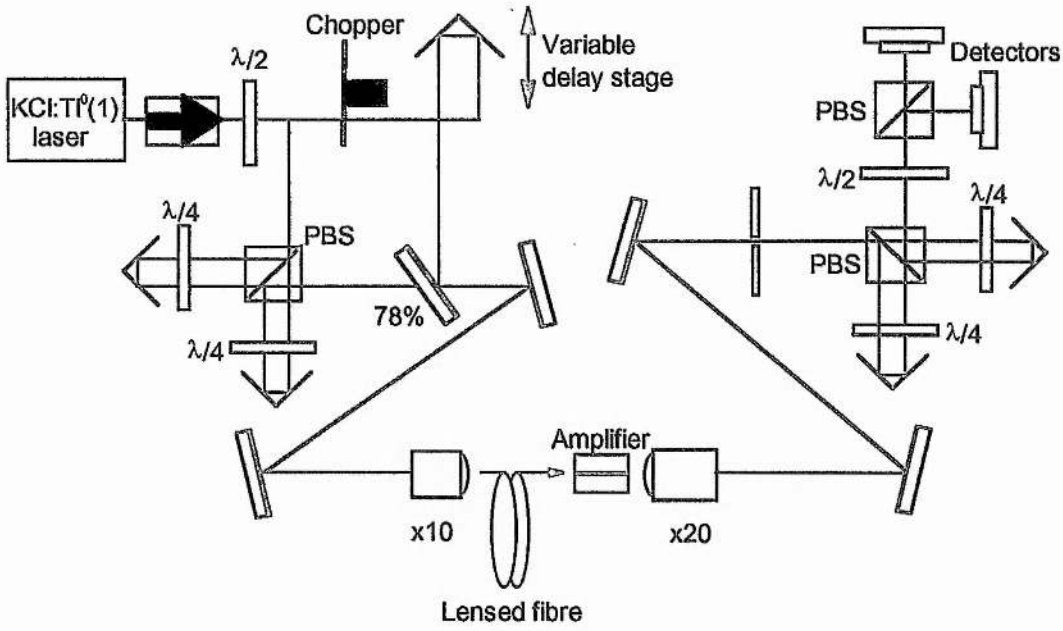

Figure 2. Setup of the time-division interferometer

A coupled-cavity mode-locked KCl:Tl^0(1) laser was used to generate pulses of approximately 100 fs duration at a wavelength of 1520 nm. The beam from the laser was passed through a Faraday optical isolator, and then passed through a half-wave plate orientated such that it transmitted the beam with a TE polarisation. The transmitted beam was then split into two beams of equal intensity by a beamsplitter with an anti-reflection coating on one side. The fraction of the beam transmitted by the beamsplitter became the pump beam, whilst the fraction reflected was used to provide the probe and reference beams.

The pump beam was incident on a retro-reflector which was mounted on a computer controlled delay stage. The delay stage was actuated by a stepper motor that moved the stage in steps of 1 μm. The pump beam was reflected by the retro-reflector through a chopper wheel to a second beamsplitter.

The fraction of the original beam reflected by the first beamsplitter was passed through a half-wave plate that rotated the polarisation of the beam to be at 45 degrees relative to the plane of the optical bench. A polarising-beamsplitter then split the beam into two equal parts, one with TE polarisation (probe), the other with TM polarisation (reference). The probe beam travelled along a delay arm 25 cm long, and the reference beam travelled along a second delay arm 16 cm long. Each of the delay arms contained a quarter-wave plate oriented such that the polarisations of the beams returning from

the delay arms to the polarising-beamsplitter was rotated through 90 degrees. Thus a probe beam with TM polarisation, and a reference beam with TE polarisation which preceded the probe by 300 ps, were transmitted by the polarising-beamsplitter

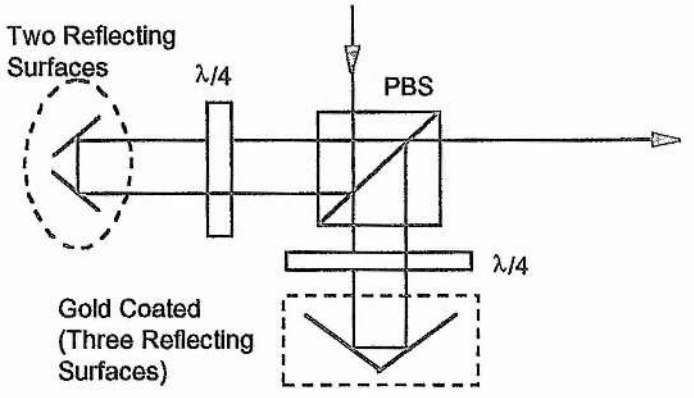

Figure 3. Delay arm

It was important to ensure that the probe and reference beams transmitted by the polarising beamsplitter were collinear and spatially overlapped. This was to ensure that they were coupled to the amplifier under investigation with equal efficiencies.

The retro-reflector used in the 'reference arm' of the interferometer was a standard gold-plated corner cube, mounted on a translation stage whose position was adjustable in the x, y, and z directions. This provided displacement of the reference beam, but did not allow adjustment of the angular orientation of the beam. A specially constructed two-mirror retro-reflector was used in the 'probe arm'. This two-mirror retro-reflector allowed adjustment of the angular orientation of the probe beam. The probe and reference beams were overlapped close to the polarising beam splitter using the translatable corner cube, and the two-mirror retro-reflector was then used to overlap the beams at a distance of ~1 m from the polarising beamsplitter. The process was iterated until the probe and reference beams were collinear.

The pump, probe and reference beams were recombined at the second beamsplitter, as shown in Figure 2. In practice this second beamsplitter was actually a mirror with 88 % reflectivity, as this gave the ratio of intensities required between the pump beam and the probe beam. Care was taken to ensure that the three beams were propagating collinearly after recombination at the second beamsplitter. This was done

by adjusting the orientation of the pump beam using a beam-steering mirror and the translatable retro-reflector mounted on the delay stage. The path length of the pump beam was adjusted so that pump pulses were temporally overlapped with probe pulses after transmission through the second beamsplitter.

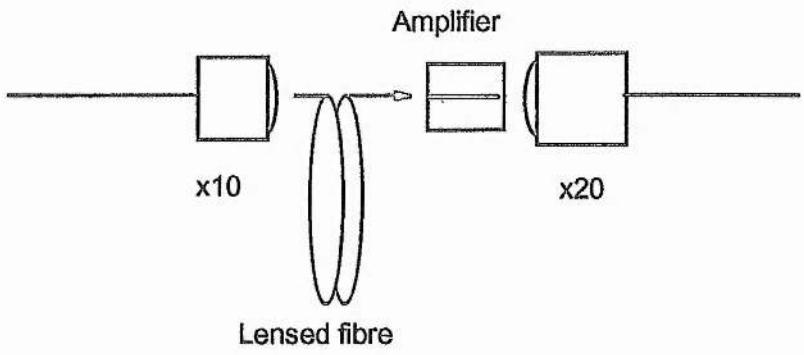

Figure 4. Coupling to and from amplifier

The three colinearly propagating beams were coupled into an optical fibre using a x10 microscope objective. The opposite end of the fibre from the microscope objective terminated at a fibre lens, from which the beams were coupled into an optical amplifier. The fibre used was short (18 cm) to avoid any distortion of the coupled pulses due to group velocity dispersion.

In order to simplify the description of the operation of the TDI, the pump, probe and reference trains of pulses (beams) will from here on be described as though each were a single pulse. It will be understood that the situation described for individual pulses can be extended to the experimental case where repeating pulses are separated by 12.2 ns.

A summary of the pulses that were coupled into the amplifier under investigation is as follows: a TE polarised low intensity reference pulse was propagated through the amplifier, 300 ps behind which were a TM polarised low intensity probe pulse which was temporally overlapped with a TE polarised high intensity pump pulse.

The pulses transmitted by the amplifier were collected using a x20 microscope objective and focused through an aperture placed 1 metre from the objective, which transmitted only light guided by the amplifier.

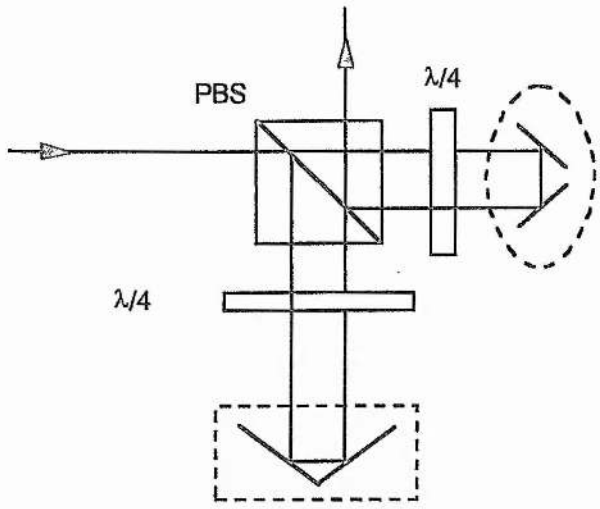

Figure 5. Delay arms on output side of amplifier

A polarising beam splitter separated the orthogonally polarised probe and reference pulses, which then passed through polarisation rotating Michelson-type delay lines as shown in Figure 5. The length of the delay arms in this second part of the interferometer was arranged so that the reference and probe pulses were temporally overlapped upon transmission by the polarising beamsplitter.

It was required to measure the phase shift of a probe pulse caused by the presence in the optical amplifier of a pump pulse. This was done using the set-up shown in Figure 6.

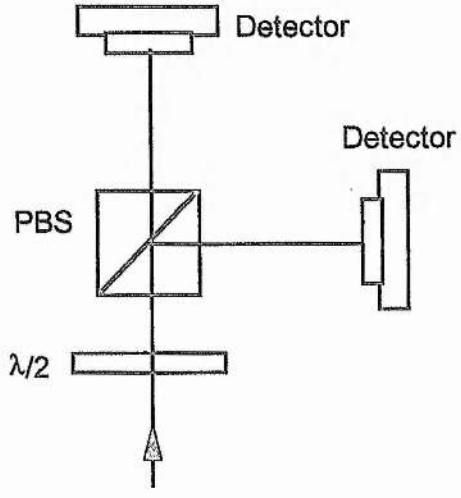

Figure 6. Balanced detector system

The temporally overlapped, orthogonally polarised probe and reference pulses transmitted from the delay arms shown in Figure 6 were passed through a half-wave plate which was orientated such that their polarisations were rotated through 45 degrees. A polarising beam splitter was used to separate each of the probe and reference pulses into their TE and TM components. The TE components of the probe and reference pulses were transmitted by the beamsplitter onto a first detector, and the TM components were reflected by the beamsplitter onto a second detector.

The intensity of light incident on each of the two detectors was determined by the phase difference between the probe and reference pulses. Any modification of the phase difference between the pulses caused equal and opposite changes of intensity at the detectors. The experimental setup was arranged such that the intensities of the probe and reference pulses were equal. This corresponded to a phase difference between the probe and reference pulses of $\pi/2$ radians.

When the pump beam, which was TE-polarised throughout the experiment, passed through the half- wave plate illustrated in Figure 6, its polarisation was rotated such that it was split by the polarising beam splitter into two components of equal intensity. The balanced detector scheme worked on the principle of measuring the difference between the intensities incident on the two detectors, and consequently did not detect the pump pulse.

3.3.2 Stabilisation and Detection of Phase Shifts

The length of the delay arm of the interferometer on the output side of the amplifier was controlled by translating the corner-cube at the end of the arm, using a piezo-electric transducer. A stabilisation signal derived from the two detectors was used to actively monitor the length of the arm such that the phase difference between the probe and reference pulses was maintained at $\pi/2$ radians when no pump pulse was present in the system. The stabilisation signal was produced using the circuit shown in Figure 7.

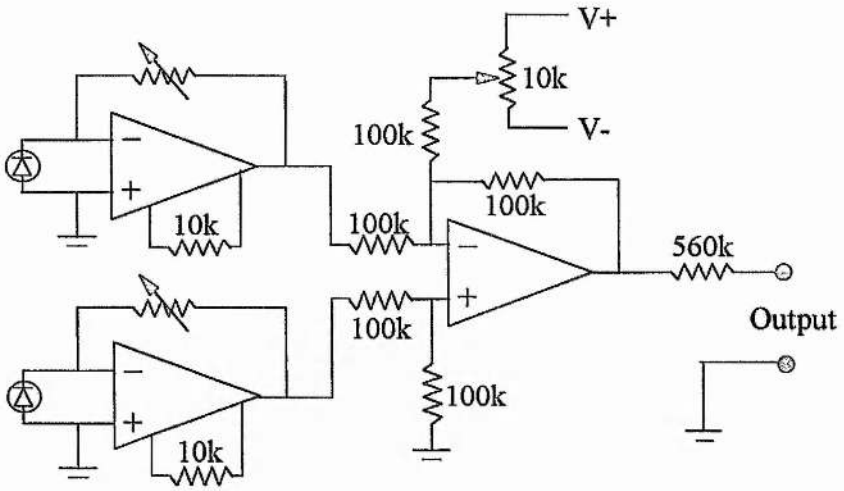

Figure 7. Circuit used to measure and amplify the difference between two optical signals.

The circuit shown in Figure 7 is based on a standard difference circuit. Voltages from each of the two detectors were input to a differential amplifier, which produced a signal proportional to the difference between the intensities incident on each of the two detectors. This difference signal was filtered, and fed to a box that converted the signal into a high voltage which controlled the position of the piezo-electric transducer and corner-cube.

The circuit that produced the high voltage signal was modified from one used to stabilise the nonlinear cavity of a coupled-cavity mode-locked laser. The frequency response of the circuit was reduced since it was required only to compensate for thermal drift and other slow changes in the length of the interferometer arms. The circuit was triggered from the reference signal of the chopper wheel used to chop the pump pulse. The circuit was set to maintain the phase difference between the probe and reference pulses at the two detectors at $\pi/2$ when the pump beam was blocked by the chopper. When the chopper was oriented so that it was transmitting the pump beam, the voltage from the circuit was held at the value it had been when the pump beam had been blocked.

Variations of the phase of the pump pulse, caused by pump-induced modifications of the refractive index of the amplifier, altered the interference condition between the probe and reference pulses. The modified interference between the probe and reference was detected as an increase of the signal from one detector, and a corresponding decrease of signal from the other detector.

3.3.3 Calibration of Phase Shift

The intensity of light detected by the two photodiodes in the balanced detector system is determined by the phase between the probe and reference pulses, with a Cos function dependency shown in Figure 8.

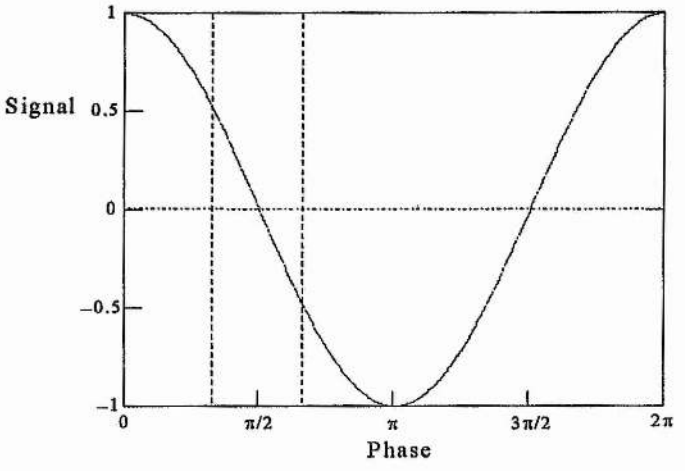

Figure 8. Normalised signal from balanced detector system

If the probe and reference pulses are in phase, no signal will be detected by the photodiode in the TM arm of the detector system, and a maximum signal will be detected in the TE arm. Equivalently, a phase difference of 180 degrees will result in an entirely TM polarised signal. Any phase difference between these two extremes will produce a signal on each of the two detectors, as indicated in Figure 8.

The phase difference between the probe and reference pulses is stabilised at $\pi/2$ so that small changes in the phase of the probe will produce a linear change of intensity as detected by the two photodiodes.

The intensity of the pump pulse in all of the experiments described in this chapter was kept below that which gave a phase shift of $\pi/6$, so that the measured signal was always within the linear region shown in Figure 8.

The phase shift detected by the interferometer was calibrated before results in any operating regime were recorded. The calibration was performed by blocking the pump pulse and switching off the stabilisation box, and then translating one of the arms of the interferometer so that it passed through several interference fringes. The

magnitude of the fringes, measured as a voltage by the balanced detector system, was recorded using a storage oscilloscope. The voltage corresponding to the height of an interference fringe relative to zero volts was a phase shift of $\pi/2$. All measurements recorded in that operating regime were then calibrated against this voltage.

3.3.4 Using the Time-Division Interferometer

As has previously been described, care was taken to ensure that the probe, reference and pump beams were all collinear on the input side of the amplifier under investigation. It was also required that the probe and reference beams be collinear upon recombination after travelling in their respective delay arms on the output side of the interferometer, so that the probe and reference would be overlapped and would produce interference fringes. This was done by introducing a vibration to one of the arms of the interferometer to produce interference fringes, and then actuating the corner-cube and two-mirror retro-reflectors until the interference pattern produced was maximised.

The intensity of the reference pulse was adjusted as necessary on the input side of the experiment, such that it was equal to the probe pulse on the output side of the experiment. This provided an interference pattern that was symmetric above and below zero, as measured by the balanced detector system (see Figure 8).

It was desirable that attenuation of the probe pulse by the pump was kept to a minimum to prevent distortion of the interference pattern produced by probe and reference pulses, and thereby avoid distortion of the phase shift measurements. To this end, the intensity of the pump beam was kept to a minimum, and phase shifts measured using the TDI are consequently small (less than $\pi/6$). This limitation of the size of measured phase shifts also ensured the linearity of phase shift measurements as described in section 3.3.3.

The time delay between the pump and probe pulses was adjusted via a stepper motor, which was adjustable in micron steps using a personal computer. The computer program used for the experiment was adapted from one previously used to perform pump-probe experiments. When taking measurements, the computer actuated the stepper motor and then paused for three tenths of a second to allow the stabilisation

circuit to re-establish a $\pi/2$ phase difference between the probe and reference beams. A lock-in amplifier then measured the signal produced from the balanced detector scheme which was recorded and plotted on a monitor screen in real time.

In theory, the effect of the pump beam on the measured signal was neutralised by virtue of its intensity being equally detected by the two detectors in the balanced detector system. However, in practice, the polarisation rotation elements used in the experiment were not perfect, and the balanced detector system picked up a signal derived from the pump beam. This signal interfered with the reference beam around the zero time delay point and obscured the detected phase shift. The problem was reduced by mounting one of the mirrors which was used to steer the pump beam on a piezo-electric transducer, and modulating the transducer so that interference caused by the pump beam was averaged to zero.

A further improvement to the signal-to-noise ratio obtained from the experiment was realised by performing each measurement three times and averaging the results.

3.4 Results

3.4.1 Preliminary results

Measurements of refractive index dynamics were performed for an amplifier containing four InGaAs quantum wells 8 nm wide, separated by InGaAsP barriers 10 nm wide (4 QW amplifier).

The coupled-cavity mode-locked KCl:Tl^0(1) laser generated pulses of 100 fs duration at a wavelength of 1520 nanometers. The average intensity of the pump beam coupled to the amplifier was 2.8 μW, which corresponded to a peak intensity of 3.0 W. The intensity of the probe and reference beams were adjusted to be one tenth of this value. The computer controlled stepper motor was set to execute a series of 100 x 20 micron (~66 femtoseconds) steps. This corresponded to a translation of the pump pulses from being 1 picosecond behind the probe pulses, to being 6 picoseconds ahead of the probe pulses.

Sets of phase measurements were performed with forward bias current applied to the amplifier at various levels. Attenuation of the probe and reference pulses prevented measurements being taken with the bias current below 7 mA. Three sets of measurements obtained using the 4 QW amplifier are shown below in Figure 9.

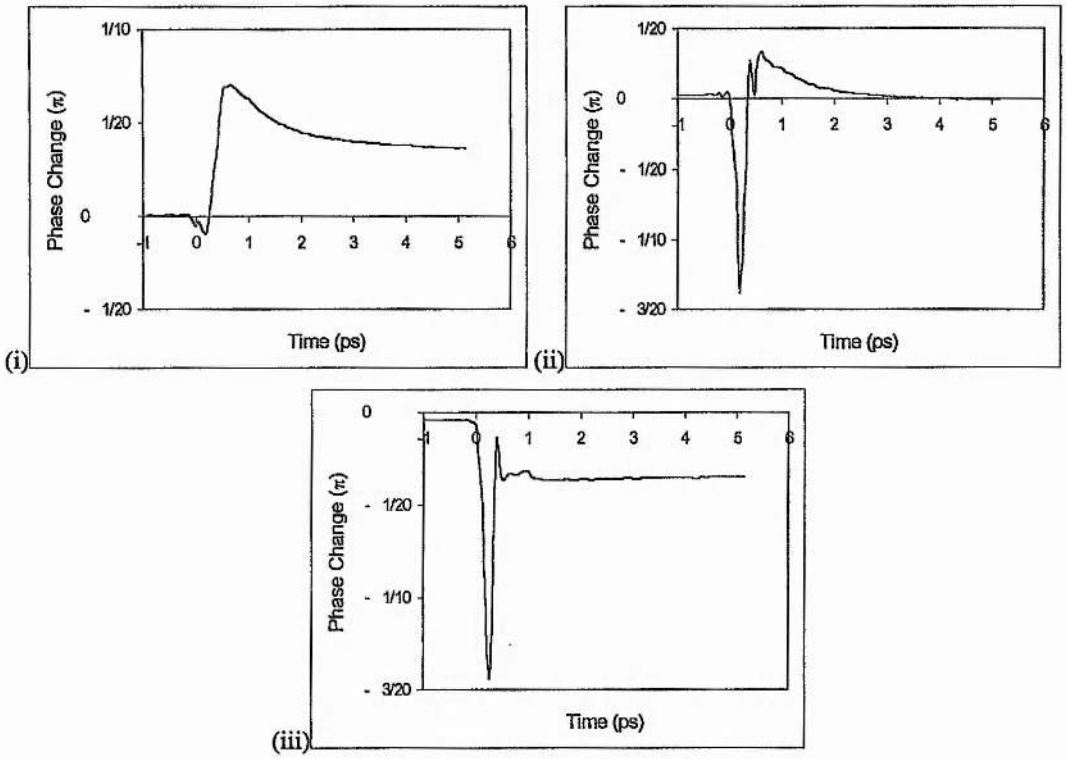

Figure 9. Preliminary results obtained from the time-division interferometer using a 4 QW amplifier, for various forward bias currents.

The plots in Figure 9 show the refractive index dynamics in the 8 quantum well amplifier when it was biased to operate in gain (i), at transparency (ii) and in loss (iii). The bias currents for each of these regimes are 15 mA, 11 mA and 7.2 mA respectively.

A step-like change of refractive index is observed in plots (i) and (iii). This corresponds to the step-like change of transmission that was observed in chapter 2, and is due to pump-induced changes in the carrier density. It has been shown in semiconductors, that increasing the carrier density will lead to a decrease of the refractive index for photon energies close to the bandgap[3-5]. Thus, in plot (i) the amplifier is operating in gain, and the effect of the pump pulse is to deplete carriers, causing the step-like increase of refractive index. The opposite case holds when the

amplifier is operating at loss, the pump pulse increasing the carrier density and causing a reduction of the refractive index. No step-like change of refractive index is observed when the amplifier is biased to transparency (plot (ii)).

A transient increase of refractive index recovering with a time constant of ~900 fs is evident from plots (i) and (ii). The transient has the same time constant as the transmission transient caused by the carrier-heating that was observed in Chapter 2. Increasing the temperature of the carrier distribution reduces the occupancy of states close to the band edge, and the effect of the carrier-heating on the refractive index is thus identical to that caused by pump-induced carrier depletion. This positive transient is consistent with that observed by other experimenters[14,15]. The carrier-heating transient is weak in the trace shown in plot (iii) and appears to have a very short time constant. The magnitude of this carrier-heating term was small because the bias current to the amplifier was low, and the carrier-heating was correspondingly reduced. The anomalous time constant was caused by interference of the pump pulse with the detected signal, an effect that also caused the sharp negative dip seen in the carrier-heating transient in plot (ii)

The negative transient seen in each of the plots in Figure 9 agrees well with previously observed responses [9,10]. This transient has been postulated to be a result of instantaneous nonlinear effects such as the electronic Raman effect and the optical Stark effect[12]. A theoretical treatment of non-resonant index dynamics in semiconductor amplifiers has shown that a combination of these effects will lead to a negative nonlinear change of the refractive index in amplifiers biased at or around the transparency point[2]. The magnitude of the transient decreases as the bias current to the amplifier is increased from 7.3 milliamps in plot (iii) to 15 mA in plot (i). Increasing the carrier density fills states near the band edge, pushing the absorption edge to higher energies and away from the probe wavelength. The reduction in the size of the transient with increasing bias is therefore consistent with a nonlinearity such as the optical Stark effect which is resonant at the band edge.

3.4.2 Comparison of refractive nonlinearities in different amplifiers

A primary objective in this project was the characterisation of the nonlinear refractive index dynamics in a range of semiconductor amplifiers. To complement the pump-probe transmission measurements recorded in Chapter 2, it would have been appropriate to use the same optical amplifiers as used in Chapter 2. Unfortunately, the amplifier containing a single quantum well was damaged before the refractive index measurements were performed. In addition, at the low pump pulse intensities required to obtain linear refractive index measurements from the time-division interferometer, the attenuation of the reference and probe pulses in the bulk amplifier was such that refractive index measurements could not be performed when the amplifier was biased to transparency.

Nonlinear refractive index measurements were performed on three different optical amplifiers. The first of these, as described above, contained four quantum wells (4 QW amplifier) and had not previously been used to provide pump-probe transmission data. The second amplifier, used in Chapter 2, contained sixteen InGaAs quantum wells 6.5 nm wide separated by InGaAsP barriers 8 nm wide (16 QW amplifier). The third and amplifier also used in Chapter 2 contained eight InGaAs wells of 8 nm thickness separated by InGaAsP barriers 10 nm wide (8 QW amplifier).

Refractive index plots obtained using the 4, 8 and 16 QW amplifiers are shown in Figure 10.

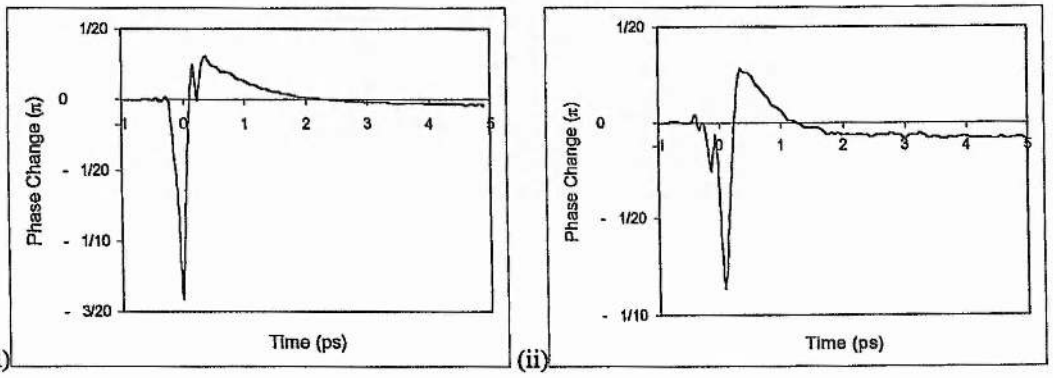

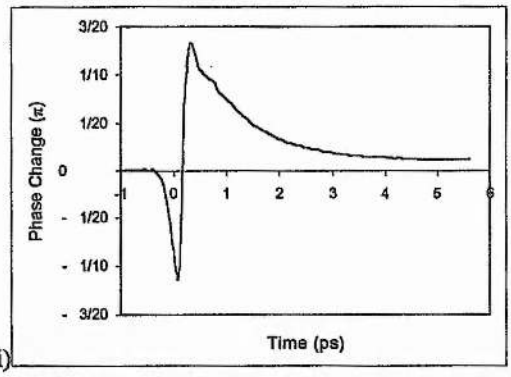

(iii)

Figure 10. Refractive index dynamics in a 4 QW (i), 8 QW (ii) and 16 QW (iii) amplifiers biased to operate at or close to transparency.

The three plots shown in Figure 10 were obtained with the amplifiers biased such that they were operating close to the transparency point. The transparency current was set by monitoring refractive index plots obtained from the interferometer, and adjusting the current until no step-like change of transmission was observed. Due to the limited resolution of the computer monitor used in the experiment, the resulting bias level did not always coincide exactly with the transparency point. This is reflected in plots (ii) and (iii) where a step in the refractive index data is clearly visible.

Each of the plots in Figure 10 displays the positive dynamic with a recovery time of less than 1 picosecond, that was attributed to carrier-heating in section 3.4.1. A negative transient with a time constant faster than the 100 femtosecond pulse duration and postulated to be due to virtual nonlinear effects is also apparent in each of the three plots.

There is clear evidence of a transient positive peak close to zero-time in the pump-probe transmission data of Chapter 2 and this is not observed in the refractive index dynamics shown in Figure 10. In Chapter 2, this transient was explained as being due to a delay in the turn on of carrier-heating. However, if a delay of carrier-heating is responsible for the positive transient seen in Chapter 2, then for these results to be consistent with the pump-probe transmission results, there must be a similar delay present in the refractive index dynamics. The solution to this apparent contradiction lies in the change of sign between the carrier-heating transient seen in transmission dynamics and that seen in refractive index dynamics. There is indeed a delay in the turn on of carrier-heating in the refractive index dynamics, but this is not observed in the

refractive index plots because it is lost in the continuation of the rise from the negative instantaneous transient to the positive carrier-heating transient. The effect of the delay is to lessen the rising gradient of the carrier-heating transient. This effect is quantified and discussed in the following section

3.4.3 Analysis

To quantify the effect that the amplifier structure had on the refractive index dynamics recorded using the interferometer, a curve-fitting program was used to separate the contributions made to the refractive index made by different nonlinear effects. The function that was fitted to the experimental data was identical to that used in the previous chapter to quantify absorptive nonlinearities, namely:

$$R(t) := \left[\left[\frac{\sinh\left(\frac{t}{a}\right)}{\cosh\left(\frac{t}{a}\right)\cdot\left(\frac{1}{a}\right)} + a\right]\cdot\left[s + d\cdot\exp\left[-\left(\frac{t}{dy}\right)\right] + c\cdot\exp\left[-\left(\frac{t}{ch}\right)\right]\right] + b\cdot\operatorname{sech}\left(\frac{t}{a}\right)^2\right]$$

The response function R(t) is constructed from a superposition of functions representing nonlinear effects, and a sech^2 pulse profile. The first bracketed term of the response function is the integral of a sech^2 pulse shape, 's' is the size of the step-like change of refractive index caused by inter-band transitions, the first exponential term represents a delay in the turn on of carrier-heating, the second exponential term represents carrier-heating, and the final term represents an instantaneous refractive index change.

The function was fitted to each of the refractive index plots obtained for the 4, 8, and 16 quantum well amplifiers. The resulting functions are plotted in Figure 11 on common axes with the experimental data.

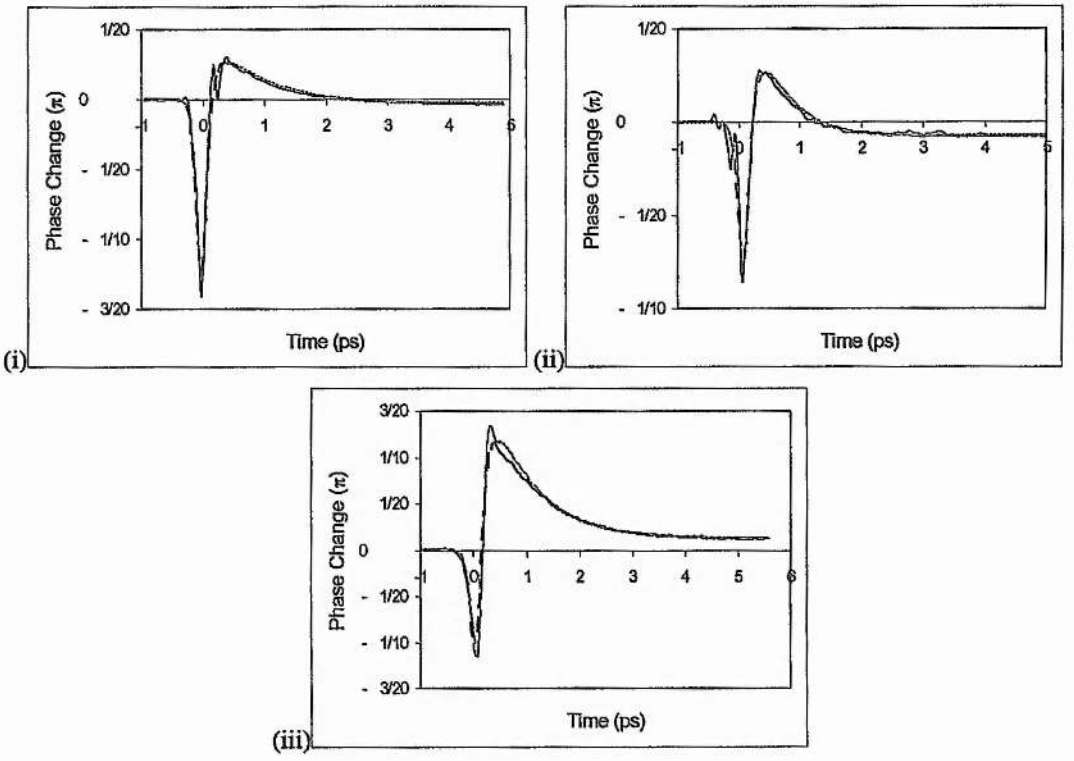

Figure 11. Refractive index dynamics in a 4 QW (i), 8 QW (ii) and 16 QW (iii) amplifiers, with experimental data shown as solid lines, fitted curve shown as dashed lines.

The fitted curves are clearly different to those that were obtained in Chapter 2, even though they were obtained using the same fitting function. The time constants associated with the delay in turn on of carrier-heating (200 femtoseconds) and the decay of the carrier-heating itself (900 femtoseconds) were the same. The sign and magnitude of the constants associated with each term of the fitting function are the only differences between the functions plotted in this and the previous chapter. In particular, the carrier-heating term 'c' and the step-like inter-band transition term 's' are both of the opposite sign to that seen in the transmission curves of chapter 2.

The size of each of the fitting terms is shown below in Table 1. The each fitting parameter in Table 1 was fitted to an accuracy of around 10%. The interdependency of the fitting terms was around 0.97, and the interplay of the terms may have reduced their accuracy to around 50%.

	4 QW	8QW	16QW
carrier-heating term	0.21	0.23	0.74
delay/hole burning term	-0.19	-0.20	-0.67
virtual effect	-0.12	-0.084	-0.12
step amplitude	-0.012	-0.027	0.040

Table 1. Fitting parameters used to fit the response function to the plots of refractive index dynamics shown in Figure 10.

The carrier-heating term obtained using the response function shows a general upward trend as the number of quantum wells in the amplifiers increases. This is in agreement with the trend observed for absorptive index dynamics discussed in Chapter 2 and corresponds to an increasing free-carrier absorption rate as the size of the active region, and the number of free carriers increases. It would be reasonable to expect the size of the carrier heating term to scale linearly with the number of quantum wells in the amplifiers. The fact that this does not happen is cannot be attributed to variations in linear loss between the amplifiers since they were all of the same design and their linear losses were measured to be within 10% of each other (α = 20+/-2 cm^{-1}). The absence of linear scaling of the carrier heating term indicates that there may be other important effects present in the nonlinear dynamics, and demonstrates a weakness of the current theory.

The second term in Table 1 is labelled as the delay/hole burning term. This term arises from the finite time required for carrier-carrier scattering to thermalise a carrier distribution after the creation of hot carriers. The carrier-carrier scattering time leads to a delay before the carrier distribution is heated (i.e. there is a delay before the rise of the positive transient seen in the plots in Figures 11), and is correspondingly equivalent to the lifetime of any spectral hole burning effects. It was not expected that any spectral hole burning would be observed in the refractive index dynamics recorded for amplifiers operating at transparency for two reasons. Firstly, no spectral-hole burning should be seen in amplifiers operating at transparency since there are no net inter-band transitions taking place. Secondly, any spectral hole that was produced as a consequence of an amplifier not being biased precisely to transparency would be

symmetric about the pump wavelength and would therefore have no effect on the refractive index of the amplifier[12]. It is not surprising therefore that the delay/hole burning term was of approximately equal magnitude (with opposite sign) to the carrier-heating term. This meant that delay term was cancelling the rise of the carrier-heating term, and there was no extra component to the term caused by carrier-heating.

The term corresponding to virtual effects in the amplifier was approximately constant for each of the three amplifiers. The magnitude of the term for the eight quantum well amplifier was less than that seen in the two other amplifiers. The dominant effect in the virtual refractive nonlinearity has been postulated to be the quadratic Stark effect [2,12]. In the quadratic Stark effect, changes in the energy of electrons in the active regions of the amplifiers are caused by interaction with the field of high intensity pulses. This leads to 'dressed' electronic states and an associated negative change in refractive index. The size of this effect is dependent on the bandgap of the active material, and the lesser magnitude of the term observed for the eight quantum well amplifier in comparison to that observed in the other two amplifiers may be a consequence of a smaller bandgap of that amplifier.

3.4.4 Nonlinear-Index Coefficients

The intensity-dependent portion of the refractive index arising from the virtual nonlinearity can be determined using the equation

$$\Delta n := \left(\frac{\lambda}{2\cdot\pi\cdot L}\right)\cdot\Delta\Phi \qquad (2)$$

where λ is the wavelength of the incident light (1520 nm), L is the length of the amplifiers (1 mm) and $\Delta\Phi$ is the phase change experienced by the probe as a result of the virtual nonlinearity (shown in Table 1). From this, the nonlinear index coefficient can be calculated using

$$n_2 := \frac{\Delta n\cdot A_{ef}}{P} \qquad (3)$$

where A_{eff} is the effective area of the mode in the amplifier and P is the peak power.

The nonlinear index coefficients calculated for the 4 QW, 8 QW and 16 QW amplifiers are shown in Table 2

	4 QW	8QW	16QW
nonlinear index coefficient (n_2) x 10^{-12} cm^2/W	-4.7	-16	-11

Table 2. Nonlinear index coefficient in 4 QW, 8 QW and 16 QW amplifiers resulting from virtual nonlinearities.

The values of n_2 shown in Table 2 are an order of magnitude higher than those observed by Ippen *et al*[14] in similar cirumstances. However, they agree well with those found by Grant and Sibbett[16] although their measurement included the effect of carrier-heating. The calculated nonlinear index coefficients do not show any discernible trend.

Equation (2) can also be used to determine the intensity-dependent portion of the refractive index arising from the carrier-heating nonlinearity. Because the pulses used in the interferometer experiments are considerably shorter than the 900 fs decay time associated with carrier-heating, the index change associated with the carrier-heating is proportional to the pulse energy density. Having calculated Δn as a function of pulse energy density, it is possible to determine the effective nonlinear index coefficient that would be experienced by pulses with durations much longer than 900fs.

The effective nonlinear index coefficient (n_2) was calculated for each of the 4 QW, 8 QW and 16 QW amplifiers.

	4 QW	8QW	16QW
nonlinear index coefficient (n_2) x 10^{-12} cm^2/W	1.2	6.8	10

Table 3. The effective nonlinear index coefficient in 4 QW, 8 QW and 16 QW amplifiers resulting from carrier-heating.

As discussed in section 3.4.3, the trend of the nonlinear index coefficient associated with carrier-heating is to increase with the number of quantum wells in the active regions of amplifiers. This is not a direct consequence of the number of quantum wells, but arises from the increased thickness of active material available to interact with optical pulses. The carrier-heating effect is caused primarily by free-carrier

absorption, and the amount of heating is thus determined by the number of free carriers which absorb incident photons.

The dependence on active region size of the nonlinear refractive index coefficient associated with carrier-heating is accentuated compared to that of the carrier-heating effect itself. This is because the A_{eff} term in equation 3 accounts for the reduced intensity of light in the active region of the amplifiers as the thickness of their active regions increased.

3.5 Summary

A time division-interferometer was constructed and used to measure refractive index dynamics in three InGaAsP amplifiers of different structure. The index dynamics measured using the interferometer were separated using a fitting function to provide information on the size of refractive nonlinearities due to virtual effects and carrier-heating. The data acquired using the fitting function were used to determine a nonlinear coefficient for the virtual nonlinearity, and an effective nonlinear coefficient for the nonlinearity arising from carrier-heating effects. The fact that the negative refractive index dynamic attributed to carrier heating did not scale linearly with the number of quantum wells in the amplifiers indicates that further effects which are not considered in the current theory may may be present in the amplifiers.

Although the uncertainties associated with the measurements of the nonlinear and effective nonlinear coefficients were large (at least 50%) as a consequence of the uncertainty associated with the estimation of mode sizes, they indicate that the cumulative nonlinearity experienced by a pulse with a duration exceeding 1 picosecond would be negative. This is in agreement with the observation by Grant and Sibbett[16] of a negative nonlinearity with a recovery time of approximately 1 picosecond . However, measurements performed by Hall *et al*[14] have shown that the index nonlinearity experienced by pulses of greater than 1 picosecond duration is positive. It is postulated that this discrepancy may be due to the fact that the carrier-heating nonlinearity and the quadratic Stark effect are linear and quadratic respectively with optical intensity. Thus, the sign of the cumulative nonlinearity in an amplifier may change with the intensity of the light coupled to it.

References

1 D. C. Hutchings, M. Sheik-Bahae, D. J. Hagan and E. W. Van Stryland, Opt. and Quant. Electron 24, 1, (1992)

2 M. Sheik-Bahae and E. W. Van Stryland, Phys. Rev. B. 50, 14171 (1994)

3 C. H. Henry, R. A. Logan and K. A. Bertness, J. Appl. Phys. 52, 4457 (1981)

4 J. Manning and R. Olshansky, IEEE J. Quantum Electron. QE-19, 1525 (1983)

5 B. R. Bennet, R. A. Soref and J. A. Del Alamo, IEEE J. Quantum Electron. 26, 113 (1990)

6 L. F. Tiemeijer, Appl. Phys. Lett. 59, 499 (1991)

7 A. D'Ottavi, E. Iannone, S. Scotti, P. Spano, J. Landreau, A. Ougazzaden and J. C. Bouley, Appl. Phys. Lett. 64, 2492 (1994)

8 J-M Halbout and C. L. Tang, Appl. Phys. Lett. 40, 765 (1982)

9 D. Cotter, C. N. Ironside, B. J. Ainslie and H. P. Girdlestone, Opt. Lett. 14, 317 (1989)

10 N. Finlayson, W. C. Banyal, C. T. Seaton, G. I. Stegeman, M. O'Neill, T. J. Cullen and C. N. Ironside, Opt. Lett. 14, 532 (1989)

11 M. J. LaGasse, K. K. Anderson, H. A. Haus and J. G. Fujimoto, Appl. Phys. Lett. 54, 2068 (1989)

12 C. T. Hultgren and E. P. Ippen, Appl. Phys. Lett. 59, 635 (1991)

13 K. L. Hall, A. M. Darwish, E. P. Ippen, U. Koren and G. Raybon, Appl. Phys. Lett. 62, 1320 (1993)

14 K. L. Hall, G. Lenz, A. M. Darwish and E. P. Ippen, Opt. Comm. 111, 589 (1994)

15 C. T. Hultgren, D. J. Dougherty and E. P. Ippen, Appl. Phys. Lett. 61, 2767 (1992)

16 R. S. Grant and W, Sibbett, Appl. Phys. Lett. 58, 1119 (1991)

Chapter 4

Intensity Dependence of the Transparency Current in InGaAsP Amplifiers

4.1 Introduction

In the preceding chapters the nonlinear mechanisms present in InGaAsP optical amplifiers were identified and quantified, and their effect on the refractive index and transmission of amplifiers biased at or close to transparency were measured. Both pump-probe transmission measurements and refractive index measurements were performed with pulses of approximately 100 fs duration. These ultrashort pulses were required to distinguish the nonlinearities through their different recovery times. However, the motivation behind the research described in this thesis was to assess the utility of InGaAsP amplifiers as optical switches, and it was therefore appropriate to perform experiments using pulses whose durations were such that the effect of nonlinearities on such pulses is instantaneous. The recovery time of the carrier-heating nonlinearity in such amplifiers has been reported in previous chapters to be less than a picosecond, and accordingly we were interested in switching pulses whose duration is 10 ps or more. To understand how the ultrafast nonlinearities in InGaAsP amplifiers could be exploited to perform optical switching, it is desirable to measure how the current required to bias an amplifier to transparency (transparency current) varies with the wavelength and intensity of a pulse propagating through that amplifier.

In this chapter, novel experimental measurements of the variation of the transparency current with the intensity of light coupled to various amplifiers are presented. The measurements, performed using bias-lead monitoring of the amplifier junction voltage, demonstrate considerable nonlinear variations of the transparency

current. Pump-probe transmission measurements, performed using ps duration pulses, illustrating the nonlinear mechanisms responsible for the variation of transparency current in a bulk amplifier are presented and discussed.

4.2 Background

4.2.1 Linear Transparency

When an amplifier is operating in a linear regime, the intensity of light propagating through the amplifier is low enough that the transmission of the light is not affected by saturation mechanisms or nonlinear mechanisms. In this regime, a pulse of light propagating through the amplifier will induce stimulated transitions of carriers between the conduction and valence bands of the amplifier. If the amplifier is biased such that a population invertion is produced, the pulse will cause more stimulated emissions than stimulated absorptions, and the number of electron hole pairs remaining in the active region of the amplifier will be reduced as a consequence of the propagation of the pulse. Conversely, if the amplifier is biased in the absorption regime, net stimulated absorption of the pulse will generate electron hole pairs in the active region. At transparency, the carrier density in the active region is such that the number of stimulated absorptions and stimulated emissions is equal, and there is no net change in the carrier density after propagation of the pulse.

As the intensity of the pulse coupled into an amplifier is increased, it begins to access nonlinear effects which will modify the forward bias required to achieve a zero net change of carrier density on propagation of the pulse. Those nonlinear processes which are expected to affect the ratio of stimulated absorptions and emissions are carrier-heating caused by free carrier absorption, and to a lesser extent two-photon absorption. Saturation of the gain/loss should not occur when amplifiers are biased at or close to transparency, and it is not expected that this or spectral hole burning will influence the transparency current. The effect of the above nonlinearities on the density of carriers in the active region of the amplifier is discussed below.

4.2.2 Opto-electronic Voltage Monitoring

To determine the effect of the propagation of a pulse through an optical amplifier on the density of carriers in the active region of that amplifier, it is necessary to monitor the population of carriers in that active region. This is done directly by measuring the opto-electronic voltage across the junction of the amplifier, a technique that is known as bias-lead monitoring. The use of the amplifier junction-voltage to monitor its carrier population is well known[1-3]. In 1990, Hall *et al.* used the bias-lead monitoring technique to perform a novel pump-probe experiment[4] which measured nonlinear dynamics of the carrier population of a bulk InGaAsP amplifier using femtosecond duration pulses generated using a colour-centre laser. The experiment revealed a strong junction-voltage transient with a recovery time of 650 fs which was attributed to carrier-heating (which has been measured to have a similar time constant using conventional pump-probe transmission measurements[5]).

Bias-lead monitoring is effected by connecting a lock-in detector to measure the voltage across the junction of an optical amplifier, and then modulating light coupled to the amplifier using a chopper which is referenced to the lock-in detector. The voltage measured by the lock-in detector across the junction of the amplifier is determined simply by the number of carriers in the active region of the amplifier. The lock-in detector is therefore able to make a comparison between the number of carriers in the active region of the amplifier, when there is light coupled into it and when the light is blocked by the chopper.

4.2.3 Detection of Optical Nonlinearities via Voltage Monitoring

As has been previously stated, the density of carriers in the active region of an amplifier which is not biased to transparency will be modified by the passage of light. If the amplifier is operating in the absorption regime, the number of carriers in the active region when light is present will exceed that when there is no light present. Thus, if a beam of light is modulated by a chopper, the light will modulate the number of carriers in the active region of the amplifier, and the voltage across the junction of the amplifier will be correspondingly affected. A lock-in detector arranged to detect the voltage across the active region of the amplifier, and referenced to the chopper, will measure

directly the modulation of the number of carriers in the active region of the amplifier. The sign of the modulation measured by the lock-in detector if the amplifier is operating at loss will be opposite to that measured if the amplifier is operating at gain. If the amplifier is biased to transparency, the number of stimulated emissions and absorptions induced in the amplifier by the light will be equal, the number of carriers in the active region will not be affected by propagation of the light, and no modulation of the voltage across the active region will be detected.

The free-carrier absorption mechanism will not affect the junction voltage of an amplifier directly because it is simply the excitation of carriers already existing in the active region of the amplifier to more energetic states, and does not increase the amount of charge in the active region. However, each free carrier absorption event corresponds to the absorption of the energy of one photon, energy which is thermalised via carrier-carrier scattering (with a time constant of approx. 50 fs) to the carrier distribution. As the energy of the carrier distribution is increased, the carrier distribution becomes smeared over a greater range of energies, and the occupancy of states at the lower ends of the conduction and valence bands is reduced. By virtue of the reduced occupancy of states at the lower end of the bands, light coupled through the amplifier which is of a wavelength close to the band-edge will experience a gain compression, and will have the effect of increasing the number of carriers in the active region of the amplifier. The heating effect caused by carrier-heating will thus be detected as an increase in the voltage across the junction of the amplifier.

The effect on the gain coefficient of an increase of the carrier temperature in a InGaAsP amplifier is shown in Figure 1.[6]

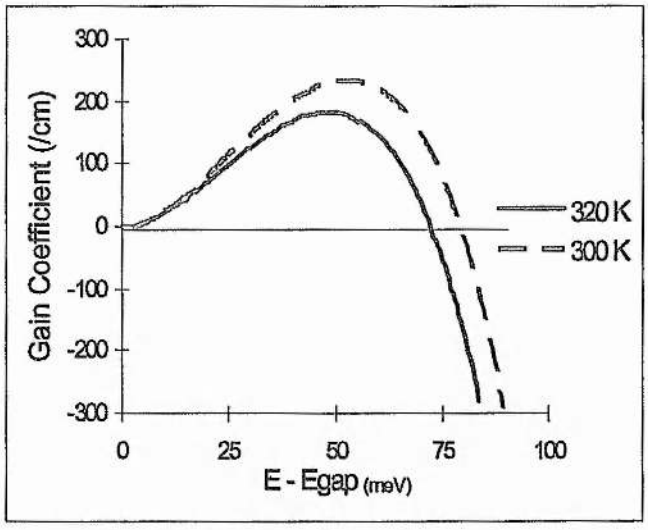

Figure 1. Calculated gain curves versus excess energy above the band-gap for a bulk amplifier with carrier temperatures of 320 K (solid line) and 300 K (dashed line).

Two-photon absorption is obviously an absorption mechanism, and as such will lead to the creation of carriers and an increased junction voltage. Its effect is two-fold because it also contributes heat to the carrier distribution leading to further compression of the gain and additional creation of carriers.

Spectral hole burning is a saturation of a transition and will oppose the effect of gain or loss saturation in an amplifier.

The amplifier junction voltage measured using the bias-lead monitoring technique is averaged over time. Thus, the signal detected across the junction of an amplifier during the propagation of pulsed light from a laser will correspond to the carrier density in that amplifier averaged over a time which is long compared to the duration of the pulses from the laser, and long compared to the time elapsed between pulses. Because the duration of optical pulses incident on the amplifier will be orders of magnitude less than the time between the pulses, the instantaneous effect of the pulses on the carriers will not be measured by the bias-lead monitoring technique. Rather, it is the long-term effect of the pulses on the density of carriers, which recovers in approximately 1 ns, which is detected.

4.3 Experiments

4.3.1 Experimental Setup

The experimental configuration used to measure intensity-dependent variations of the transparency current in various InGaAsP optical amplifiers is illustrated in Figure 2.

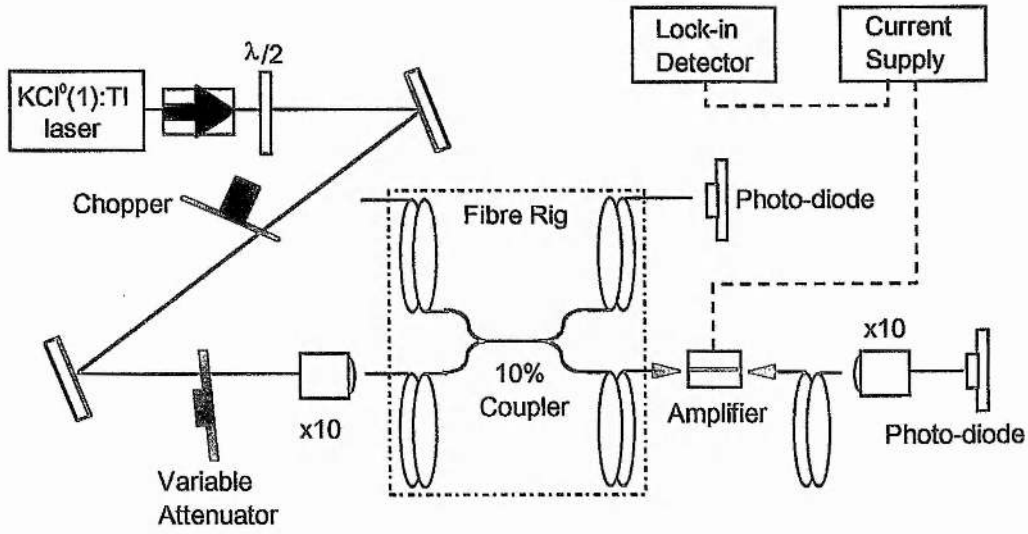

Figure 2. Experimental setup used to measure the intensity dependence of the transparency current in optical amplifiers.

The KCl:Tl^0(1) colour-centre laser shown in Figure 2 was pumped synchronously by an acousto-optically modelocked Nd:YAG pump laser to produce pulses with a duration of ~12 ps. The beam of pulses produced by the laser was passed through an isolator to reduce feedback from the experiment into the laser cavity, and through a half-wave plate which was used to control the linear polarisation of the pulses used in the setup.

The beam was modulated by a chopper which was referenced to a lock-in detector, and then passed through a neutral density attenuator wheel before being incident at a x10 microscope objective, from which it was coupled to a fibre rig. The fibre rig comprised of a fibre coupler which split off approximately 10% of light coupled to it, the remaining 90% being coupled, via a fibre lens, to the optical amplifier under investigation. The optical power that was incident from the fibre lens to the front facet of the amplifier was calibrated from the fraction of light that was transmitted by

the 10% arm of the coupler. The splitting ratio of the fibre coupler was wavelength dependent, and a calibration of that wavelength dependence was used to ensure that the incident power was correctly calculated. Coupling from the amplifier to the fibre lens was estimated by increasing the forward bias to the amplifier until it oscillated, and then comparing the total light emitted by the input facet of the amplifier with that which was coupled through the fibre lens. Using this method, the coupling efficiency of the fibre lens was estimated to be 33%. Coupling of light to and from the amplifier was monitored using a second fibre lens coupled to the output facet of the amplifier, and measuring the transmission from the amplifier using a photo-diode.

4.3.2 Results for 4 QW and 8 QW amplifiers

The experimental setup described above was used to determine the intensity dependence of transparency currents in amplifiers containing 4, 8, and 16 quantum wells (4 QW, 8 QW and 16 QW amplifiers), and also in a bulk amplifier. The 4 QW and 8 QW amplifiers were of similar structure, and both contained InGaAs wells 8 nm thick, separated by InGaAsP barriers of 10 nm thickness. The 16 QW amplifier contained InGaAs wells of 6.5 nm thickness, separated by InGaAsP barriers 8 nm thick; and the bulk amplifier contained an InGaAsP active region 180 nm thick.

The intensity dependence of the transparency current that was measured for the 4 QW and 8 QW amplifiers conformed to that which was expected, and these results are discussed in this and the following section. The results obtained using the 16 QW and bulk amplifiers were more complex, and these are presented and discussed in section 4.3 of this chapter.

The plots in Figure 3 show the transparency current in milliamps measured for the 4 QW and 8 QW amplifiers as a function of the intensity of continuous wave (CW) light and pulsed light of the same average power.

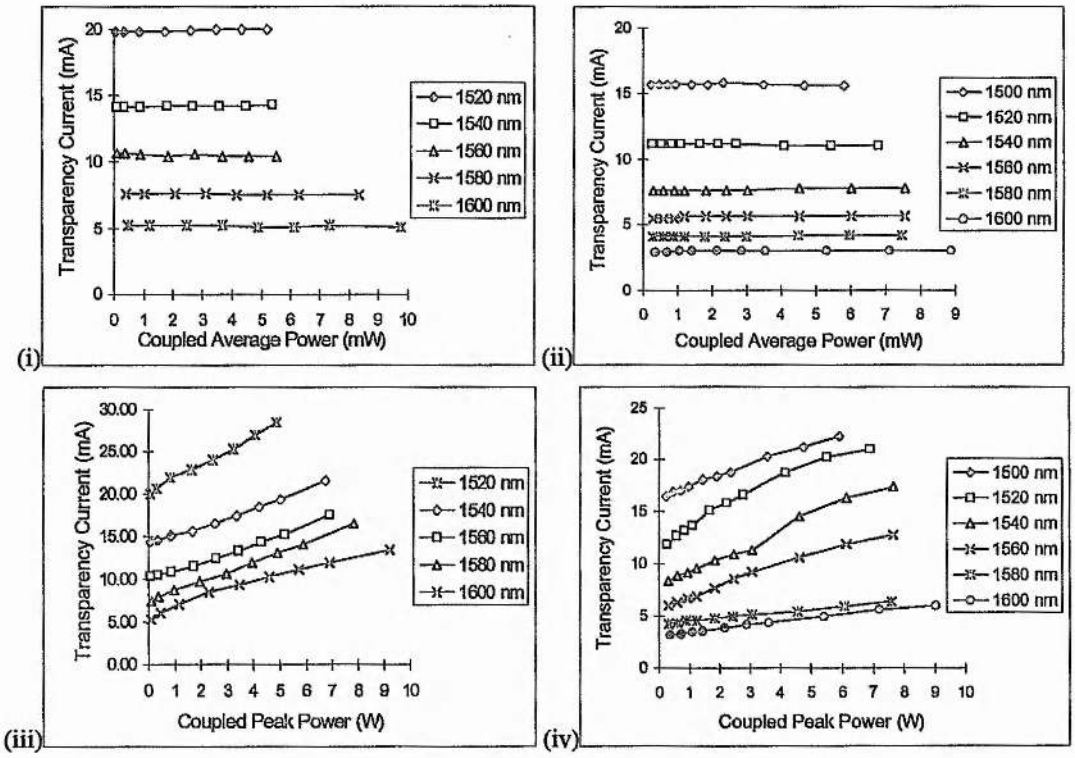

Figure 3. Transparency current measured for CW light in a 4 QW (I) and an 8 QW (ii) amplifier, and for pulses of ~10 ps duration in the same 4 QW (iii) and 8 QW (iv) amplifiers.

Each measurement of the transparency current was performed by first adjusting the power of the pulses coupled to the amplifier under investigation using the variable attenuator wheel, and then adjusting the bias to that amplifier until the lock-in detector indicated that there was no modulation if the carrier density in the active region of the amplifier caused by the propagation through it of the modulated light from the KCl:Tl^0(1) laser. These measurements were discrete and are marked as points on the plots in Figure 3. The lines connecting the set of points obtained for each wavelength of incident light are intended as a guide to the eye and they have no physical significance.

The transparency current measurements were performed at various wavelengths at intervals of 20 nm over the tuning range of the KCl:Tl^0(1) laser. From the plots in Figure 3 it is clear that the transparency current is wavelength dependent. This is due to the increasing number of carriers interacting with the coupled light as its wavelength is reduced and it reaches higher into the conduction and valence bands of the amplifiers. As the wavelength of the coupled light gets shorter, the bias to an

amplifier must be increased to maintain equality between the number of stimulated emissions and stimulated absorptions which are induced by the light.

There is no detectable variation of transparency current in the amplifiers as the power of CW light coupled to them is increased (plots (i) and (ii) of Figure 3). This was expected and is due to the fact that the intensity of the light coupled to the amplifiers is not sufficient to cause a significant number of nonlinear interactions.

Plots (iii) and (iv) indicate that there is a marked variation of the transparency current in the amplifiers when high intensity pulsed light is coupled to them. From comparison of plots (iii) and (iv) with plots (i) and (ii), it is clear that the variation of the transparency current is caused by an intensity dependent effect and is not related to the average power of the light coupled to the amplifiers.

As expected, the transparency current observed for the coupled pulses at low powers is the same as that observed for CW light of the same wavelength. As the intensity of the pulses coupled to the amplifiers is increased, the transparency current increases in a generally linear manner. The cause of this linear increase of the transparency current in the 4 QW and 8 QW amplifiers will be discussed in the next section where more detailed results obtained using an 8 QW amplifier are presented.

4.3.3 Results for 8 QW Amplifier

The experiment described in section 4.2 above was repeated at a later date using a modified experimental setup to obtain further information on the nature of the intensity dependence of the transparency current. The motivation behind this experiment was to use the technique of coherent-photon seeding[7] (CPS) to control the duration of pulses generated by a NaCl:OH^- colour-centre laser. Using the coherent-photon seeding technique it was possible to control the duration of pulses coupled to an optical amplifier whilst keeping the average optical power constant, and this allowed a novel measurement of the intensity dependence of the transparency current to be performed.

The setup that was used for this experiment is illustrated in Figure 4.

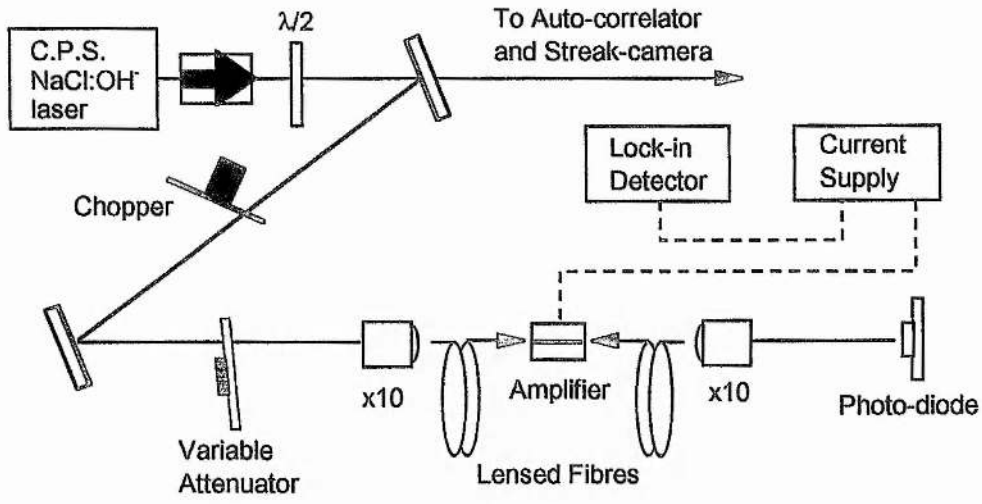

Figure 4. Experimental setup of a second investigation of intensity dependence of transparency current, using a NaCl:OH⁻ colour-centre laser.

The NaCl:OH⁻ colour-centre laser was used in preference to the KCl:Tl^0(1) colour-centre laser used in the previous experiment because it is more suited to CPS by virtue of its upper-state lifetime (150 ns[8]). The duration of pulses produced by the NaCl:OH⁻ laser was adjusted from a minimum of 10 ps to a maximum of 30 ps by varying the length of the cavity of the laser. It was not possible to monitor the duration of the longer pulses produced by the laser using a scanning auto-correlator, and a synchro-scan streak-camera was used in conjunction with an auto-correlator to provide monitoring of the pulses from the laser over the 10 - 30 ps range of durations. Coupling to the 8 QW amplifier of the light generated by the laser was performed using an anti-reflection coated x10 microscope objective and a single lensed fibre. The lensed fibre was used in preference to the fibre rig described in section 4.2 to provide the additional bench space required to accommodate the optical beams needed to operate the streak-camera. A lensed fibre was coupled to the output facet of the amplifier to allow continuous monitoring of the coupling of the first lens to the amplifier.

Plots of the transparency current versus intensity of incident light obtained using the above described experiment as shown in Figure 5.

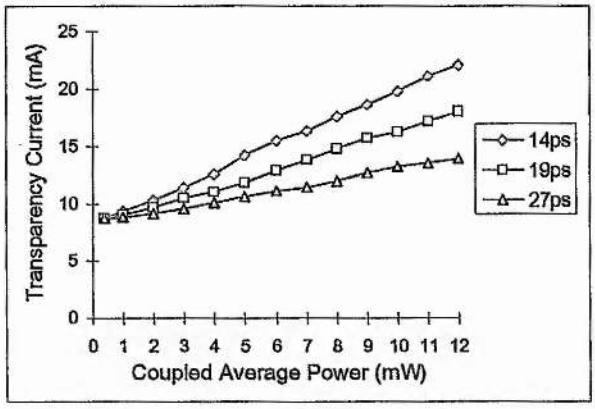

Figure 5. Transparency current of an 8 QW amplifier plotted against coupled average power for beams of pulses of 14, 19 and 27 ps duration at a wavelength of 1540 nm.

Figure 5 shows the transparency current plotted against the average power of pulsed light at 1540 nm coupled to an 8 QW amplifier whose construction was identical to that used in the experiment described in section 4.2 (the first one was destroyed). The transparency current has a linear dependence with respect to the coupled average power, with a gradient dependent upon the duration of the pulses (i.e. the intensity of light) coupled to the amplifier. The linear nature of these results does not agree entirely with the results presented for the other 8 QW amplifier in section 4.2 of this chapter, where the points obtained do not follow a linear relationship. This discrepancy is attributed to the difficulty in maintaining a constant duration of the pulses from the KCl:Tl^0(1) laser, and the consequent variation of the intensity of light coupled to the amplifier. The duration of the pulses obtained from the coherently-seeded NaCl:OH^- laser was very stable, and the linear dependence of the transparency is therefore believed to be accurate.

In order to confirm that the transparency current was entirely linear with intensity, the transparency current data of Figure 5 was plotted as a function of peak coupled power. The gradients of the lines connecting the points for each set of results obtained with 14, 19 and 27 ps duration pulses are identical within experimental error, and the transparency current is therefore linear with intensity.

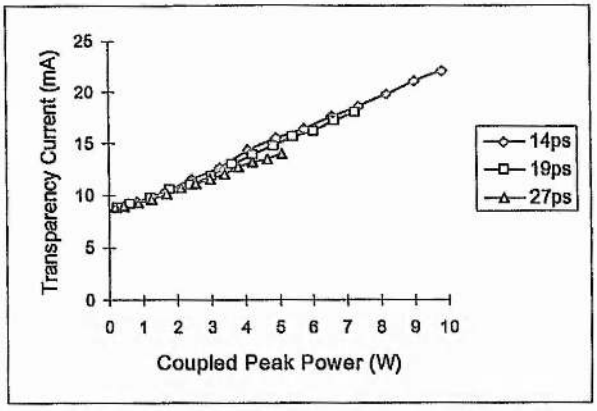

Figure 6. Transparency current of an 8 QW amplifier plotted against coupled peak power for beams of pulses of 14, 19 and 27 ps duration at a wavelength of 1540 nm.

The linear dependence of the transparency current with respect to the intensity of coupled light indicates that the origin of the observed variation in the transparency current cannot be due to two-photon absorption, which has a quadratic dependence on intensity. Saturation of inter-band transitions is also discounted as a possible cause of the intensity dependence of the transparency current as there are by definition no net inter-band transitions taking place in an amplifier which is biased to transparency.

It is postulated that the intensity dependence of the transparency current is due to the effect of free-carrier absorption on the temperature of the carrier distribution in the conduction band of the amplifier. The effect of heating the carrier distribution, as discussed in section 4.1, is to smear the distribution of carriers in the bands of an amplifier, reducing the occupancy of states at the wavelength of the incident light and causing gain compression. To compensate for this gain compression it is necessary to increase the bias to the amplifier to increase the density of carriers in the bands of the amplifiers such that the probability of a photon inducing a stimulated emission once again becomes equal to the probability of the photon inducing a stimulated absorption. Free-carrier absorption has a linear intensity dependence, which is in agreement with the results shown in Figure 6.

Further confirmation that the intensity dependence of the transparency current in the 8 QW amplifier is caused by heating of the carrier distribution is obtained by reducing the duration of pulses coupled to the amplifier until they are comparable to the recovery time of the heated carrier distribution (~1 ps). Figure 7 shows results

obtained for the 8 QW amplifier for incident light at three different wavelengths and with pulse durations varying from 30 ps to 10 ps.

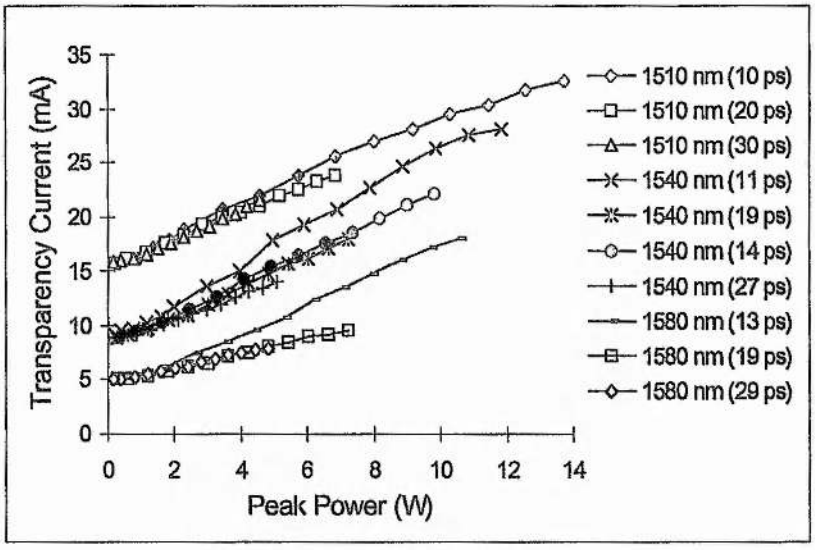

Figure 7. Transparency current of an 8 QW amplifier plotted against coupled peak power for beams of pulses of 10 - 30 ps duration at various wavelengths.

From Figure 7 it can be seen that the rate of increase of the transparency current with intensity is constant for pulses whose duration is well in excess of the recovery time of the carrier-heating effect. However, as the duration of the pulses is reduced to ~10 ps, the gradient of the transparency current as a function of coupled peak power increases. This is because the temperature of the carrier distribution ceases to follow adiabatically the profile of the pulse propagating through the amplifier, the gain compression caused by heating the carrier distribution being correspondingly increased. The variation of gradient with pulse duration seen in Figure 7 demonstrates that the intensity dependent transparency current cannot be due to an instantaneous nonlinearity.

Although it would have been instructive to perform the above experiment using pulses with a duration shorter than 10 ps, at the time the experiment was carried out there were no suitable sources available.

4.3.4 16 Quantum well and Bulk amplifier results

The results presented thus far in this chapter were obtained using a 4 QW and an 8 QW amplifier of similar construction. The transparency current in these amplifiers was linearly dependent on intensity, and this variation was explained as being due to heating of the carrier distribution in the active region of the amplifiers via the absorption of free carriers. The experimental measurements of the variation of transparency current in a bulk amplifier and a 16 QW amplifier are presented in this section (the structure of these amplifiers is described in section 4.2).

The experimental setup used to measure the transparency current was identical to that described in section 4.2 of this chapter. A reproduction of the Figure showing the experimental setup is shown below.

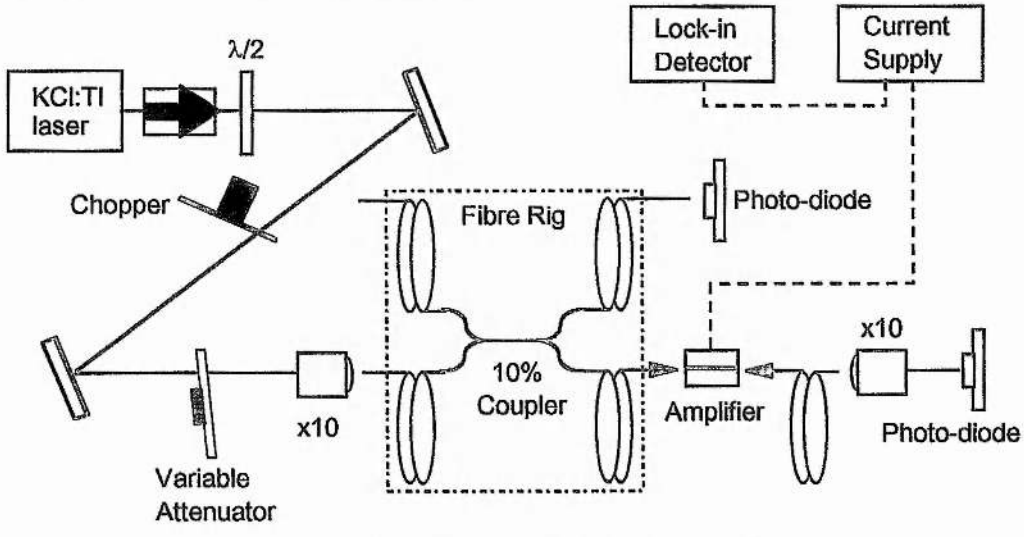

Figure 8. Experimental setup used to measure intensity dependence of the transparency current in a 16 QW and a bulk amplifier

The transparency current in the 16 QW and bulk amplifiers was monitored as before by chopping the light coupled to the amplifier and monitoring the voltage across the junction of the amplifier using a lock-in detector. Results obtained using pulses of ~12 ps duration from the KCl:Tl^0(1) laser are shown in Figure 9.

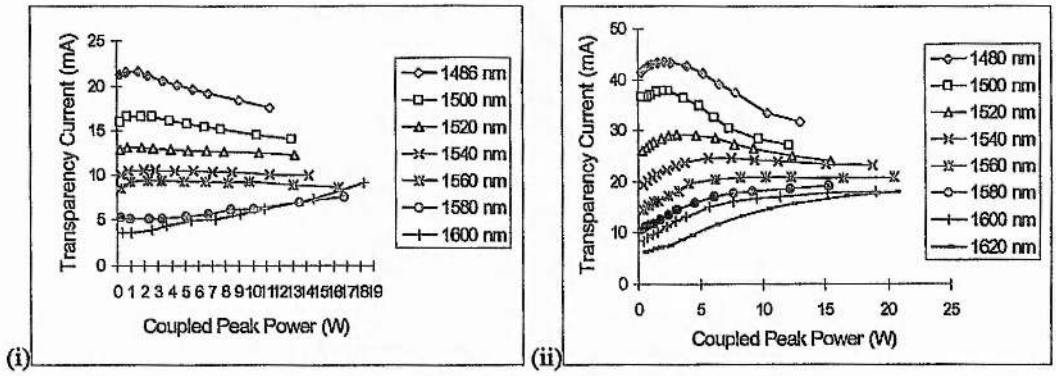

Figure 9. Intensity dependence of the transparency current in a 16 QW amplifier (i), and in a bulk amplifier (ii).

It can be seen from the plots in Figure 9 that the intensity dependence of the transparency current in the 16 QW and bulk amplifiers was very different to that seen for the 4 and 8 QW amplifiers. The gradient of increase of the transparency current varies considerably with intensity and wavelength, and furthermore, at short wavelengths and high coupled peak powers the transparency current decreases as the coupled intensity is raised.

The beginnings of a theoretical model based on a density matrix description of the semiconductor[9] and following the framework developed by Mark and Mork in their analysis of gain dynamics in InGaAsP amplifiers[10], was developed by Davies at B.T. labs to simulate this nonlinear transparency current variation. However, although the model was able to show that the transparency current was intensity dependent, no set of parameters were found that would cause the gain of an amplifier to rise as the optical intensity coupled to the amplifier was increased.

One physical mechanism which would lead to an intensity-dependent increase in the density of carriers available to interact with light coupled to an amplifier is cooling of the carrier distribution. Carrier cooling will occur when the light coupled to an amplifier removes carriers whose temperature is above the average temperature from the active region of the amplifier. An equivalent effect will occur if carriers whose energy is below the average energy are created. However, because the investigations described in this chapter are concerned with amplifiers which are biased to transparency, neither of these mechanisms can arise.

4.3.5 Picosecond Pump-Probe Measurements

In an attempt to obtain further insight on the behaviour of the transparency current in the bulk amplifier, a pump-probe transmission experiment was devised to measure the transmission by the amplifier of 25 ps pulses. The pump-probe setup used was identical to that described in chapter 2, except that the KCl:Tl^0(1) laser used was actively modelocked by pumping it synchronously with a Nd:YAG laser, as opposed to the coupled-cavity modelocked KCl:Tl^0(1) laser used in the pump-probe experiments of chapter 2.

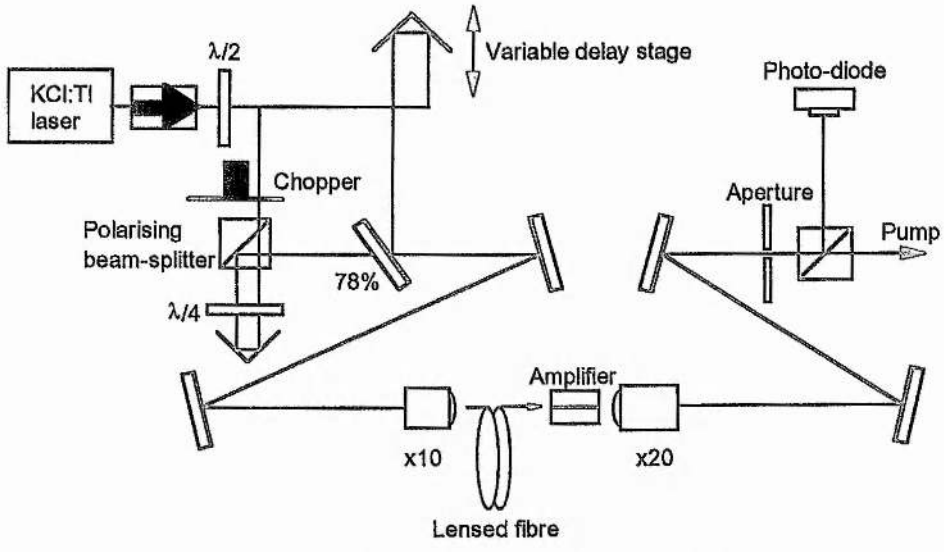

Figure 10. Setup of the pump-probe transmission experiment used to measure the transparency current in a bulk amplifier.

Using the experimental setup depicted in Figure 10, pump-probe measurements of the transmission of the bulk amplifier were performed with pulses of 25 ps duration at 1500 nm, 1540 nm and 1580 nm for a range of pulse intensities. It was intended to examine the resulting transmission curves for discrepancies between the transmission of the amplifier at low intensities and long wavelengths, and the transmission at high powers and short wavelengths. It was also intended to measure the current required to bias the amplifier to transparency by comparing the transmission of the probe pulse before and after the arrival of the pump pulse.

Transmission curves obtained using the bulk amplifier with ps duration pulses are shown below in Figure 11.

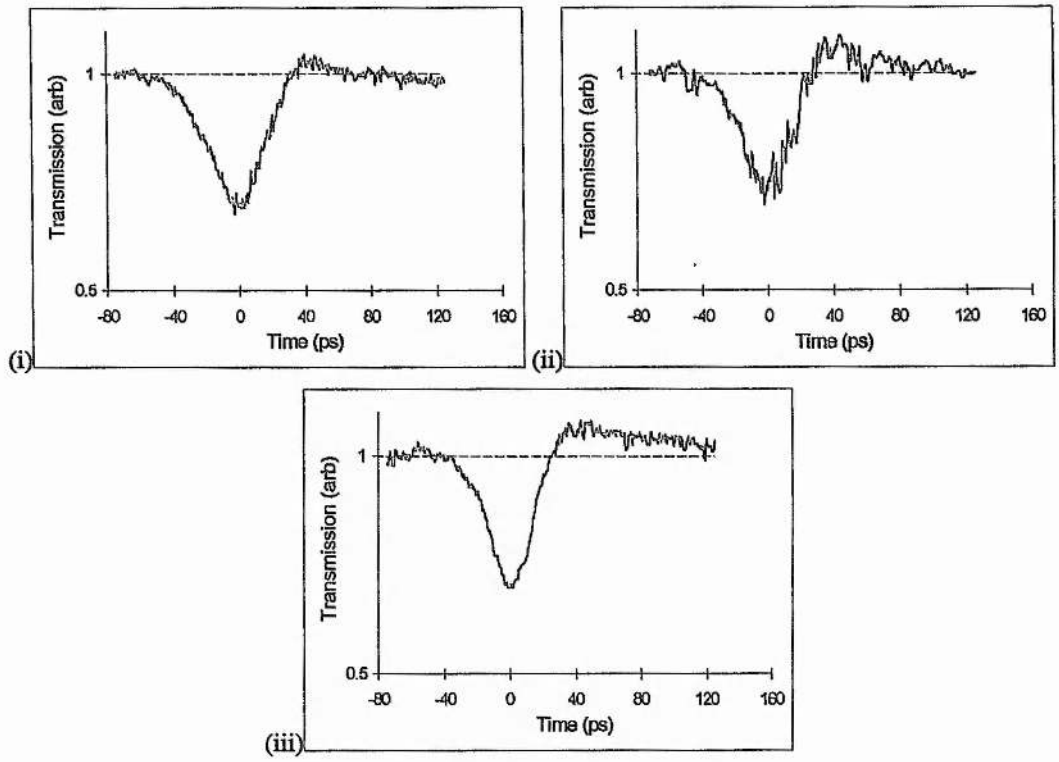

Figure 11. Pump-probe transmission profiles for a bulk amplifier at 1500 nm (i), 1540 nm (ii) and 1580 nm (iii)

All of the transmission measurements shown in Figure 11 were obtained using incident pulses of 1.6 W peak power (44 pJ). The dip in each transmission curve centred around time equals zero (where the pump and probe pulses overlap) is caused by heating of the carrier distribution as a result of excitation of free carriers by the pump pulse. The downward slope of the dip caused by heating of the carrier distribution follows the profile of the pump pulse. However, the gradient of the up-slope is enhanced compared to that of the down-slope, and the carrier-heating dip is clearly not symmetric about time equals zero. This is due to the gain provided to the second half of the pulse by the heated carrier distribution as it cools from its maximum temperature (at time equals zero) through the emission of LO-phonons. This is a dynamic process, with some carriers being excited by photons in the trailing portion of the pulse, but the general trend of the temperature of the carrier distribution is downwards, and the resulting increase in the gain experienced by the second half of the pulse leads to the steeper recovery of the gain compression. The peak of transmission seen at the top of the carrier-heating dip is also caused by this effect, with the tail of

the probe pulse being heated by carriers which were heated by the pump pulse as they return to the lattice temperature.

An unexpected property of the transmission curves is that none of them return to a constant transmission after the propagation of the pump-pulse. It was expected that by biasing the amplifier to transparency it would be possible to obtain a transmission curve which essentially followed the profile of the pump pulse auto-correlation and recovered to a constant transmission (the slow recovery time associated with inter-band transitions being avoided). The motivation behind this experiment was to set the transparency current using the transmission curves by comparing the transmission of a probe pulse before and after the transmission of a puma pulse, and varying the bias to the amplifier until the two transmissions were equal. Unfortunately, it was not possible to set the transparency current using this method because, as is evident from plot(i) of Figure 11, the transmission of the amplifier did not behave as expected. The transmission of the bulk amplifier at 1500 nm in plot(i) recovers after the propagation of the pump pulse to a level slightly above its initial value, but then starts to decrease at a steady rate with a time constant too long to be measured using the experimental setup. This slow change of transmission cannot be explained as the carrier density recovering to the level that it was at prior to the arrival of the pump pulse because it is tending away from that initial value. It is clear that the properties of the amplifier have been modified in such a way that its transmission is decreasing at a steady rate away from its equilibrium value.

It is the opinion of the author that the anomalous behaviour of the transmission of the bulk amplifier may be an effect of the heat which is added to the amplifier by the free-carrier absorption mechanism. If the heated carrier distribution were to 'bottle-neck' it would be unable to return to the temperature of the lattice of the amplifier with the normal ~1 ps recovery time and may have an effect with a much longer time constant on its transmission.

It is clear that if the slow reduction in transmission seen in the plots of Figure 11 is associated with a decrease in the number of carriers in the active region of the amplifier, then this would be detected as a modification of the junction voltage measured across the amplifier using the lock-in detector as described earlier in this chapter. A reduction in the carrier density is the effect that would occur if a pulse was

coupled through the amplifier when it was operating in gain. Thus, the slow decrease in transmission observed in the pump-probe transmission traces would necessitate a reduction in the current supplied to the amplifier to return it to the transparency bias as measured by the lock-in detector.

There is little in the transmission plots of Figure 11 to differentiate between the effects observed at 1500, 1540 and 1580 nm, particularly in view of the fact that a carrier-density induced step may inadvertently have been included in the 1540 and 1580 nm transmission curves. However, if a mechanism which leads to carrier recombination due to heating of the amplifier lattice is the cause of the decrease in transmission, then this could explain the wavelength and intensity dependence of the transparency current curves shown for the bulk amplifier in section 4.3. This is because the amount of heat added to the amplifier by free carrier absorption will increase as the wavelength of light decreases and the number of carriers in the active region needed to bias the amplifier to transparency increases. It should be emphasised that, because this is a slow effect, its effect on the signal detected by the lock-in amplifier (which is averaged over time) will be enhanced.

4.4 Summary and implications for nonlinear switching

The intensity dependence of the transparency current in InGaAsP optical amplifiers, one with a bulk active region, and three with active regions containing variously 4, 8, 16 quantum wells has been measured. To the best of the author's knowledge, this measurement has not been previously performed.

The variation of the transparency current in the 4 QW and 8 QW amplifiers has been shown to be linear with intensity for pulses with durations in excess of 10 ps. The increased gradient of the intensity dependence of the transparency current as the duration of pulses incident on the amplifiers was reduced below 10 ps indicates that the effect responsible for the intensity dependence is not instantaneous, and furthermore it has a time constant of less than a few picoseconds. The evidence suggests that the transparency current in the 4 QW and 8 QW amplifiers is a result of gain compression caused by heating of the carrier distribution from free-carrier absorption (it has been shown that heating the carrier distribution reduces the occupancy of states adjacent to

the band edge, thereby reducing the gain of the amplifiers at the wavelengths used for the experiments described in this chapter).

The transparency current in the 16 QW and bulk amplifiers had an anomalous behaviour with respect to the intensity of incident light. The variation of the transparency current measured varied in gradient and sign as a function of both intensity and wavelength. An attempt to explain this dependency by performing pump-probe investigations of the transmission of the bulk amplifier using ps regime pulses showed that a slow negative transient was present. This transient was not due to the recovery of the carrier density distribution to an equilibrium value because the sign of the transmission variation was such that it was tending away from the equilibrium transmission of the amplifier. It was suggested that the slow negative change in transmission was connected to the effect on the bulk amplifier of the heat added to the amplifier by absorption of the pump pulse via free-carrier absorption. This slow negative transient was of the correct sign to explain the anomalous transparency current variations seen in the bulk and 16 QW amplifiers, but did not appear to have the correct wavelength dependency. Further work is required to explain these results completely. A calculation of the effect on a carrier distribution of adding heat through free-carrier absorption would perhaps provide an insight into the intensity dependence of the transparency current described in this chapter.

The strong intensity dependence of the transparency current in the amplifiers has important implications for the use as all-optical switches of optical waveguides biased to transparency. A waveguide which is biased to transparency for one intensity of light may not be operating at transparency for light coupled to it at a different intensity. This important point requires further investigation, although spectral evidence presented in Chapter 5 of this thesis demonstrates that the effect on the ultrafast switching capabilities of amplifiers operating in this regime may be minimal.

Monitoring the voltage across the junction of an optical amplifier has been demonstrated to be an effective method of determining whether an amplifier is biased to transparency. This simple technique could be used to automatically maintain the bias to switching devices at the transparency point in future communications systems. The finding that the transparency current in some waveguide structures may tend to a

consant level further enhances the potential applicability of the nonlinearity at transparency in optical switching devices.

References

1 A. Apling, B. Bentland and S. T. Eng, Electron. Lett. **20**, 794 (1984)

2 W. B. Joyce and R. W. Dixon, J. Appl. Phys. **49**, 3719 (1978)

3 Y. Mitsuhashi, J. Shimada and S. Mitsutsuka, IEEE J. Quantum Electron. QE-17, 1216 (1988)

4 K. L. Hall, E. P. Ippen and G. Eisenstein, Appl. Phys. Lett. **57**, 129 (1990)

5 K. L. Hall, J. Mark, E. P. Ippen and G. Eisenstein, Appl. Phys. Lett. **56**, 1740 (1990)

6 K. L. Hall, G. Lenz, A. M. Darwish and E. P. Ippen, Opt. Comm. **111**, 589 (1994)

7 G. J. Valentine, G. T. Kennedy and W. Sibbett, paper CThl38, Conference on Lasers and Electro-Optics, Baltimore 1995

8 G. T. Kennedy, Ph.D. Thesis, 1993

9 M. Asada, M. Yamada and Y. Suematsu, JARECT **17**, 12 (1985-86)

10 J. Mark and J. Mork, Appl. Phys. Lett. **61**, 2281 (1992)

Chapter 5

Optical Switching

5.1 Introduction

In the preceding chapters, refractive index nonlinearities in optical amplifiers that have been forward biased to operate at transparency have been examined. The primary objective of this investigation was to determine the suitability of the nonlinearities for possible application in all-optical switching. In this chapter the results of two experiments which demonstrate optical switching in the transparency regime for two different switching geometries are presented

In the first part of the chapter, the technique of producing optical switching via intensity-dependent polarisation rotation is discussed. Transmission curves obtained from a bulk amplifier exploited in this way are presented, with a discussion of how best to optimise the operation of the switch. The second part of the chapter deals with switching in a nonlinear directional coupler, and the relevant theory thereof.

5.2 The Polarisation Rotation Switch

5.2.1 Introduction

Polarisation rotation is observed when light with linear polarisation is launched into a waveguide whose TE and TM axes have different refractive indices. If the light is launched at some angle relative to the axes of the waveguide, the TE and TM fields of the light in the waveguide will experience unequal refractive indices. At the exit of the waveguide, one field will be retarded relative to the other, and there will be a phase

difference between them. The combined polarisation of the two transmitted fields will in general be an elliptical state. If the refractive index of the waveguide has an intensity dependent component, the phase difference induced between the TE and TM fields on propagation through the waveguide will also be a function of the intensity. An intensity dependence has thereby been introduced to the polarisation of the light transmitted by the amplifier. Therefore, by arranging polarisation elements at the output of the amplifier to block the transmission of coupled light at low intensities, it is possible to create a switch that will discriminate between low intensity and high intensity optical signals.

The conversion of intensity-dependent polarisation into intensity-dependent transmission was first demonstrated in 1982 by Stolen *et al.*[1] using a birefringent optical fibre. They described their experimental setup as an intensity discriminator, indicating that it could be used for the separation of intense subpicosecond duration pulses from low intensity pedestals generated from soliton pulse compressors.

Following on from the idea of an intensity discriminator, Katayama *et al.*[2] used the same principle to produce a fibre-optic logic device operating as an AND gate, with a very high contrast between *on* and *off* states. In common with other optical fibre switches the AND gate required a long interaction length (11m) to accumulate sufficient phase shift to switch between states.

More recently, there has been considerable interest in optical switching in semiconductor waveguides, favoured for their small dimensions, large nonlinearities and potential for integration with electronic circuitry and semiconductor lasers. One of the techniques of optical switching which has been demonstrated in semiconductor waveguides is polarisation rotation[3-6].

The first polarisation rotation gates demonstrated using semiconductors were constructed from AlGaAs and GaAs/AlGaAs multiple quantum well waveguides[3-5]. These switches operated below half the bandgap of AlGaAs (typically at 1.55 μm), exploiting the resonant enhancement of the ultra-fast third order susceptibility whilst avoiding two-photon absorption. The virtual nonlinearity utilised by the switches gave them switching times of the order of hundreds of femtoseconds, fast enough for even the most ambitious of telecommunications applications, but the peak powers required

for operation (typically in excess of 100 W) are prohibitively large for practical device implementations.

More recently, Day *et al.*[6] have constructed a low power polarisation gate in a passive InGaAsP multiple quantum well waveguide operating at 1.53 μm, using a carrier-enhanced nonlinearity. The energy of the photons at 1.53 μm was just below the bandgap of the well material. Electron-hole pairs formed through the absorption of photons at this wavelength caused a nonlinear change in the refractive index via bandfilling and the plasma effect. The different effective band-edges for TM and TE polarised light in the waveguides gave a greater change of refractive index for TE light than for TM light, facilitating the construction of the polarisation switch. The system was estimated to have a switching time of the order of 20 ps, and required a coupled peak power of 350 mW.

We have constructed a low power polarisation switch[7], operating via the above-band gap nonlinearity in amplifiers biased to transparency which has been described in previous chapters. As has been shown, the time constant for this nonlinearity is of the order of a few ps. The peak optical power required to produce switching was of the order of 1 W.

5.2.2 Theory

The most efficient angle of polarisation at which to launch light into a polarisation switch is determined by the relative size of the refractive index nonlinearity in each axis of the waveguide, and the power of the coupled light. The power transmitted by the polarisation switch depends upon the phase shift induced in the waveguide, and the angle between the polarisation of the incident light and the principle axes of the waveguide. This can be expressed[1] as

$$P_t = P_o \cdot \mathrm{Sin}\left(\frac{\phi}{2}\right)^2 \cdot \mathrm{Sin}(2\theta) \qquad (1)$$

where P_0 is the incident power, P_t is the transmitted power, and θ is the angle of polarisation of the coupled light relative to the x axis. The phase shift ϕ between the x and y components of light is given by

$$\phi := \frac{2\pi L}{\lambda}\cdot\left(n_x - n_y\right) \qquad (2)$$

where L is the length of the waveguide, λ is the wavelength of the light, and n_x and n_y are the intensity dependent components of the refractive indices of the x and y axes of the waveguide respectively.

For any given coupled intensity of light, reducing the angle of the coupled polarisation (θ) will increase the size of the TE component relative to the TM component, increasing the phase difference between the TE and TM fields. However, the above expression indicates that reducing the angle θ will decrease the transmission of the system. Stolen *et al.*[1] discussed this trade-off in their paper using the case of a lossless birefringent fibre. In the birefringent fibre, the intensity dependent phase shift between the TE and TM fields has a $\cos(2\theta)$ dependency. They determined that, for a required phase shift of π radians, a switching efficiency of 50% can be achieved using only 1.41 times the minimum power if the incident light is launched at 22.5^0. A switching efficiency of 99% will occur for a launching angle of 42^0, but will require 10 times the minimum incident power.

The angular dependence of the switching efficiency is complicated in the case of semiconductor waveguides because of the difference in the confinement factor for the TE and TM modes. Furthermore, coupling to the waveguide via the coupling optics is likely to be different for the TE and TM modes. Consequently, an experimental approach was used to find the best switching efficiency in the setup described below.

5.2.3 Experiment

A polarisation switch was constructed using the experimental configuration illustrated in figure 1. A KCl:Tl^0(1) laser was synchronously modelocked by a CW acousto-optically modelocked Nd:YAG laser to generate pulses of ~20 ps duration at 1530 nm, with a repetition rate of 82.2 MHz. These pulses from the laser were passed through an optical isolator to ensure that there was no feedback from the experiment into the laser cavity. A calibrated half-wave plate rotated the polarisation of the pulses to an angle measured relative to the plane of the optical bench (TE). The pulses passed

through a variable neutral-density filter wheel before being coupled into an optical amplifier using a x20 microscope objective. Two of the coupling mirrors were partially transmitting. The transmission through the first mirror was directed to an SHG autocorrelator to allow continuous monitoring of the pulse duration. Light transmitted by the second mirror was incident on a germanium photodiode, which gave a calibrated measurement of the power incident on the facet of the amplifier.

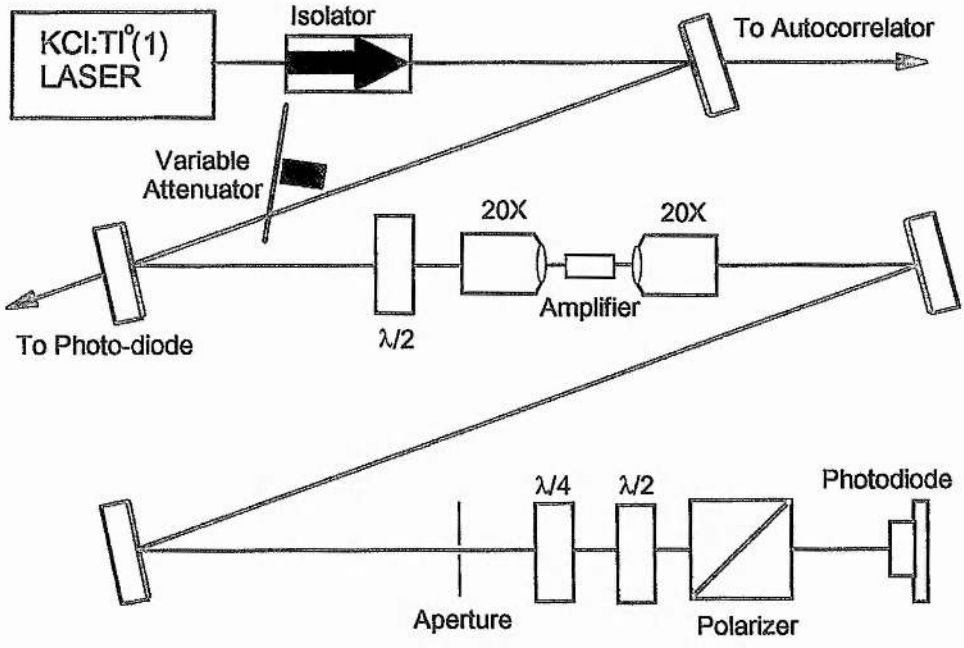

Figure 1. Configuration of polarisation switch experiment.

Light transmitted by the optical amplifier was collected using a second x20 microscope objective and focused through an aperture situated approximately 1 m away from the objective. The aperture selected only the guided mode from the amplifier and prevented the detection of unguided light. Bulk optics were used in preference to the optical fibre lenses that had been used in other experiments because they preserved the polarisation of the coupled light and thus gave a better extinction ratio between TE and TM polarisations.

A quarter-wave plate and a half-wave plate were placed after the aperture to linearise and rotate the polarisation of light transmitted by the amplifier. A polarising beam-splitter, the element that converts the intensity dependent rotation of polarisation to intensity dependent transmission, was placed after the half-wave plate. The beam-

splitter was arranged to allow the transmission of TE light onto a second calibrated germanium photodiode.

A forward bias was applied to the optical amplifier such that it was operating at transparency at the wavelength of the pulses generated by the laser. The transparency current was determined by referring to results from previous experiments. At low intensities of coupled light, with the neutral density filter set to maximum attenuation, the quarter-wave plate was arranged to linearise transmission from the amplifier, and this linearly polarised light was rotated by the half-wave plated such that its transmission by the polarising beam-splitter was minimised. As the intensity of light coupled to the amplifier was increased, the polarisation of the transmitted light was rotated. The component of the transmission whose polarisation was perpendicular to the low intensity transmission passed through the polarising beam splitter and was detected by the photodiode.

The two photodiodes were connected via a linear amplifier box to the X and Y channels of a digital storage oscilloscope. The timebase on the oscilloscope was set at two seconds per division so that a full traverse of the screen occurred in eight seconds. By slowly rotating the neutral density wheel it was possible to ramp the power incident at the amplifier, and record in real time the input and output powers detected by the photodiodes. Once the data had been recorded, they were transferred to a computer where the transmitted power was plotted as a function of incident power. This method of measuring the switching power was advantageous because it recorded many more data points than could be acquired using an x-y plotter, enabling comprehensive averaging which reduced noise on the resulting curves.

Having recorded a measurement of the power transmitted by the polarising beam-splitter (effectively the first channel of the switch) for a given set of experimental criteria, the photodiode was moved to measure the power reflected by the beam-splitter (effectively the second channel of the switch) under the same conditions.

5.2.4 Results

The amplifier used as a polarisation switch was a bulk amplifier, 0.5 mm in length having a 180 nm thick InGaAsP active region. The power transmitted by the

switch was measured for coupled incident polarisation at an angle of 20^0 relative to the TE axis. Two sets of measurements were taken, the first using CW light and the second using pulses of 20 picoseconds duration. The average power coupled to the amplifier was the same for both measurements. Figure 2 shows the transmission curves obtained under these conditions. In this and all subsequent figures the open boxes represent light reflected by the polarising beam-splitter (TM), and the black diamonds represent light transmitted by the beam-splitter (TE).

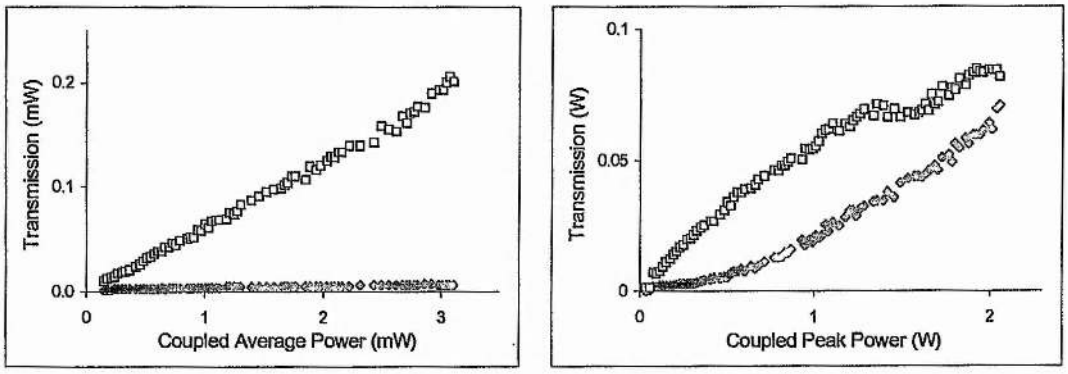

Figure 2. Transmission of bulk amplifier polarisation switch for CW (left), and 20 ps pulses (right) with the same average intensity.

The transmission of CW light by the switch is a straight line. This indicates that there was no rotation of polarisation at these low input intensities and also confirms that the amplifier was operating at transparency (through the absence of any curvature indicating absorption saturation or loss saturation). The transmission of the 20 picosecond pulses is clearly intensity dependent, with the TE and TM transmissions initially curving away from each other and then curving back the other way at high intensities.

A more informative view of these results is obtained by plotting the normalised transmission of each channel of the switch against the incident power as shown in Figure 3.

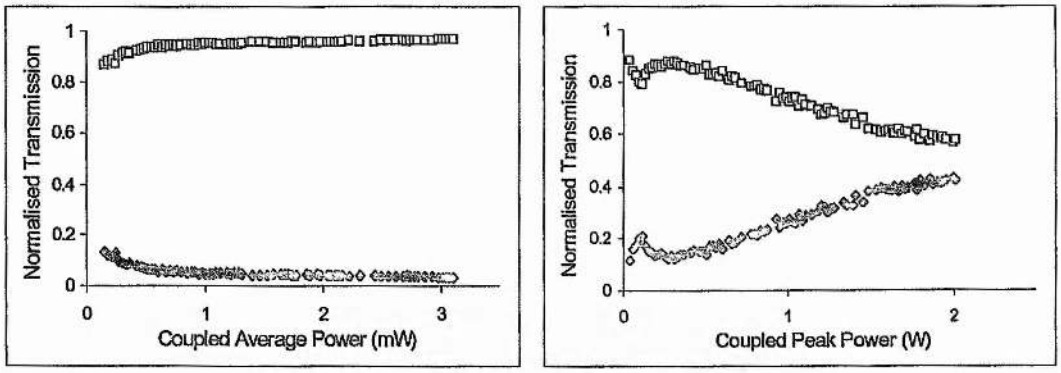

Figure 3. Normalised transmission of bulk amplifier polarisation switch for CW (left) and 20 ps pulses (right).

The normalised transmission curves enhance the contrast between the nonlinear transmission, which leads to partial switching, and the linear transmission. In both plots of Figure 3, the normalised transmission tends towards 0.5 at low coupled powers as the unpolarised spontaneous emission from the amplifier becomes a significant portion of the signal detected by the photodiode. The discontinuity in transmission of the 20 picosecond pulses at very low powers arose as a result of blocking the output from the amplifier in order to verify that the zero of the detection system was correctly set.

The maximum switching efficiency possible for light launched into a polarisation switch with its polarisation at 22.5 degrees is 50%, and indeed, in the second graph of figure 3, the normalised transmissions of the two channels can be seen tending towards this value at high coupled incident powers. In fact, the transmission curves are tending towards a value less than 50%. This is because the coupling of light into the TE mode is more efficient than the coupling to the TM mode, effectively reducing the angle of the polarisation coupled to the amplifier.

The strength of the nonlinearity producing the intensity dependent phase shift in the amplifier determines the angle of incident polarisation required to achieve the maximum possible switching efficiency for any given coupled power. In order to find this optimum angle transmission curves were obtained for angles of incident polarisation from zero to 0 degrees in steps of 10 degrees. The results obtained for incident polarisations of 10, 20, 30 and 40 degrees are shown in figure 4.

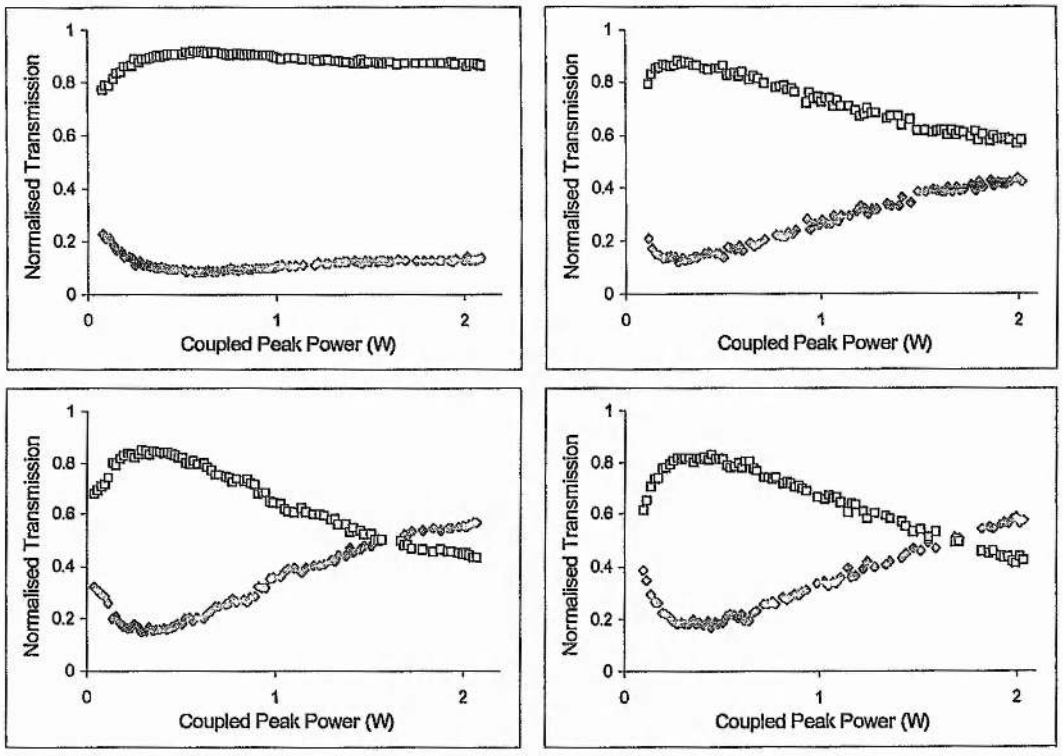

Figure 4. Transmission of the bulk amplifier polarisation switch for incident polarisations increasing from 10 degrees (top left) to 40 degrees (bottom) in steps of 10 degrees

The first graph of figure 4 shows the normalised transmission of the switch with the incident light polarised at 10 degrees. The transmission of TE polarised light by the switch can be seen to rise to a maximum at a coupled peak power of around 1.5 W, beyond which the transmission stays constant. This corresponds to a maximum of the $\sin^2(\phi/2)$ term from equation (1) as discussed in section 5.2.2 of this chapter. As the angle of the incident polarisation is increased, the maximum efficiency of the switch increases as expected. However, the transmission of the switch no longer reaches a maximum because the difference between the phase shifts induced by the TE and TM fields does not reach π radians. The transmissions of the switch for incident light polarised at 30 and 40 degrees were very similar, and the maximum switching efficiency was found to lie somewhere between the two. In practice, varying the angle of incident polarisation between these two values did not produce an appreciable difference in the response of the system. This was in part due to the limitation in accuracy of the orientation of the half-wave plate at the input of the amplifier.

The efficiency of the switch for incident light polarised at 40 degrees reached 60% for a maximum coupled input power of 2.1 W. The crossover point of the switch was at 1.7 W (1.6 W for 30 degrees launch), corresponding to a coupled average power of less than 3 mW. The proportion of incident optical power transmitted by the switch was ~ 5%, the rest of the power being lost through absorption and scattering losses in the amplifier.

This result demonstrates switching at optical powers that are orders of magnitude less than those required for a similar experiment in passive AlGaAs waveguides[3]. Whilst the power requirement is greater than that reported by Snow *et al.* from their passive InGaAsP waveguide polarisation switch, the speed of operation is significantly faster.

5.3 The Nonlinear Directional Coupler

5.3.1 Introduction

If two identical optical waveguides are placed in close proximity with one another, the evanescent field associated with light propagating through one of them will overlap into the other. The overlap of the field from the first waveguide results in a transfer of power into the second. The exchange of power between these two synchronously coupled waveguides is periodic with a 'beat length' characterised as being the length over which the power transfers from the first waveguide to the second, and then back to the first. If the waveguides have an intensity-dependent refractive index, the phase matching condition between them will be altered for the propagation of high intensity light. A sufficiently large refractive index nonlinearity will decouple the waveguides, preventing any transfer of power between them. If the waveguide geometry is chosen so that the coupled region extends over half a beat length, then low intensity light launched into the first waveguide will be coupled into the second, whereas high intensity light will not couple between the waveguides and will remain in the first. This form of optical switch is known as a nonlinear directional coupler (NDC).

The first description of a nonlinear directional coupler (then termed a nonlinear coherent coupler) was presented as a conference paper by Jensen[8] in 1980. This was followed in 1982 with a full theoretical model of the operation[9] of the NDC based on the coupled mode theory of Yariv[10]. The paper discussed the potential for realising extremely fast switching times using an NDC, emphasising the fact that the interaction of fields in the device is both spatially and temporally localised, allowing the simultaneous processing of a stream of pulses.

The first demonstration of all optical switching in a semiconductor NDC was observed by Li Kam Wa *et al.*[11] in 1984. The refractive index nonlinearity used in the multiple quantum well GaAs/GaAlAs structure was the result of excitonic absorption saturation. The pulses used in the experiment were not short enough to resolve the recovery time of the switch, but since it utilised a carrier enhanced nonlinearity this is likely to have been of the order of a few nanoseconds. The power required to observe switching was ~ 1 mW, and the NDC was held in a cryostat at a temperature of 180 K. In the time since this demonstration, NDC's in AlGaAs structures using excitonic or Kerr-like nonlinearities have evolved considerably[11-15].

Current state of the art AlGaAs NDC's have been demonstrated both multiplexing[16] and demultiplexing[17] operations at 1.55 μm with pulse durations as short as 600 fs. These devices operate just below the two-photon band edge, avoiding two-photon absorption, but taking advantage of the resonant enhancement of the Kerr nonlinearity at that wavelength. To avoid coupling very high peak powers into the devices, which would lead to considerable three photon absorption, the NDC's are designed to have a long interaction length (~2 cm), spreading the nonlinear interaction along the length of the device and reducing the maximum peak power required to obtain switching. A high bit-rate demonstration of these devices has not been performed, because the colour-centre laser used to generate the pulses used has a repetition rate of 76 MHz. However, the nonlinearity utilised in the devices is effectively instantaneous, and bit-rates in excess of 1 THz are theoretically possible.

Nonlinear directional couplers that are switched by external means (for example, a modulation of the bias to the NDC) do not fall within the scope of this thesis. However a description of a recent switching experiment performed using such a device will illustrate the state of the art in that field. The refractive index of one of the

guides in a InGaAlAs/InAlAs multiple quantum well coupler was modified by putting a variable reverse bias across it, moving the peak of the heavy-hole exciton absorption. Using this technique light at 1549 nm was switched at a rate of 10 Gbit/s in a fully packaged system with an error rate of 1 bit per second.[18]

5.3.2 Theory

Light propagating in one channel of a linear directional coupler can be described by:

$$P(Z)_1 := P(0)_1 \cdot \frac{1 + \mathrm{Cos}(2Z)}{2} \qquad (3)$$

where $P_1(0)$ is the power coupled into that channel and $P_1(Z)$ is the power in the channel at a distance Z along the coupler from the input facet. A similar expression for the second channel of the coupler conserves the total power propagating along the coupler. Power in the coupler oscillates from one channel to the other, the period of this oscillation being determined by the overlap of the two fields in the channels. The period, or 'beat length', can be controlled by varying the separation of the channels in the coupler.

Equation (3) is limited in that it only applies when all of the light in the coupler has been launched into one channel. It is also limited because it only describes linear interactions in a coupler, the more general case which takes account of nonlinear coupling is:

$$P(Z)_1 := P(0)_1 \cdot \frac{1 + \mathrm{cn}\left(\frac{2Z}{m}\right)}{2} \qquad (4)$$

where

$$m := \frac{P(0)^2}{\left(P_c\right)^2} \qquad (5)$$

and cn(2Z/m) is a Jacobi elliptic function with a period K(m), and P_c is the critical power relating to the coupling of the guides. Below this power, increases of the coupled input intensity lead to an increase in the period (beat length) of the coupler. Above the critical power the refractive index in the channel carrying the high intensity

light is altered to the extent that coupling between the two channels is lost, and power is not to transferred to the second channel.

A graphical representation of the analytic solutions produced by Jensen[8] of light propagating in a nonlinear directional coupler is shown in Figure 5.

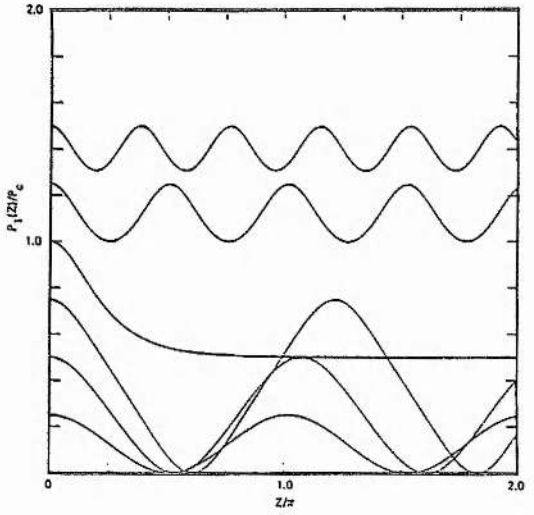

Figure 5. Optical power in a first channel of a directional coupler (measured as a fraction of the critical power P_c) plotted as a function of its position along the length of the coupler (measured as the beat length z of the coupler divided by π).

Figure 5 shows a number of curves representing the optical power in one channel of a directional coupler as it propagates along the coupler. The period of the oscillation of power to and from the first channel of the coupler is clearly intensity dependent. Optical power well below the critical value P_c is coupled between the channels of the coupler with a period of z/π. As the intensity of light in the channel is increased, the period of the coupling is increased. When the power in the channel reaches the critical value P_c, optical power is no longer completely coupled from the channel, but rather reaches a stable intermediate level. For powers in excess of the critical value, only a fraction of the optical power switches between the channels of the coupler.

Nonlinear directional couplers used as optical switches are cleaved to be half of the beat length z/π so that, at low intensities, the power coupled into one channel is transferred to the other at the output of the device. This maximises the contrast with the high intensity transmission, where all of the light remains in the original channel.

5.3.3 Experiment

BT supplied four nonlinear directional couplers 1 mm long, with epitaxial structure comprising six InGaAs wells separated by InGaAsP barriers. The ridges that formed the waveguides for the two channels were of a range of thickness from 1.5 μm to 3 μm, with separations also ranging from 1.5 μm to 3 μm.

The experimental configuration used to investigate the switching properties of the couplers is shown in figure 6. An NaCl:OH$^-$ colour-centre laser was synchronously pumped using a CW acousto-optically modelocked Nd:YAG laser to produce pulses of approximately 20 ps duration, at 1520 nm. Pulses from the laser were coupled into and out of the NDC using lensed fibres adjusted by piezo-electric controllers. When the output from the laser was blocked, it was possible to distinguish between the two channels of the coupler by forward biasing it, and adjusting the position of the lensed fibres to maximise the spontaneous emission coupled through them. In this way, it was possible to choose either a bar state (measuring transmission from the same channel as the incident light) or a cross state (measuring the transmission from the other channel) of the coupler.

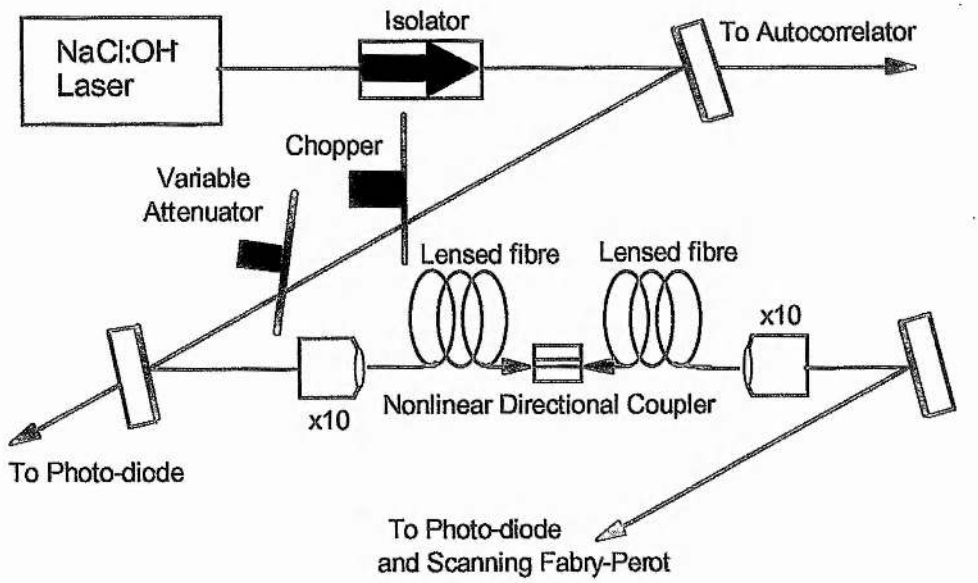

Figure 6. Configuration of nonlinear directional coupler switch experiment.

A mirror with 88% reflectivity on the input side of the configuration allowed calibrated measurement of the power incident on the coupler using a germanium

photodiode. The power transmitted by the coupler was measured using a second photodiode. Both of the signals detected were recorded and plotted, the incident power along the X axis, and the transmitted power along the Y axis. Power incident on the coupler was ramped from a minimum to a maximum using a rotatable neutral density wheel. The duration of the pulses from the NaCl:OH^- laser (which was stabilised by coherent-photon seeding) were continuously monitored using an autocorrelator.

5.3.4 Results

A preliminary investigation of the spectra transmitted by the coupler for varying intensities of coupled light was performed using a scanning Fabry-Perot interferometer. The spectra obtained showed that a peak coupled power of ~ 7 W was required to produce self-phase modulation in the NDC corresponding to a $3\pi/2$ phase shift. For pulses of 22 ps duration, this corresponded to an average power of ~ 40 mW incident on the front facet of the coupler. The input facet of one of the NDC's was damaged by incident light at this high intensity, the damage seemingly caused by heating of the facet. Accordingly, a chopper wheel with a transmission ratio of 1 in 5 was placed in the beam incident on the coupler, allowing high intensities to be coupled to the NDC's without damaging the facets. Because the incident and transmitted light measured by the photodiodes was chopped, it was not possible to use the storage-oscilloscope method of measurement described in the first half of this chapter. Instead, an XY-plotter was used, which had a response time considerably less than the modulation of the chopped beam and thus averaged the detected powers.

To set the forward bias to the NDC's such that they were operating at transparency, the optoelectronic voltage across them was measured with a lock-in amplifier (using the method described in chapter 3 of this thesis). However this method was rather inaccurate at the relatively high currents that were required to reach transparency in the couplers (~100mA). Consequently, the forward bias was set using a second method which involved monitoring the transmission by the cross and bar states of the coupler for incident CW light. A plot of the transmitted power against incident power demonstrated whether the coupler was operating at loss (concave

transmission curve), gain (convex transmission curve) or transparency (the transmission is a straight line).

All of the couplers were cleaved to be 1mm long, and as such, were not necessarily the half beat length required to demonstrate all optical switching. Four different couplers had been supplied, each with different channel widths and separations. The low power transmission of all of the couplers was investigated to see which of them had the greatest contrast of transmission between the cross and the bar states (the cross state carrying the majority of the power). A coupler with channels 2.5 μm wide, separated by a 2.5 μm gap gave the best result and was chosen to demonstrate optical switching.

The transparency current of the coupler was found to be 105 mA. Pulses of 22 ps duration at 1530 nm were coupled into one channel of the coupler, and the transmission curves shown in Figure 6 were recorded for the bar and cross transmission channels.

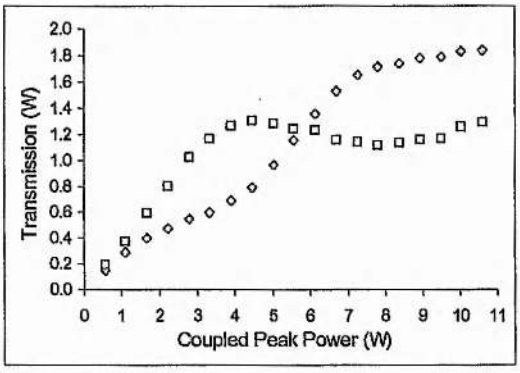

Figure 6. Transmission of the bar and cross states of the nonlinear directional coupler.

The transmission of the coupler is clearly nonlinear. Switching by the coupler is better illustrated by plotting the normalised transmission of the cross and bar states as shown in figure 7.

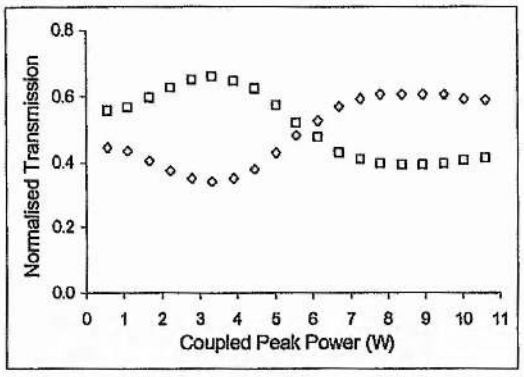

Figure 7. Normalised transmission of the bar and cross states of the nonlinear directional coupler.

In figure 7, the transmission of the cross state is represented by the squares, and that of the bar state is represented by the black boxes. The curves are not the same as those normally associated with nonlinear directional couplers, where the cross and bar states begin at a maximum and minimum respectively. This is because, as was previously mentioned, the NDC did not extend for half a beat length long, but was actually a little longer. The results shown in figure 7, indicate that as the incident power was increased from zero to three Watts, the effective beat length of the NDC was increased, and a larger proportion of the transmission came from the cross state, until the cross coupling was maximised. The beat length of the NDC continued to increase until the incident power reached the critical level (~ 7 W) above which the light was permanently confined in the bar state.

The poor contrast between the transmission of the two states was a result of the fibre lenses not coupling light exclusively into the required channel, but also coupling a lesser amount of light into the second channel. The reduction in contrast at high intensities was seen because the nonlinearity did not switch the low intensity wings of the propagating pulses.

The coupled incident power required to reach the crossover point of the transmission from the two channels was ~ 5.8 W. This high value (in comparison with the results obtained using the polarisation switch) was due to the ridge structure of the NDC, which increased the size of the propagating optical mode, reducing the intensity of light in the active region and lowering the nonlinear refractive index change induced by a given coupled incident power. The total optical power transmitted by the NDC was approximately 30 % of that which was coupled to it. Attenuation of power on

propagation through the NDC could be reduced by lowering the doping levels in the cladding regions. A buried heterostructure NDC would provide better confinement of the mode in the active region, and would require less power to achieve optical switching.

To verify that the NDC's were exhibiting ultrafast switching (and were not merely switching the high intensity pulses and then recovering with a time constant of a few nanoseconds), spectra of pulses transmitted by both the cross and bar states were recorded using a scanning Fabry-Perot interferometer as shown in figure 8.

The vertical line marked on each of the spectra shown in figure 8 represent the peak of the low power transmission. The spectra are generally symmetric about this line, indicating that the nonlinear refractive index change causing the phase shift is not due to absorption saturation or gain saturation, but rather is equally strong on both sides of the propagating pulse. This confirms that the switching seen in the directional coupler was indeed the result of an ultrafast effect. Further confirmation that the switching observed was ultrafast could be obtained by performing a pump-probe experiment on the directional coupler using 100 fs pulses.

The spectra in figure 8 also bear out the earlier suggestion that the switching of high intensity pulses is incomplete, with the propagation of the low intensity wings of the unaffected by the intensity-dependent refractive index. This is shown in the lowest two spectra of figure 8, where the transmission of the bar state shows a broad $5\pi/2$ phase shift, with the cross state transmitting the remaining low intensity unmodulated central wavelength with a slightly broadened pedestal.

These results represent a considerable improvement over the partial optical switching demonstrated by Davies and co-workers (including the author) in an InGaAsP NDC biased to transparency in 1993.[19]

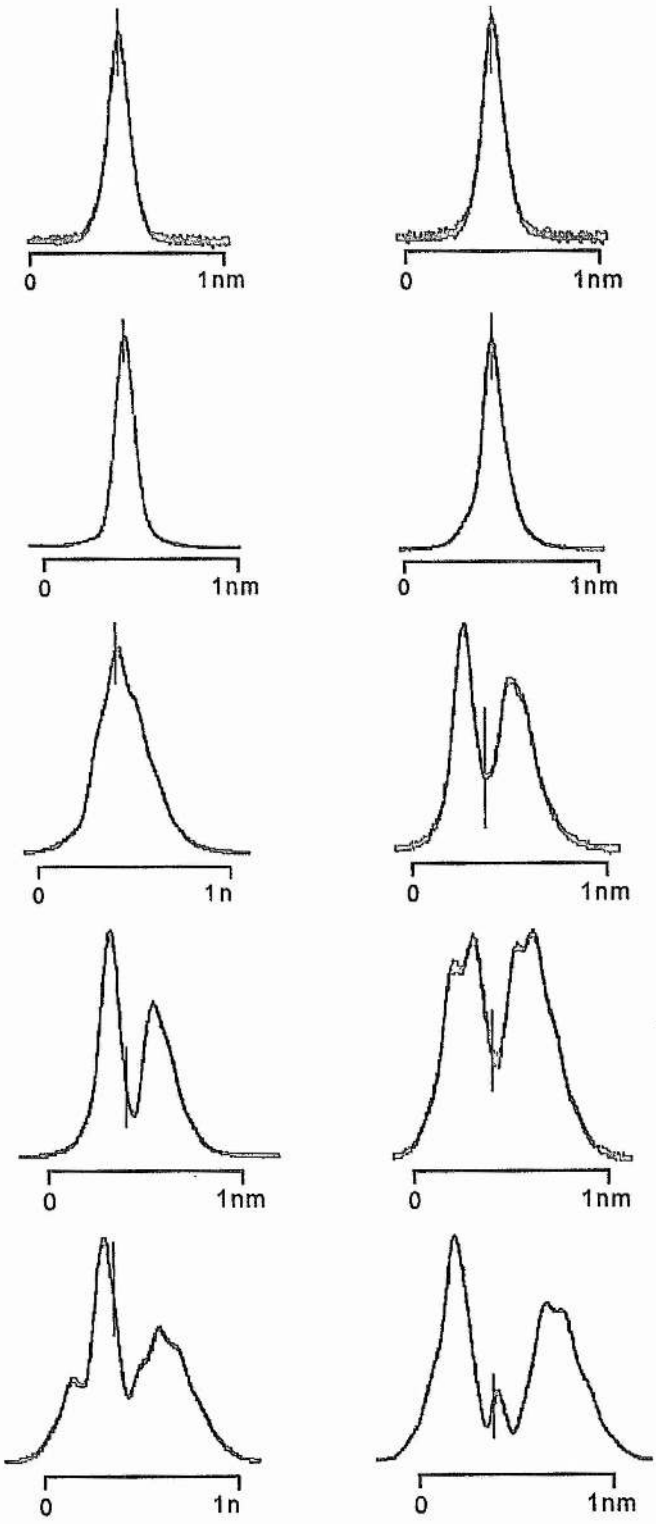

Figure 8. Transmission spectra from the cross (left hand column) and bar (right hand column) states of the NDC. The peak power coupled to the NDC was 0.1, 3.3, 6.7, 10 and 13.4 W reading down the page.

5.4 Summary

Ultrafast optical switching of 20 ps duration pulses at a wavelength of 1530 nm has been demonstrated in a bulk InGaAsP amplifier operating in a polarisation switch geometry, and biased to transparency. Switching between the TE and TM modes of the switch occurred with a crossover point corresponding to 1.6 W of coupled peak power. The intensity-dependent polarisation state arose from the different confinement factors of the TE and TM modes in the amplifier and corresponding differences in refractive index nonlinearities experienced by the modes.

Ultrafast switching was also demonstrated in a nonlinear directional coupler for 20 ps pulses at a wavelength of 1520 nm. The directional coupler consisted of two ridge guides, each 2.5 μm wide and containing six quantum wells, separated by a gap of 2.5 μm. The crossover point in the nonlinear directional coupler corresponded to 5.8 W of coupled peak power.

The experiments presented in this chapter demonstrate all-optical switching of picosecond regime pulses at intensities of coupled light which are orders of magnitude less than that required in previously published experiments (for example refs 6 and 15). The reduction in optical intensity required to perform all-optical switching opens up the possibility of switching light generated by semiconductor lasers, and the future integration of monolithic integrated switching structures and sources.

References

[1] R. H. Stolen, J. Botineau and A. Ashkin, Opt. Lett. 7, 512 (1982)

[2] K. Katayama, Y. Kimura and S. Seika, Appl. Phys. Lett. 46, 317 (1985)

[3] P.A. Snow, I. E. Day, I. H. White, R. V. Penty, H. K. Tsang, R. S. Grant, Z. Su, W. Sibbett, J. B. D. Soole, H. P. Leblanc, A. S. Gozdz, N. C. Andreadakis and C. Caneau, Electron. Lett. 28, 2346 (1992)

[4] C.C. Yang, S. Villeneuve, G. Stegeman, C. Lin, H. Lin and I. Chiou, Technical Digest of Ultra-Fast Phenomena Conference (1993) Paper MA2-1

[5] P. A. Snow, I. E. Day, R. V. Penty, G. T. Kennedy, W. Sibbett and J. S. Aitchison, Technical Digest of Ultra-Fast Phenomena Conference (1993) Paper TuC5-1

[6] I. E. Day, P. A. Snow, Z. Jiang, R. V. Penty, I. H. White, D. A. O. Davies, M. A. Fisher and M. J. Adams, Electron. Lett. 30, 1050 (1994)

[7] P. D. Roberts, G. T. Kennedy, W. Sbbett, D. A. O. Davies, M. A. Fisher and M. J. Adams, Conference on Lasers and Electro-Optics (1995) Paper CFB2

[8] S. M. Jensen, Conf. Integrated and Guided-Wave Optics, Incline Village, CA, 1980.

[9] S. M. Jensen, IEEE J. Quantum. Electron., QE-18, 1580 (1982)

[10] A. Yariv, IEEE J. Quantum. Electron., QE-9, 919 (1973)

[11] P. Li Kam Wa, J. E. Sitch, N. J. Mason, J. S. Roberts and P. N. Robson, Electron. Lett. 21, 26 (1985)

[12] R. Jin, C. L. Chaung, H. M. Gibbs, S. W. Koch, J. N. Polky and G. A. Pubanz, Appl. Phys. Lett. 53, 1791 (1988)

[13] J. S. Aitchison, A. H. Kean, C. N. Ironside, A. Villeneuve and G. I. Stegeman, Electron. Lett. 27, 1710 (1991)

[14] A. Villeneuve, C. C. Yang, P. G. J. Wigley, G. I. Stegeman, J. S. Aitchison and C. N. Ironside, Appl. Phys. Lett. 61, 147, (1992)

[15] K. Al-hemyari, A. Villeneuve, J. U. Kang, J. S. Aitchison, C. N. Ironside and G. I. Stegeman, Appl. Phys. Lett. 63, 3562, (1993)

[16] J. U. Kang, G. I. Stegeman and J. S. Aitchison, Electron Lett. 31, 118, (1995)

[17] A. Villeneuve, K. Al-hemyari, J. U. Kang, C. N. Ironside, J. S. Aitchison and G. I. Stegeman, Electron. Lett. **29**, 721, (1993)

[18] T. Ito, M. Kohtoku, N. Yoshimoto, K. Kawano, S. Sekine, M. Yanagibashi and S. Kondo, Electron. Lett. **30**, 1936, (1994)

[19] D. A. O. Davies, M. A. Fisher, D. J. Elton, S. D. Perrin, M. J. Adams, G. T. Kennedy, R. S. Grant, P. D. Roberts and W. Sibbett, Electron. Lett. **29**, 1710, (1993)

Chapter 6

General Conclusions

An in-depth study of the effect of the dependence of structure on the nonlinearities in InGaAsP optical amplifiers has been presented in this thesis. Femtosecond-regime measurements of refractive index dynamics, and picosecond and femtosecond measurements of transmission dynamics were performed variously on a bulk amplifier and amplifiers containing four, eight and sixteen quantum wells (4 QW, 8 QW and 16 QW). The pump-probe transmission measurements, described in Chapter 2, were analysed by fitting a transmission function with terms representing each of the nonlinear transmission effects present in the amplifiers. With this curve-fitting method it was possible to attribute distinctive separate contributions to transmission curves resulting from carrier heating, two-photon absorption, stimulated absorption/recombination and delayed thermalisation of the carrier distribution. Although the curve-fitting function used was empirical in origin and not based upon a theoretical model, it was nonetheless a useful tool for the comparison of transmission curves obtained from the amplifiers.

A comparison was performed of the carrier-heating terms and two-photon absorption transmission terms obtained from the 4 QW, 8 QW, 16 QW and bulk amplifiers when they were biased to the transparency point. The results showed clearly that there was a correlation between the magnitude of the carrier-heating effect and the number of quantum wells in the amplifiers (or the thickness of the active region in the case of the bulk amplifier). Carrier-heating was predominantly caused by the creation via free-carrier absorption of highly excited carriers and their subsequent thermalisation with the carrier distribution. The overlap of the optical mode with free-carriers in the active region of the amplifiers depends upon the thickness of the active region and the confinement factor of the mode, and these factors were used to explain the carrier-heating effect.

In contrast to the clear trend observed in the size of the carrier-heating effect, the transmission curves demonstrated that the magnitude of the two-photon absorption term was independent of amplifier structure. The energy of carriers created via two-photon absorption is considerably greater than the bandgap of both the active and the cladding regions of the amplifiers, and the two-photon absorption thus depended predominantly on the intensity of light coupled to the amplifiers and not on the structure of the amplifiers.

A time-division interferometer was developed and used to obtain plots of the refractive index dynamics in the 4 QW, 8 QW and 16 QW amplifiers, as described in Chapter 3. The refractive index plots, obtained using pulses of 100 fs duration, showed an instantaneous negative transient and a positive transient with a time constant consistent with the carrier-heating effect recorded in Chapter 2. A fitting function identical to that used in relation to the transmission plots was used to distinguish the contributions to the refractive index plots made by different effects. The magnitude of the refractive index dynamic associated with carrier-heating was observed again to follow the number of quantum wells in the amplifiers. The carrier heating effect did not scale linearly with the number of quantum wells as would be expected, and this suggests a limitation of the current theory. The instantaneous negative transient was attributed to the quadratic Stark effect.

A value for the intensity-dependent refractive index $n_2 \sim -(4 - 16)\times10^{-12}$ was calculated for the instantaneous nonlinearity in each of the amplifiers. An effective intensity-dependent refractive index ($n_2 \sim 1 - 10 \times10^{-12}$) associated with the carrier-heating effect was determined for pulses whose duration was in excess of the carrier-heating recovery time of ~ 1 ps. From these measurements it was seen that a high intensity pulse with a duration of > 1 ps would experience a cumulative negative nonlinearity on propagation through the amplifiers. However, it is noted that the carrier-heating and quadratic Stark effect have linear and quadratic respective dependencies on intensity, and the sign of the cumulative nonlinearity experienced by an optical pulse will depend on its intensity.

The measurements performed using the time division interferometer were limited to the regime of small ($<\pi/6$) phase changes. Further work to develop a time division interferometer working via heterodyne detection would allow the

measurement of larger phase changes which more accurately reflect the operation of all-optical switches.

An investigation of the intensity-dependence of the current required to bias the 4 QW, 8 QW, 16 QW and bulk amplifiers to transparency was presented in Chapter 4. No previous investigation of the transparency current variation has been published, and this novel measurement is the highlight of this thesis. The transparency current was measured by modulating light coupled to the amplifiers and detecting the resulting modulation of the voltage across them. The transparency current was found to have a linear intensity-dependence in the 4 QW and 8 QW amplifiers. The effect responsible for the intensity-dependence was demonstrated to be carrier-heating. This was done by reducing the duration of pulses coupled to the amplifiers, and observing an increase in the gradient of the intensity dependence of the transparency current as the duration of the pulses approached the carrier-heating recovery time.

Measurements of the intensity-dependence of the transparency current in the 16 QW and bulk amplifiers showed a very nonlinear response which varied as a function of both wavelength and intensity. The transparency current in these amplifiers tended to converge towards a single value. To further investigate this surprising result, pump-probe transmission measurements were performed on the amplifiers using pulses of the same duration (25 ps) as those used for the transparency current measurements. The transmission curves revealed a slow negative trend whose time constant was in excess of the 200 ps span of the measurements. This effect may be a consequence of heating of the carrier distribution caused by free-carrier absorption, which is related to the thickness of the active region and is thus accentuated in the bulk and 16 QW amplifiers. It was noted that the slow negative trend would result in the detection of a decrease of the transparency current with increasing intensity as observed for short wavelengths in the bulk and 16 QW amplifiers. Future work is required to clarify the interesting effects observed in this part of this project.

The motivation behind the work described in this thesis was to investigate the potential applicability for all-optical switching at 1.55 μm of the enhanced intensity-dependent refractive nonlinearity observed in optical amplifiers. It was appropriate therefore to include the results of two switching experiments which exploited this effect. In Chapter 5, all-optical switching in a bulk-amplifier polarisation switch and in

a multiple quantum well directional coupler is demonstrated. The intensities of coupled light required to operate these switches are orders of magnitude less than that required to switch picosecond regime pulses in previously published experiments.

The experiments presented in this thesis indicate that the enhanced intensity-dependent refractive nonlinearity in waveguides biased to transparency is an attractive mechanism for the development for all-optical switching. The size of this nonlinearity opens up the possibility of ultrafast optical switching of light at lower powers than those previously required.

It is within the capability of currently available semiconductor laser sources to produce peak powers of the magnitude required to obtain optical switching, using the enhanced nonlinearity described in this thesis. In the future, it will be possible to produce monolithic structures combining optical sources with optical switching geometries. Such structures could be a few millimetres in length or less and would have a variety of applications.

Optimisation of waveguide structures to further enhance the nonlinearity in forward biased optical amplifiers may eventually allow exploitation of the nonlinearity for switching tasks in optical fibre communications links. In such applications, the forward bias to the switches would need to be monitored to ensure that the switches were maintained at the transparency point; this could be done by designing a stabilising circuit which measured the opto-electronic voltage across the switch and varied the current accordingly.

Appendix

List of Publications

Journal Publications

Sub-milliwatt optical bistability in a coated InGaAs/InP multiple quantum well waveguide Fabry-Perot cavity,

D. T. Neilson, J. E. Ehrlich, P. Meredith, A. C. Walker, G. T. Kennedy, R. S. Grant, P. D. Roberts, W. Sibbett and M. Hopkinson,

Election. Lett. 29, 1537 (1993).

Nonlinear switching in InGaAsP laser amplifier directional couplers biased at transparency,

D. A. O. Davies, M. A. Fisher, D. J. Elton, S. D. Perrin, M. J. Adams, G. T. Kennedy, R. S. Grant, P. D. Roberts and W. Sibbett,

Electron. Lett. 29, 1710 (1993).

Conference Publications

Effect of quantum-well number on nonlinear refraction in semiconductor laser amplifiers biased at transparency,

D. A. O. Davies, M. A. Fisher, D. J. Elton, C. P. Seltzer, M. J. Adams, G. T. Kennedy, P. D. Roberts, R. S. Grant and W. Sibbett, Annual Meeting IEEE Lasers and Electro-Optics Society (LEOS) 1993.

Low power polarisation switching in InGaAsP semiconductor amplifiers,

P. D. Roberts, G. T. Kennedy, W. Sibbett, D. A. O. Davies, M. A. Fisher and M. J. Adams,

Paper CFB2, Conference on Lasers and Electro-Optics (CLEO), Baltimore, May 1995.

Intensity dependence of transparency current in InGaAsP optical amplifiers,

P. D. Roberts, G. T. Kennedy, W. Sibbett, D. A. O. Davies, M. A. Fisher and M. J. Adams,

Paper 9-4, Twelfth National Quantum Electronics Conference (QE-12), Southampton, September 1995.

Intensity dependence of the transparency current in InGaAsP semiconductor amplifiers,

G. T. Kennedy, P. D. Roberts, W. Sibbett, D. A. O. Davies, M. A. Fisher and M. J. Adams,

Accepted for Conference on Lasers and Electro-Optics (CLEO), June 1996.

Acknowledgements

I would like to thank my supervisor, Professor Wilson Sibbett for his support and encouragement through the duration of this project. I am indebted to my CASE supervisor Dr. Mike Adams for his advice and for providing the optical amplifiers and other equipment. I would also like to thank Dr. Gordon Kennedy for his assistance in the lab and elsewhere, and for his patience.

I am also grateful to:

Robert Grant for many enlightening discussions and practical help,
Dave Burns for sharing his knowledge on many subjects,
Bill Sleat for advice on things electronic and for mending the laser,
Gareth 'Super G' Valentine for his enthusiastic help,
and all the other members of the 'W' squad for their cheerful stoicism in the face of adversity;
Dave Davies and Mike Fisher for their experimental suggestions and theoretical ideas, and the other 'B.T.' boys for making my time at Martlesham memorable.

Thanks are due also to all the members of the technical staff of the Physics Department, particularly:

Bob Mitchell for his cryogenic expertise,
Reg Gavine for his instruction in the workshop,
Andy Barman for keeping the dewar supplied with liquid nitrogen,
and the members of the Mechanical Workshop for constructing numerous bases and mounts.

I am most grateful to Stephanie Rogers for her encouragement when things were not going as smoothly as I would have liked, and to the Hangovers for many hours of harmonising. Thanks also to my parents for providing the computer on which this thesis was written.

Finally, I am grateful to the Engineering and Physical Science Research Council, and to British Telecom for financial support.